

Capillary and permeability seal capacity of mudstones

E.P. Imberechts

MSc. Thesis

Earth Structure and Dynamics, Utrecht University

March 2014

Under supervision of Prof. J. de Jager (Utrecht University)
and Dr. J.M. Verweij (TNO)

Abstract

Two main goals are pursued in this research, firstly a better correlation between two grain size measuring devices, for the mud content specifically has been established. Secondly, a grain size based work flow, developed by Daza, 2012 at TNO, to calculate permeability and capillary seal capacity of mudstones, has been calibrated, extended and improved. First of all, to obtain a better correlation, the first data set was applied, containing samples of the Rupel Clay Formation, Netherlands, and a core derived from the Belgian Boom Clay. The Belgian Boom Clay has been a target for nuclear waste disposal for decades and recently the Rupel Clay Formation has been targeted for the same reasons. These two formations are basically the same formation. Clay formations have a high permeability which is highly preferred with nuclear waste storage. The issues with the devices is that in the Netherlands, the laser diffractor is applied while in Belgium the sedigraph is used and the results are not directly comparable. It has been shown that the laser diffractor underestimates the clay fraction of the sample with respect to the sedigraph. Therefore a first step in this research is to calibrate these two grain size results. Grain size analysis of this data set has been carried out by both measuring devices and in total 16 boreholes in the Netherlands have been investigated and one core was derived from the Belgian nuclear waste disposal project. The depth of these samples ranges from 20-736m, indicating that some of the samples are of very shallow depths. In the literature, the clay fraction results should be comparable when for the laser diffractor a grain size of 8 μm is applied and for the sedigraph 2 μm . In this research a new correlation has been established at 5 μm for the laser diffractor compared to 2 μm with the sedigraph. With this improved correlation, the workflow can be continued. A next step is to integrate the improved correlation into the workflow. The workflow starts off with calculations based on formulas developed by Yang and Aplin. They established equations relating pressure coefficients to porosity and permeability, based on the clay fraction of the sample. This part of the workflow has been calibrated with a second data set, completely derived from 4 boreholes of the Boom Clay, in a synthesis research. These relationships are however for homogenous mudstone samples. Therefore to improve the workflow, heterogeneity calculations, based on Drews relationships have been implemented. Drews developed in his PhD thesis several equations relating effective stress to porosity and eventually porosity to permeability. All relationships are developed for a specific clay fraction ranging from 50% clay to 100% clay. A fourth step in this research is to select a third data set. This time a closer look was taken at the muddy cap rocks overlying the shallow gas fields, offshore northern Netherlands. The samples were derived from the A and B blocks. In total 4 cores and 49 cuttings were carefully selected in the cap rocks above the gas accumulations in order to have calibration points. The depth of these samples ranges from 312-1044m. In the sedimentological lab at the VU, these samples were analyzed by laser diffraction. These samples were implemented to verify the workflow and the calculations were carried out according to the new correlation for the clay fraction. The last step in this research is to extend the workflow, therefore 2 alternative pore throat calculation methods have been implemented. The first method is the equivalent grain size

method by Nakayama and Sato. They converted pore throats into grain size by using a theoretical relation of COEF, which is the ratio of pore throat to grain size. Then this grain size is used to evaluate top seal capacity. The second alternative pore throat calculation method is the critical grain size method of d10 method, by Nordgård Bolås et al. Here the size of the critical pore throats is important to a cap rock's seal capacity. When this workflow is carried out, there will be 12 calculations of seal capacities, 6 of these seal capacities will have the heterogeneity incorporated and 6 will assume homogenous samples. In order to calibrate the computed seal capacities with the shallow gas fields, an interpretation will be made of seismic images indicating gas columns and NPHI-RHOB cross-overs, depth contour maps, and production plans. This results in the selection of three methods that render the most accurate seal capacities, two of them are based on the integration of the equivalent grain size method with and without heterogeneity calculations; the other on the critical grain size method.

Contents

Abstract.....	1
Introduction	6
Objective	6
Background	6
Mudrocks	6
The Rupel Clay Formation	6
Shallow gas fields	7
Seal capacity.....	7
Improvements needed for calculating porosity, permeability, pore throats, seal capacity of mudrocks using grain size data	10
Previous studies on calculating porosity, permeability and seal capacity Porosity-Permeability studies	10
Empirical models.....	10
Theoretical model: Kozeny-Carman equation	10
Theoretical models based on pore size distributions	11
Data bases	11
Methodology.....	13
Method 1. Comparison between different grain size measurement methods (Sedigraph and laser diffraction)	13
Method 2. Porosity- effective stress and porosity-permeability calculations with Belgian Boom Clay measurements.....	16
Method 3. Application of heterogeneity: Drews methodology.....	18
Method 4. Sampling and grain size analysis of Plio-Pleistocene mudrocks	20
Method 5. Calculation of pore throat and capillary seal capacity.....	21
1.1 The equivalent grain size method (1)	21
1.2 The equivalent grain size method (2)	23
2. The d10 method.....	23
Results.....	27
Results Method 1.Comparison of grain size measurement methods (Laser diffraction vs. sedigraph)	27
Results Method 2 for homogeneous mudrocks (Yang & Aplin) + method 3 for heterogeneous mudrocks (Drews).....	33
Porosity- effective stress and porosity-permeability calculations.....	33
Results Method 4. Sampling, new grain size analysis, new calculations and calibration	36
Results Method 5. Calculation of pore throat and capillary seal capacity	37

1. d10 method.....	37
2. Seal Capacity, d10 methods and equivalent grain size method	39
Discussion.....	41
Method 1. Laser diffraction vs. sedigraph	41
Method 2. And 3.	42
Method 5. Alternative pore throat calculations	44
2. The d10 method.....	44
2.1. The Schlömer and Krooss, 1997 data set.....	44
2.2. The Yang and Aplin data set.....	45
2.3. The Katsube et al., data set.....	45
2.4. All data sets combined.....	46
2.5. Comparison d10 graphs	46
2.6. Comparison seal capacity graphs.....	47
2.7. Evaluation of the different methods.....	48
A12-03.....	48
A12-01.....	50
B16-01.....	52
B17-05.....	54
B10-03.....	56
2.8. Overview methods.....	58
Conclusions and outlook.....	60
Method 1. Laser diffraction vs. sedigraph	60
Method 2. Porosity- effective stress and porosity-permeability calculations with Belgian Boom Clay measurements.....	60
Method 5. Alternative pore throat calculations	60
1. The equivalent grain size method (1)	60
2. The d10 method.....	60
3. Seal capacity.....	61
Acknowledgments.....	62
References	63
Appendix A: shallow gas field data.	67
Appendix B: results sedigraph vs. laser diffraction.....	68
Appendix C permeability values.....	74
Appendix D: selection shallow gas field samples.....	75

Appendix E: contour maps shallow gas fields.....	76
Appendix F: Grain size analysis results: shallow gas fields	81
Appendix G: Shallow gas fields: Calculated properties.....	83

Introduction

Objective

In this masters research, several goals are pursued. Firstly an attempt is made to improve the correlation of the clay fractions, between two grain size measurement techniques, the sedigraph and the laser diffractor. The calibration is based on the data set derived from the Rupel Clay Member, Netherlands (also used in the OPERA project, TNO). Secondly this new clay fraction is taken into account for the calibration of a grain size based workflow specific for the calculation of porosity and permeability, developed by Daza, 2012 and TNO. This calibration is based on a second data set derived from the Belgian Boom Clay. Thirdly this workflow is extended in order to compute capillary pressure and seal capacities for mudstones. For this last step a new data set, derived from the shallow gas fields offshore Netherlands, is selected.

Background

Mudrocks

They are the most abundant sedimentary rocks and are of great relevance to many aspects of the geosciences. Due to their specific properties such as high capillary entry pressure and low permeability they baffle fluid flow effectively on moderate timescales (Aplin *et al.*, 2010). Therefore mudstones can act as seals, fluid barriers and shale gas reservoirs in petroleum systems, targets for nuclear waste deposits in the subsurface, CO₂ storage, etc., Daza, 2012; Drews, 2012.

The components of mudstones are derived from weathering, primary production and diagenesis. In general, depositional porosities of mudstones are high, reaching 80-90%. Porosity reduces with burial depth, at shallow depths the reduction is mainly due to mechanical compaction, driven by the increase of effective stress. The degree of compressibility is dependent on the dominant grain size of the mud. The finer the grains the higher the initial porosities and the higher their compaction rates, Yang and Aplin, 2004; Aplin and Macquaker 2011.

Natural mudstones are rarely homogenous. Their grain size varies from less than 0.1 μm to larger than 100 μm and the clay fractions range from 10 to 100%, Fawad *et al.*, 2010. This heterogeneity is mainly caused by the sedimentary architecture and the paleo-environment. On the sample scale, shales and mudstones are fairly well understood, on the sub-metre scale, many typical properties are dependent on spatial heterogeneity.

The Rupel Clay Formation

The Rupel clay formation consists out of three members: the Vessem Member, the Rupel Clay Member and the Steensel Member, Herngreen, 2005. The Rupel Clay Member was targeted because of a recent interest in possible locations for subsurface nuclear waste deposition. The Rupel clay member is more or less equivalent to the Belgian Boom Clay, which has been subject of interest for the same reasons in Belgium. Seen that this research

has been going on in Belgium for almost three decades, it would be useful to compare permeabilities for both researches. First of all a clay fraction is measured in the Members. In Belgium this is carried out by the sedigraph, in the Netherlands by applying laser diffraction. For these two grain size measurement devices, the resulting clay fractions are not consistent. In order to make a correlation, the results of a core of the Belgian Boom Clay were provided.

Shallow gas fields

The third data set used in this thesis originates from the Southern North Sea, mainly the A and B blocks. This part of the North Sea is characterized by the presence of shallow gas. This gas occurs in unconsolidated sediments of Cenozoic age. The sediments in which the gas originated are of Plio- to Pleistocene age and are shallow marine to continental origin. Commonly these sediments are referred to as part of the Eridanos delta system. The gas is trapped in anticlines above salt domes, in stratigraphic or depositional traps, Overeem *et al.*, 2001; De Haan, 2010. At certain locations gas accumulation are stacked on top of each other in subtle anticlines. The gas occurs in relatively shallow reservoirs, typically at depths of less than 1000m.

Seal capacity

The seal capacity of a mudstone is defined as the height of the hydrocarbon column that the seal can hold prior to leaking. It is a function of heterogeneous pore throat size distribution along the largest interconnected pore throat path, the formation water pressure, the density of the hydrocarbons, and other factors, Barboza *et al.*, 2009. The seal capacity for hydrocarbons of a water wet mudstone is strongly controlled by the capillary entry pressure. This is on its turn dependent on the pore throat size of the most favorable path, as described above. This indicates that grain size is the most important factor in seal capacity and not the thickness of the seal itself.

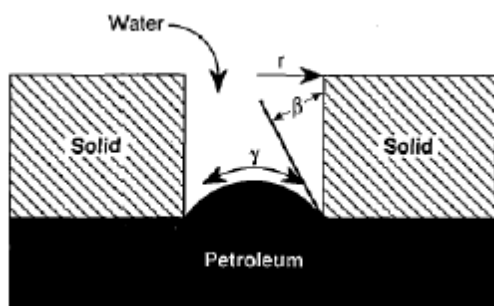


Figure1. Capillary resistance sketch, Clayton, 1994.

For failure to occur, the upward buoyancy pressure and an excess overpressure, must exceed the capillary pressure

$$P_{buoy} + \Delta U > P_c \quad (1)$$

$$(\rho_w - \rho_{hc})gh + \Delta U > P_c \quad (2)$$

Where P_{buoy} , is the upward buoyancy pressure; ΔU is any excess overpressure; P_c the capillary pressure.

Theoretically, a few centimeters of shale could form an adequate seal and trap large columns of hydrocarbons. The height of the hydrocarbon column that is held by a thin seal is the same as the height of the column trapped by a thick seal. Therefore the thickness of the seal is not incorporated in the equations to compute seal capacities, see equations (1), (23) and (29). There is however a small probability that a very thin seal could be continuous, unbroken, unbreached and maintain a stable lithic character over a sizable accumulation Downey, 1984.

A distinction can be made between a capillary seal, a permeable seal and a pressure seal. The first one indicates that sealing occurs at the hydrocarbon water interface and a sharp pressure discontinuity is retained across the seal. The second one indicates that the hydrocarbons have invaded the seal and a pressure gradient is maintained throughout the seal. A pressure seal indicates that the buoyant fluid is held back by water flowing downwards through the pores as consequence of a pressure potential. This occurs in under-compacted shales, highly strained shales or in shaly seals with a high organic matter content, Ingram *et al*, 1997.

Different stages in nonwetting phase breakthrough processes in a fine grained medium can be distinguished. Firstly, the nonwetting fluid only fills the largest pores on the surface contact. This occurs when the pressure of the injected fluid exceeds the capillary entry pressure. This initiates migration of the nonwetting fluid into the seal. With a further increase in nonwetting fluid, the smaller pore throats start to open, thereby displacing the wetting phase and increasing nonwetting phase saturation in the pore system. In this phase, the gas pressure is higher than the capillary pressure, but it is still lower than the threshold pressure or breakthrough pressure. Therefore the seal retains its sealing properties. A third step comprises the creation of a continuous flow path along the cross-section of the seal. Now interconnected fluid paths arise along the largest pore diameters. The pressure at which a gap forms in the capillary sealing system is the capillary breakthrough pressure. During this stage the fluid flow only comprises a small part of the pore network. With increasing pressure, the flow extends to other pore throats, thereby increasing the saturation of the nonwetting phase and so increasing the effective permeability. After nonwetting phase breakthrough a pressure reduction occurs, resulting in wetting phase re-imbibition, starting with the smallest pore diameter. The closing of the flow paths decreases permeability for gas and eventually leads to a stop in fluid flow or leakage Klimkowski *et al.*, 2012; Schowalter, 1979; Dullien, 1992; Hildenbrand *et al.*, 2002; and Li *et al.*, 2005.

A first step in the computation of the seal capacity is the determination of the grain size. Mostly this is carried out by the laser diffractor or the sedigraph. Here the objective is to determine the clay fraction of the samples. The clay content appears to be a reasonably robust indicator of the overall grain size of the mudrocks. Additionally, void ratio at liquid

limit is strongly correlated to the clay fraction, Skempton, 1944 Yang and Aplin, 2004. Moreover the clay fraction is one of the important parameters to calculate capillary seal capacity. To establish the grain size, two methods were used, the first one being the Micromeritics Sedigraph 5100 and the second one the laser diffraction analysis. Previous studies stated that laser diffraction results are only comparable to sedigraph analysis for coarse silt and sands, Konert *et al.*, 1997.; Buurman *et al.*, 2001. For the clay fraction, Konert *et al.*, 1997 made the suggestion that the results of both methods could be compared when for the laser diffraction fraction, a grain size of $<8 \mu\text{m}$ is applied and for the sedigraph fraction a grain size of $<2 \mu\text{m}$. Many other authors concluded in their research that the $<8 \mu\text{m}$ grain size correlation for the laser results in an underestimation of the silt fraction and an overestimation of the clay fraction. They suggested that the grain size for the laser diffraction should be smaller than $8 \mu\text{m}$. (e.g. Ferro *et al.*, 2009; Konert *et al.*, 1997; Pieri *et al.*, 2006; Arriaga *et al.*, 2006; Kowalenko *et al.*, 2012). In 2006, Ramaswamy and Rao investigated this discrepancy and concluded from their research that a new grain size of $6.2 \mu\text{m}$, should better be applied as clay fraction for the laser diffraction.

The next step is the calculation of the porosity of the sample. Porosity can be determined from measurement techniques directly, such as mercury intrusion. With this technique, pores between $500 \mu\text{m}$ and 3.5nm can be investigated. The analysis gives information about the largest entrance to a pore, the smallest pore size, pore size distribution and much more, Giesche, 2006. Other methods to compute porosity are based on equations relating effective stress to porosity, e.g. Drews, 2012, Nordgård Bolås *et al.*, 2005.

A last step is to compute the seal capacity. Several methods are able to produce accurate seal capacities. In 2002, Nakayama and Sato developed the equivalent grain size method. This is a method that links critical grain sizes to seal capacity. Two relationships were developed one based on mudstone data and one based on artificial tests. Nordgård Bolås *et al.*, 2005, developed relationships in order to calculate seal capacities based on critical pore throat diameters.

All the above described methods, with exception of Drews, 2012, are based on homogeneous mudstones. Heterogeneity has qualitatively been investigated by many authors e.g. Norhdal *et al.*, 2008; Schneider, *et al.*, 2011; Deutsch, 2002; Chiles and Delfiner, 1999; Schieber, 1999; Macquaker and Gawthorpe, 1993. The two most standard approaches in heterogeneity investigations taken are, firstly the sedimentological processes behind the formation of the heterogeneities, which involve detailed studies of sequence stratigraphy, paleontology and depositional environments. The second method takes the geometric shape of the heterogeneity into account and only minorly refers to sedimentological processes, Drews, 2012. In order to incorporate heterogeneity in the calculations, Drews, 2012, developed different relationships, by investigating the core and borehole images and integrating them into a model. The equations are based on the clay fraction of the sample, and are thus leading to results specific for depth and grain size.

Improvements needed for calculating porosity, permeability, pore throats, seal capacity of mudrocks using grain size data

1. The sedigraph and laser diffractor. A better correlation between the two grain size measuring devices needs to be established, especially with respect to clay content.
2. More extensive calibration of porperm calculation with models of Yang and Aplin, 2004, 2010 and of the equivalent grain size method to calculate pore throats.
3. Integration of heterogeneity in mudstone in the permeability calculations, by including methods developed by Drews, 2012.
4. Evaluation of the pore throat calculations by Nakayama and Sato, 2002.
5. Selection of the methods which represent the best permeability and seal capacity results.

Previous studies on calculating porosity, permeability and seal capacity

Porosity-Permeability studies

A routine measurement of permeability, brings along many difficulties, especially when it concerns mudstones. Therefore, a variety of models have been developed in order to relate permeability to variables that are more easily measured. These are preferentially porosity and permeability. In general there are two major approaches, the first by using laboratory measurements to build equations relating porosity to permeability. A second approach is theoretical, by making use of the Kozeny-Carman and Hagen Poiseuille equations, Tavenal *et al.*, 1983; Tokunaga *et al.*, 1994 and Dewhurst *et al.*, 1999 .

Empirical models

In attempt to correlate permeability to easily determinable physical characteristics of clays, Tokunaga *et al.*, 1994, developed an equation for stresses to geological conditions in the sediments.

$$K = k_0 \left[\frac{n}{n_0} \right]^a \quad (3)$$

Where K is the permeability; n is the porosity; K_0 is the permeability at n_0 , the initial porosity and a is an experimentally determined constant.

Theoretical model: Kozeny-Carman equation

This equation has been used to predict sand permeabilities. When applying this relationship the assumption is made that all pores are capillary tubes with the same cross-section area.

$$K = \frac{1}{k_0 k_T} \frac{n^3}{S^2 (1-n^2)} \quad (4)$$

Where k_0 and k_T , are shape and tortuosity factors; n is porosity; and S in the specific surface area ($m^2 m^{-3}$). This relationship implies that when flow rate through a pore is exponentially

proportional to its radius, the majority of the flow occurs through the larger interconnected pores, Carman 1965; Yang and Aplin, 1998.

Theoretical models based on pore size distributions

The majority of these models are based on the Hagen-Poiseuille equation, which serves as base to derive permeability from pore size distributions.

$$q = \frac{\gamma l}{8\eta} a y^2 \quad (5)$$

Where γ is the unit weight of the fluid, y is the radius of the tube, l the hydraulic gradient, a the cross-sectional area of the tube and η the viscosity of the fluid, Dewhurst *et al.*, 1999. In 1998, Yang and Aplin developed a permeability model based on the Hagen Poiseuille equation. The pore shape was defined as two frustums of cones which are connected at the base and the pore shape was allowed to change as function of effective stress.

Yang and Aplin developed several models based on effective stress and clay content, Aplin *et al.*, 1995; Yang and Aplin, 1998, 2004, 2010. The majority of the models results in sub-nano to micro-darcy permeabilities and a logarithmic permeability and porosity decrease with increasing effective stress, depth. Another feature is the anisotropic behavior for horizontal and vertical permeabilities, displayed by clay rich sediments. Shales and mudstones are characterized either by mineralogy or grain size, Mondol *et al.*, 2007. In this study, the grain size will be subject of interest.

Data bases

This research used grain size analysis data of mudrocks of Oligocene and Plio-Pleistocene age:

Grain size analysis data of the Rupel Clay from the onshore Netherlands Member (146 samples from 17 wells; depth range 20-736m), see figure 3. For this dataset both laser and sedigraph measurements were available. These data were used to improve the correlation between the sedigraph and laser diffractor and to calibrate the workflow developed by Daza, 2012 and TNO.

Grain size analysis data and hydraulic conductivity data of the Boom Clay in Belgium (124 samples from 4 wells; depth range 56-381m), see figure 2. This dataset was used to calibrate the workflow developed by Daza, 2012 and TNO.

New samples for grain size analysis were taken from Plio-Pleistocene mudrocks in the Dutch northern offshore (5 wells, 53 samples, depth range 312-1044m), see figure 4. These mudrocks act as sealing cap rocks for shallow gas accumulations. The new grain size analysis data and the available information on e.g. HC column heights etc. were used to verify and improve the workflow.

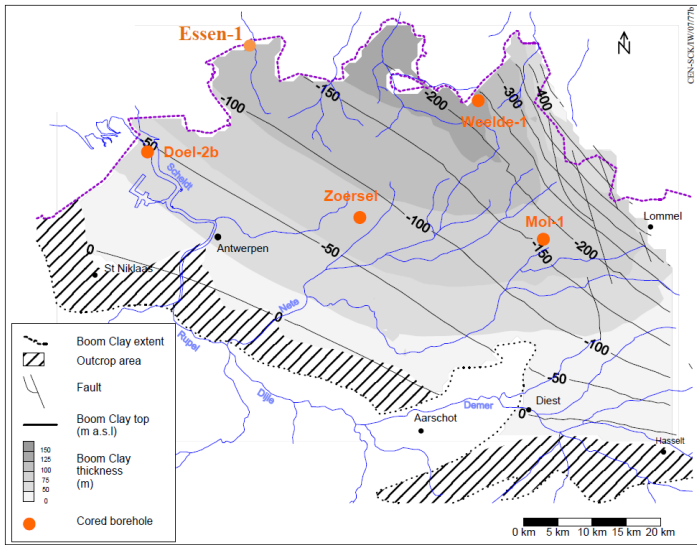


Figure 2. Left: location of the samples of the Belgian Boom Clay, from Yu *et al.*, 2011.

Figure 3. Lower left: location of the boreholes where the samples were derived, only locations of 16 wells are presented, the 17th well is confidential.

Figure 4. Lower right: location of the boreholes of the second data set.



Methodology

The workflow starts with obtaining a better correlation between the sedigraph and laser diffractor for the clay content. It is succeeded by the calculation of effective stress, porosity and permeability. These calculations are based on relationships developed by Yang and Aplin 2004; 2010. Thirdly, to include heterogeneity in the clay measurements, an attempt was made to include the workflow of Drews, 2012. Next alternative pore throat calculations, the equivalent grain size method by Nakayama and Sato, 2002; and the d10 method, developed by Nordgård Bolås *et al.*, 2005 are implemented. With these last methods the workflow can be extended to the calculations of capillary forces and eventually seal capacities.

Method 1. Comparison between different grain size measurement methods (Sedigraph and laser diffraction)

The first data set, derived from the Rupel Clay Member, was selected and analyzed by TNO, the third data set, derived from the shallow gas fields was personally selected and analyzed. The first data set was analyzed both by the laser diffractor and sedigraph, the third one only by laser diffraction.

The grain size analysis, for 17 boreholes of the Rupel Clay Member in the Netherlands was carried out by Qmineral bvba in Belgium. The samples originated from boreholes spread over the Netherlands and one core originated from the Belgian Boom Clay, figure 3. For the 5 boreholes of the shallow gas fields offshore northern Netherlands, see figure 4., the grain size analysis was carried out in the sedimentological lab at the University of Amsterdam, for the laser diffraction the same analysis was made for both data sets. Samples of the first data set were only taken onshore, where the thickness of the Rupel Clay Member exceeded 100m and the top of the formation was situated at a depth of at least 400m. Before the actual grain size analysis could be carried out a pre-treatment was applied. The first step taken was to reduce the bigger samples into a smaller, more convenient size. Secondly the organic compounds were dissolved. Subsequently the samples were rested overnight in an acid (HCl) solution to dissolve all carbonates present. Finally $\text{Na}_4\text{P}_2\text{O}_7 \cdot 10\text{H}_2\text{O}$ was added to detach the clay plates from each other.

The sedigraph, an X-ray measurement, is used for fine grained clay rich sediments. Due to technical reasons the largest grains that this method can do not exceed 250 μm . The fraction of the sample smaller than 250 μm was centrifuged and dried. Then a suspension was made by adding water. Next, a peptizer was added to make the suspension stable.

Finally, the sample was shaken and analyzed by the Micromeritics Sedigraph 5100. Three-fifth of a prepared sample was used for analysis by the Sedigraph.

One fifth of the sample was used to determine the fraction larger than 250 μm . The sample was wet sieved. Both the fraction smaller and larger than 250 μm were weighed after drying, in order to obtain the fraction larger than 250 μm .

Laser diffraction analysis, a low angle laser light scattering, or LALLS, is a technique that measures particle size distributions. The remaining one fifth of the prepared sample was used for this analysis. It was subdivided into ten equally sized samples using a Rotary Cone Sample Divider. The laser beam, of monochromatic light, passes through a dispersed particle sample, which causes the light to scatter. The scattered light is focused onto detectors, which measure the intensity of this scattering. Large particles scatter light at small angles with respect to small particles which scatter light at larger angles. This angular intensity scatter data is then analyzed to obtain a particle size distribution (Cajjgal, 2012; Ferro *et al.*, 2009). An important assumption is, that the transformation of the scattering patterns to grain sizes relies on matrices, which are calculated for spheres (Konert *et al.*, 1997). At least two separate measurements were carried out, of which the average was calculated.

When the results were obtained, they were implemented in the EXCEL spreadsheet GRADISTAT V8, see figure 6.



Figure 5. Laser diffractor at the VU sedimentological lab.

To investigate which grainsize for the laser diffraction is in better agreement with the clay fraction determined by the sedigraph, an analysis was made. Subsequent to the grain size analysis in GRADISTAT, the grain sizes and according fractions of the samples are presented. Several grain sizes were selected, ranging from 2 µm to 8 µm. The different clay fractions of the laser diffractor are then plotted together with the standard 2 µm grain size of the sedigraph.

Size, µm		Frequency, %		
Low	High	Average	VIII1	VIII2
0,05	0,06	0,05	0	0
0,06	0,07	0,06	0	0
0,07	0,08	0,07	0	0
0,08	0,09	0,09	0,01	0,01
0,09	0,11	0,10	0,02	0,01
0,11	0,13	0,12	0,03	0,02
0,13	0,15	0,14	0,05	0,05
0,15	0,17	0,16	0,09	0,08
0,17	0,20	0,18	0,15	0,14
0,20	0,23	0,21	0,24	0,22
0,23	0,27	0,25	0,33	0,32
0,27	0,31	0,29	0,41	0,40
0,31	0,36	0,34	0,45	0,44
0,36	0,42	0,39	0,44	0,44
0,42	0,49	0,46	0,44	0,43
0,49	0,58	0,53	0,44	0,44
0,58	0,67	0,62	0,44	0,43
0,67	0,78	0,72	0,47	0,45
0,78	0,91	0,84	0,57	0,53
0,91	1,06	0,98	0,70	0,64
1,06	1,24	1,14	0,87	0,78
1,24	1,44	1,33	1,11	0,99
1,44	1,68	1,55	1,40	1,24
1,68	1,95	1,81	1,74	1,55
1,95	2,28	2,11	2,18	1,95
2,28	2,65	2,46	2,68	2,45
2,65	3,09	2,86	3,23	3,01
3,09	3,60	3,33	3,80	3,64
3,60	4,19	3,88	4,37	4,28
4,19	4,88	4,52	4,91	4,93
4,88	5,69	5,27	5,38	5,51
5,69	6,63	6,14	5,72	5,97
6,63	7,72	7,15	5,92	6,27
7,72	9,00	8,33	5,98	6,41

Figure 6. Copy of the Excel program Gradistat. The average grain size was used to select the according clay fractions of the sample. The different rectangles indicate all the different grain sizes. VIII indicates that it is borehole VIII and the number refers to a specific sample depth.

Method 2. Porosity- effective stress and porosity-permeability calculations with Belgian Boom Clay measurements

With the intention to obtain the permeabilities for the Rupel Clay Member and sealing capacity for the samples of the shallow gas fields, relationships by Yang and Aplin (2004; 2010) are applied. First of all a division in grain size classes is made. The first class is clay, which consists out of particles with a diameter smaller than 2 μm . The second class is silt, where the particle size ranges from 2- 62.5 μm and the last class is sand, which ranges from 63-2000 μm in particle diameter. Yang and Aplin developed in 2004, several equations to describe the mechanical compaction of fine grained clastic sediments, such as muds and mudstones. The relationships can adequately describe mechanical compaction up to 40 MPa.

In order to calculate the permeability, first the clay fraction of the sample needs to be determined. This is carried out by the Sedigraph and the laser diffraction. Once this value is known, the porosity can be computed. Therefore equations based on the effective stress principle derived in soil mechanics are applied, Yang *et al*, 2004. (also described in Daza Cajigal 2012 and Chapter 6 in Ten Veen et al 2013).

$$e = e_{100} - \beta \ln\left(\frac{\sigma'v}{100}\right) \quad (6)$$

$$\sigma'v = \sigma v - u \quad (7)$$

$$e = \frac{\emptyset}{1-\emptyset} \quad (8)$$

With e being the void ratio; e_{100} the void ratio at 100 kPa effective stress; β the slope of the linear relation between void ratio and the natural logarithm of vertical effective stress; $\sigma'v$ is the effective stress, the difference between the total stress σv and the pore fluid pressure u . Coefficients e_{100} and β , are the compression coefficients which describe the mechanical compaction of mudstones.

Equation (8) can easily be rewritten in order to calculate the porosity of the sample

$$\emptyset = \frac{e}{1+e} \quad (9)$$

Yang and Aplin, 2004 were able to derive equations linking the compression coefficients to the clay fraction of the sample, based on the data sets of Skempton, 1970 and Burland (1990).

$$e_{100} = 0.3024 + 1.6867\text{clay} + 1.9505\text{clay}^2 \quad (10)$$

$$\beta = 0.0407 + 0.2479\text{clay} + 0.3684\text{clay}^2 \quad (11)$$

In order to calculate the permeability, the effective stress has to be computed. It was estimated from the following relationship

$$\sigma_v - P_w = 11.1 z \quad (12)$$

Where z [mTVDss]; $\sigma_v - P_w$ is the effective stress [kPa]

The vertical stress, σ_v , is derived from the RHOB log at well B18-02 for depths between 400-1200m.

$$\sigma_v = 21.6 * z \quad (13)$$

The water pressure in this part of the North Sea is based on pressure gradients derived from measured RFT pressures at 9 wells.

$$P_w = 10.5 * z \quad (14)$$

Where P_w is in kPa.

With the effective stress the permeability of the sealing layers can be compute. Therefore a permeability-porosity relationship for mudstones as a function of clay content, developed by Yang and Aplin, 2010, is applied. Here a relationship between bedding perpendicular, absolute, permeability and porosity is established. It was developed for homogenous fine grained clastic sediments.

$$\begin{aligned} \ln(K) = & -69.59 - 26.79 * CF + 44.07 * CF^{0.5} + (- 53.61 - 80.03 * CF + 132.78 * CF^{0.5}) * e \\ & + (86.61 + 81.91 * CF - 163.61 * CF^{0.5}) * e^{0.5} \quad (15) \end{aligned}$$

CF is the clay fraction of the sample.

Method 3. Application of heterogeneity: Drews methodology

Drews collected many clay rich samples with a wide range of lithological variability. A first step undertaken was the division in the grain size. A distinction was made between the cohesive fraction, grains with a diameter smaller than 10 μm and a sortable fraction, which consist out of coarse silt and sand. Drews defined mud and mud content as follows “Bulk lithological property on all scales beyond sample scale (centimetre-scale). A sample can be called mud, if its cohesive content is equal or greater than 50%” (Drews, 2012, p. 13). For analyzing the samples a Sedigraph was applied. Drews used these clay contents to calculate porosity and permeability with the models developed by Yang and Aplin (2004, 2010) on cm-scale. The investigated mud contents range from 50-100%. Subsequently, an extended version of Yang and Aplin’s models (2004; 2010) are implemented in a geostatistical 2D modelling workflow, to predict porosity and permeability for the full spectrum of grain size fraction combinations of fine grained siliciclastic sediments. Porosities and permeabilities were calculated for different effective stresses at a fixed ratio of clay to fine silt. Drews developed relationships for porosity as function of effective stress and for horizontal and vertical permeabilities as function of porosity, both with a fixed mud content. To address the various types of heterogeneity in mudstones, relationships were developed for continuous beds, discontinuous beds, isotropic structures, small vertical structures and large vertical structures.

The first step in this approach is to calculate the effective stress. This is carried out by implementing equation (12). With the computed effective stress, the above table can be applied. Once the porosity is known for the desired mud content, the porosity can be implemented in the following relationships, see table 2. in order to compute the permeability.

Mud content [%]	$\varphi = f(\sigma)$	R^2
50	$2.29\text{e-}004*\sigma^2 - 1.49\text{e-}002*\sigma + 4.16\text{e-}001$	0.99
60	$2.53\text{e-}004*\sigma^2 - 1.64\text{e-}002*\sigma + 4.34\text{e-}001$	0.99
70	$2.77\text{e-}004*\sigma^2 - 1.78\text{e-}002*\sigma + 4.52\text{e-}001$	0.99
80	$3.01\text{e-}004*\sigma^2 - 1.93\text{e-}002*\sigma + 4.70\text{e-}001$	0.99
90	$3.25\text{e-}004*\sigma^2 - 2.08\text{e-}002*\sigma + 4.87\text{e-}001$	0.99
100	$3.49\text{e-}004*\sigma^2 - 2.23\text{e-}002*\sigma + 5.05\text{e-}001$	0.99

Table 1. Various relationships to calculate the porosity as function of effective stress and mud content, Drews, 2012.

Model_ID	Structure	Variogroup	Mud Content [%]	Kh - f(ϕ)	R ²
Mod01	Laminated	Zonal, horizontal	50	$-1.86e+001\phi^2 + 1.90e+001\phi - 1.87e+001$	1
			60	$5.64e+000\phi^2 + 8.05e+000\phi - 1.97e+001$	1
			70	$4.26e+000\phi^2 + 7.83e+000\phi - 2.01e+001$	1
			80	$3.47e+000\phi^2 + 7.39e+000\phi - 2.04e+001$	1
			90	$2.77e+000\phi^2 + 6.99e+000\phi - 2.06e+001$	1
			100	$2.23e+000\phi^2 + 6.60e+000\phi - 2.08e+001$	1
Mod03	Laminated	Geometric, horizontal	50	$6.64e+000\phi^2 + 8.55e+000\phi - 1.98e+001$	1
			60	$5.58e+000\phi^2 + 7.99e+000\phi - 2.02e+001$	1
			70	$4.47e+000\phi^2 + 7.61e+000\phi - 2.05e+001$	1
			80	$3.41e+000\phi^2 + 7.34e+000\phi - 2.06e+001$	1
			90	$2.69e+000\phi^2 + 6.99e+000\phi - 2.08e+001$	1
			100	$2.26e+000\phi^2 + 6.58e+000\phi - 2.08e+001$	1

Table 2. Some of the relationships to compute permeability, in this case horizontal permeability, as function of fixed mud content and porosity. (For all the equations, see Drews 2012, p. 156.)

Method 4. Sampling and grainsize analysis of Plio-Pleistocene mudrocks

In the TNO core shed, 54 cm scale samples were collected, of which five are core samples and 49 cuttings. Logs of the several wells were analyzed and just above bright spots or known gas accumulations, in the sealing clay/mud layer, the samples were collected. The depth of these samples ranges from 275m to 1007m (mTVDss). See appendix A for more information about the samples.



Figure 7. Selection of the cuttings at the TNO core shed.

The samples were analyzed at the VU sedimentological lab, according to the same methods as described above with the samples of the Rupel Clay Member. Only laser diffraction was carried out.

Method 5. Calculation of pore throat and capillary seal capacity

These calculations are carried out for the new grain size analysis data of Plio-Pleistocene mudrocks, with this data set the workflow can be extended to the calculation of capillary pressure and seal capacity.

For these calculations the newly established correlation between the sedigraph and laser diffraction of the clay fractions will be applied. Calculations resulting from method 1. and 2., i.e. calibration of the grain size measurement devices and porperm calculations, will be carried out with a clay fraction of 5 μm . Method 3., incorporation of heterogeneity, will have a cohesive content of $<10 \mu\text{m}$.

1.1 The equivalent grain size method (1)

This method aims to derive a specific pore throat radius, which directly influences the sealing capacity of a layer of interest. The authors concluded that the pore throat radius is not a convenient parameter for geologist, therefore they converted it into a critical grain size. For this conversion a theoretical relation of COEF, which is the ratio of pore throat to grain size, as a function of porosity is contrived. The calculations are based upon Nakayama and Sato's, 2002, equivalent grain size method. Important assumptions made by applying this method are a) the cap rock consist of equalized grains, b) the pore throat is a function of grain size and porosity only if the geometrical ratio of pore-throat and grain size is considered, c) porosity changes according to packing. This gives the next equations:

$$\text{COEF} = 1.92(\phi)^2 - 0.0882(\phi) \quad (16)$$

$$R = \frac{1}{2} (\text{COEF})d_e \quad (17)$$

Where COEF is the ratio of pore-throat size to grain size, ϕ is the porosity, d_e is the equivalent grain diameter and R is the pore-throat radius. Here, we use the median grain size diameter for d_e .

Combining (16) and (17) gives (18):

$$R = \frac{1}{2} [1.92 (\phi)^2 - 0.0882 (\phi)] d \quad (18)$$

In order to calculate capillary seal capacity,

$$h = \frac{P_{ce}}{(\rho_w - \rho_g)g},$$

where

$$P_{ce} = \frac{2\gamma}{R}$$

We first calculate of the interfacial tension. Nordgård Bolås *et al*, estimated the interfacial tension variation of the water-gas system with depth by a depth- interfacial tension relationship. Daza, 2012 developed a relationship in order to compute interfacial tension for the according depth.

$$\gamma = \frac{5222.2-z}{69.44} \quad (19)$$

Where γ is the water-gas interfacial tension in mN/m.

With the interfacial tension and pore throat radius, the theoretical capillary pressure can be computed.

$$P_{ce} = \frac{2\gamma}{R} \quad (20)$$

With P_{ce} is the theoretical capillary pressure in Pa.

The last parameters that are required to calculate the seal capacity are the temperature at each specific depth and the gas density.

The gas densities for the specific depths were calculated by the Material Measurement laboratory from the National Institute of Standards and Technology. The required input data are the temperature and pressure at a certain depth. Since, most chemical analyses from shallow gas fields indicate that the gas is biogenic in origin, it consist mostly of methane, Muntendam-Bos, *et al.*, 2009. The pressure gradient 10500Pa/m is used to calculate the pressure. Temperature data for the Dutch northern offshore show some spatial variations in geothermal gradient, therefore equation (22) was selected to calculate the temperature at a certain depth. The general pressure equation is:

$$P = (0.0105 * z(m)) + 0.101325 \quad (21)$$

The temperature gradient was derived from the following equation

$$T = 0.030(z) + 10 \quad (22)$$

Where T is the temperature in °C.

The final step is to calculate the seal capacity

$$h = \frac{P_{ce}}{(\rho_w - \rho_g)g} \quad (23)$$

Where h is the seal capacity in m; ρ_w is the water density, 1070 kg/m³; ρ_g is the gas density in kg/m³; and g is the gravitational acceleration.

1.2 The equivalent grain size method (2)

In 2005 Sawamura and Nakayama computed a second method to calculate the COEF and R respectively. The same set up and assumptions, for the experiments were used as with the calculation of the first equivalent grain size method, hereafter EGM (1) or (2). The obtained formula is:

$$\text{COEF} = 2R/D_m = 3.085\phi^2 + 0.2087\phi \quad (24)$$

The authors stated that the difference in coefficients between formula (16) and (24) are due to the drag effect at the grain surface for the case of the experiment. They also suggest that formula (24) is closer to nature than the more theoretical case (16).

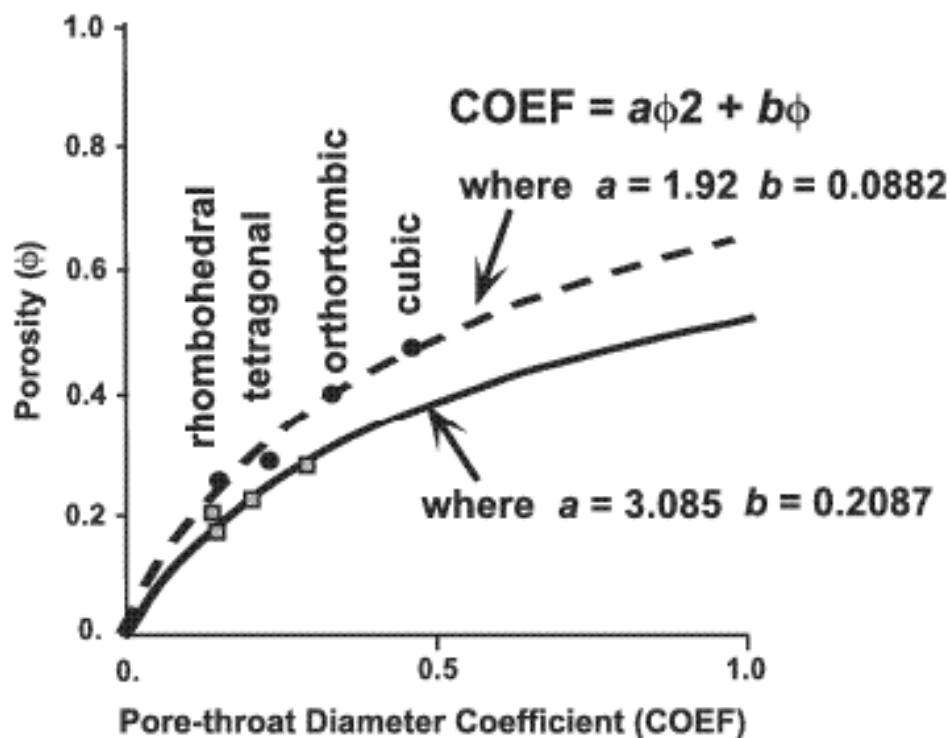


Figure 8. COEF vs. porosity for both the EGM's. The top curve represents the theoretical case using different packing types, equation (16), and the physical experiment, equation (24). (from Sawamura *et al.*, 2005.)

2. The d10 method

This is a method developed by Nordgård Bolås *et al.*, 2005. The aim was to calculate membrane seal capacities. The seal capacities are dependent on the flow paths for hydrocarbon escape through the seal. The flow paths themselves, comprise the largest interconnected pores and the actual hydrocarbon flow will be limited by the sizes of the smallest pore throats in these flow paths. The diameter of these pore throats are referred to as the critical pore throat diameter. Since the transmissibility of a seal is mainly controlled

by the according permeability, and this permeability can be estimated from the mean pore diameter, it has been suggested that a quantitative relationship between these quantities could be derived Amyx *et al.*, 1960. Nordgård Bolås *et al.*, 2005, made an attempt to derive such an equation. Three different data sets from three different authors, Schlömer and Krooss 1997; Yang and Aplin (submitted) and Katsube *et al.*, 1998, were investigated and for each a relationship of the critical pore throat in function of permeability were derived.

The first data set, Schlömer and Krooss, was derived from the Haltenbanken area offshore Norway and from Carboniferous and Permian red claystones of northern Germany. Mercury displacement pressures at approximately 10% pore saturation, of all the samples are presented and defined as “the pressure required to form a continuous filament of nonwetting fluid through the largest interconnected pore throats”, Nordgård Bolås *et al.*, 2005, p 587. These pore throats correspond to the critical pore throats. The following relationship was derived:

$$\text{Log } d_{cS} = 0.3085 * \log K + 3.0103 \quad R^2 = 0.4798. \quad (25)$$

The permeability used in this equation can be calculated with equation (15) or by selection an appropriate equation developed by Drews, 2012.

The second data set by Yang and Aplin (submitted) consist of samples from the North Sea, the Gulf of Mexico and the Caspian Sea. The mean pore throat diameters, 50% percentile and the 10% percentile are presented. Nordgård Bolås *et al.*, 2005 concluded that the d_{10} data should be comparable with the pore throat diameters that were calculated by Schlömer and Krooss.

$$\log d_{cY} = 0.7187 * \log K + 5.5655 \quad R^2 = 0.8970. \quad (26)$$

The last and final data set, by Katsube *et al.*, 1998, was derived from the Venture gas field (offshore Nova Scotia), the Beaufort-Mackenzie Basin and the Western Canada Basin. Here mean pore throat sizes were presented. However these pore sizes are smaller than the critical pore throats and are therefore not comparable to the data of the two above data sets. A conversion of the reported pore sizes was carried out by Nordgård Bolås *et al.*, 2005.

$$\text{Log } d_{cK} = 0.2454 * \log K + 2.6099 \quad R^2 = 0.2934. \quad (27)$$

Finally an integration of all data sets was made. All data was collected in one plot and an new equation was derived.

$$d_{cAll} = 0.4295 * \log K + 3.8013 \quad R^2 = 0.4359. \quad (28)$$

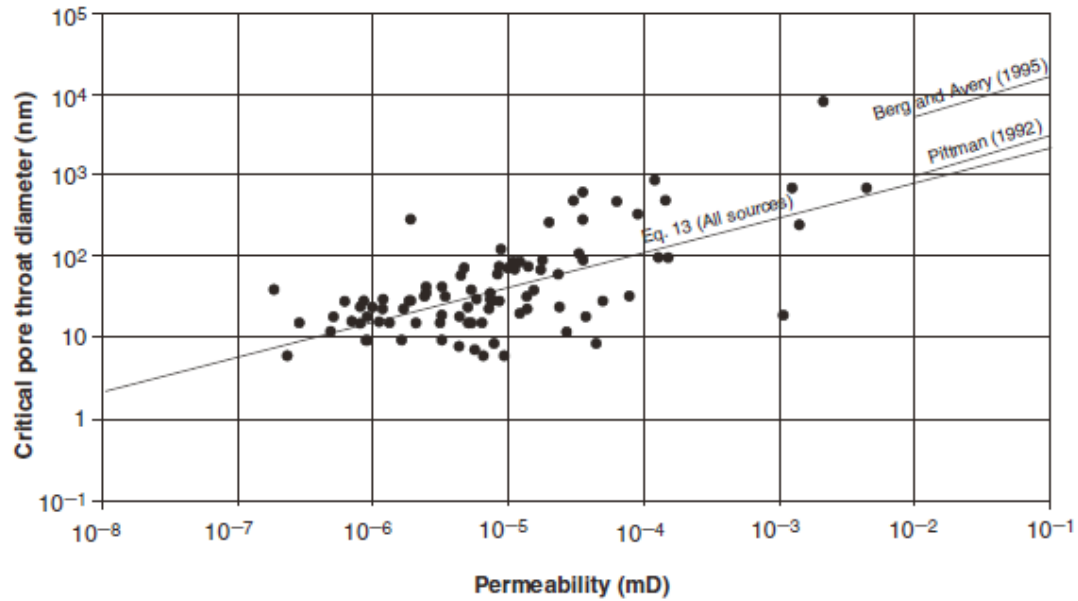


Figure 9. all samples from the combined data sets, Nordgård Bolås *et al.*, 2005.

The next steps are to calculate first interfacial tension, the theoretical capillary pressure, gas density and temperature, see equations (20), (21), (22) and (23).

Finally the seal capacity can be calculated

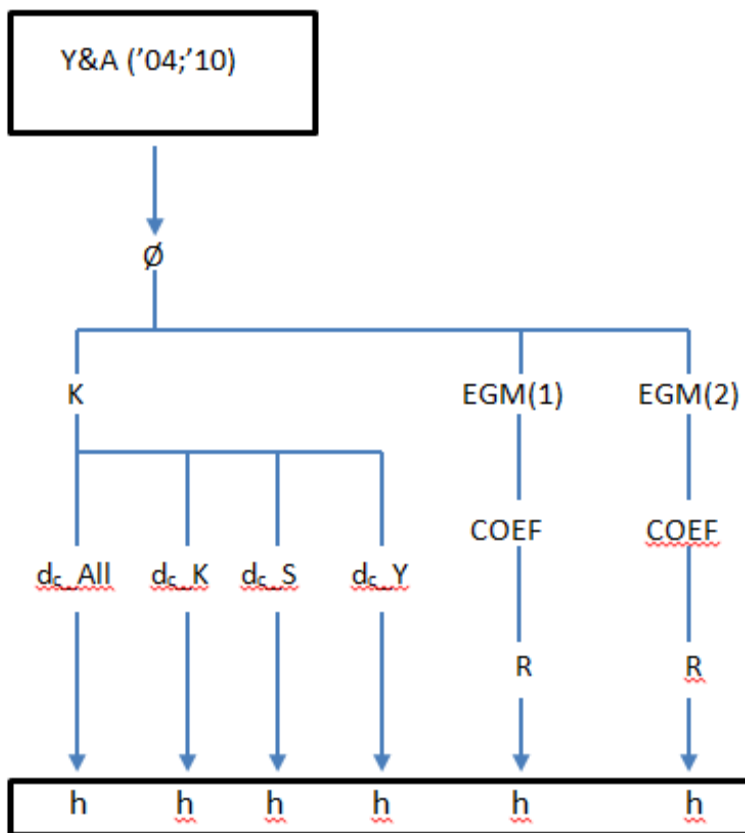
$$h = \frac{4\gamma}{\Delta\rho g d c} \quad (29)$$

Where $\Delta\rho$ is the difference between the water density and the gas density.

A first critical note to keep in mind is that all the above formulae apply for homogenous mudstones. In this research the Rupel Clay Formation is investigated, which strongly resembles the Belgian Boom Clay. This clay is characterized by its strong banded structure found in the alternation of siltier and more clay rich layers, Aertsens *et al.*, 2004. Therefore it would be useful to try and incorporate this heterogeneity in mudstone permeabilities. For this reason the methodology of Drews 2012, was investigated. Secondly, these methods are developed and tested for mud rocks of mainly great depths. For example the data set from Drews, 2012 was based on samples with a depth range of 1500-2500m; the Yang and Aplin data sets, 2004; 2010, are derived of 3 different data sets ranging from 400-3500m; the critical grain size methods has samples from 1000-5000m depth and for both the equivalent grain size methods, the specific depths are not mentioned. Both the data sets used in this research are based mainly on shallow samples.

On the next page, figure 10. gives an overview of the workflow and all the calculations that will be carried out. In total 12 seal capacities will be computed.

Homogeneous



Heterogeneous

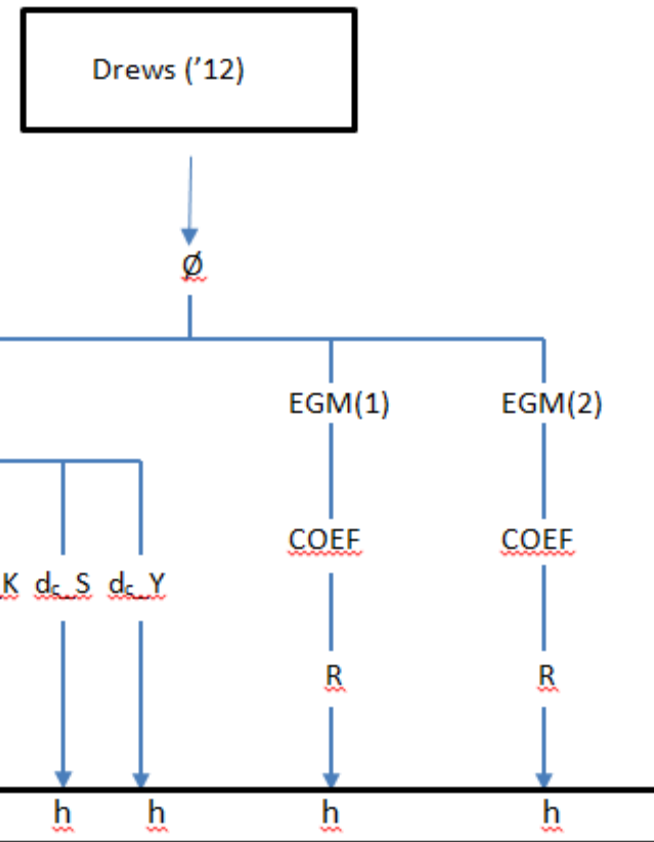
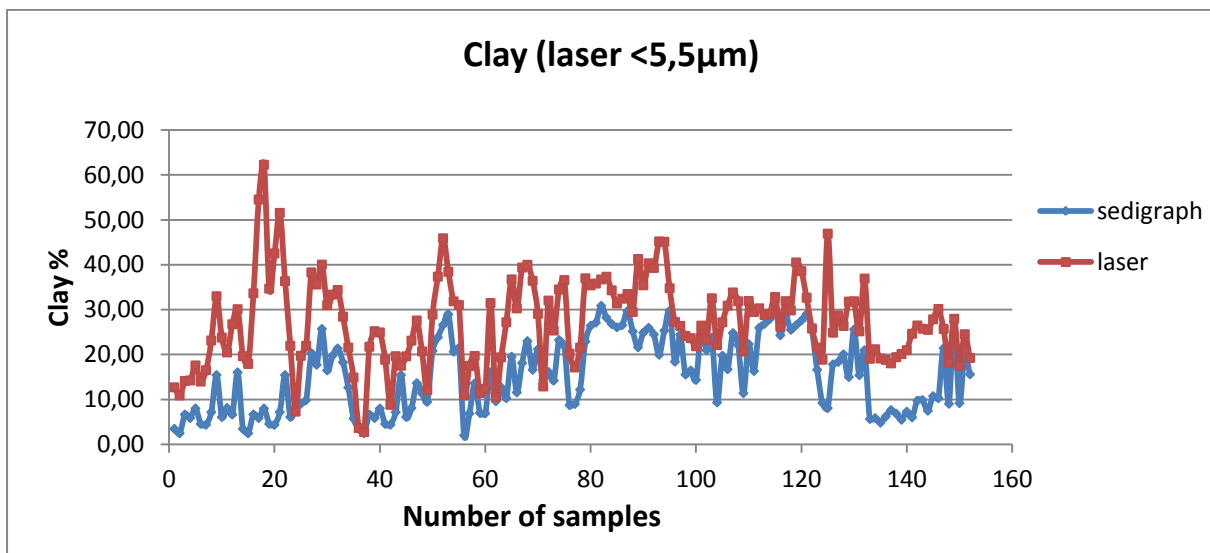
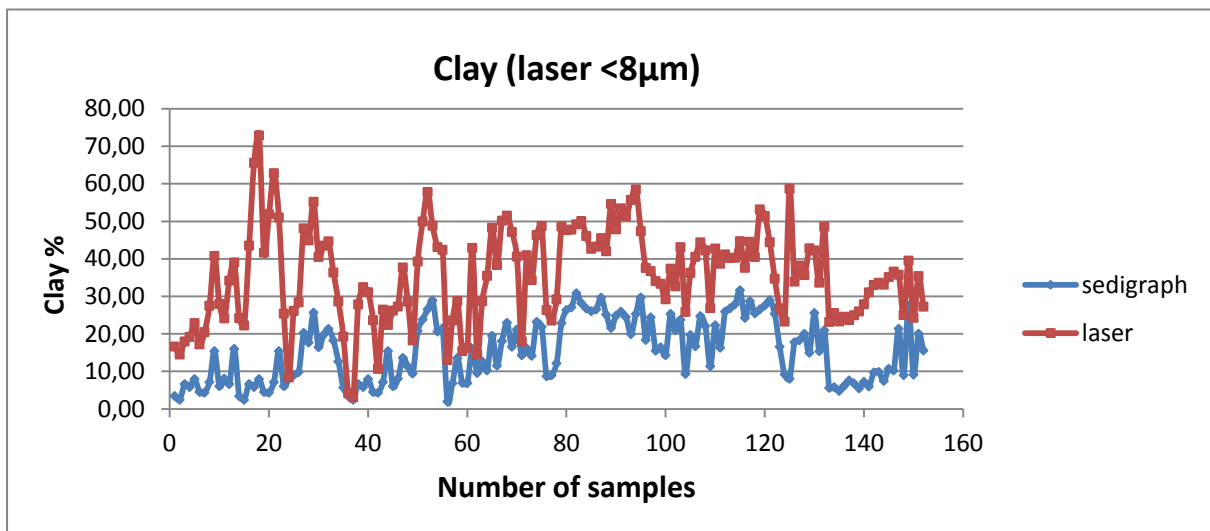


Figure 10. Schematic representation of the workflow and the results that will be obtained

Results

Results Method 1. Comparison of grainsize measurement methods (Laser diffraction vs. sedigraph)

Here data from the Rupel Clay Formation, the first data set is used. In total 146 samples of 17 boreholes is used as calibration. Five different grain sizes, 2, 5, 5.5, 6.5 and 8 μm , for the laser diffraction were plotted against the 2 μm clay fraction of the sedigraph. The best agreement was found for laser diffraction 5 μm vs. sedigraph 2 μm . Below some of the graphs are represented in figure 11., more graphs and input data can be found in Appendix B.



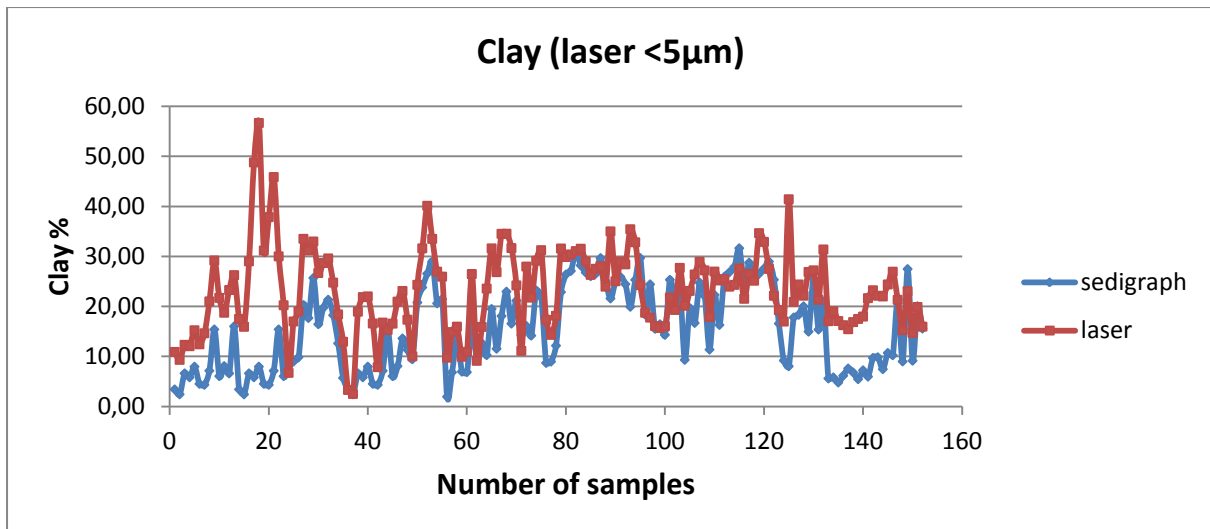


Figure 11. The above graphs represent the sedigraph clay fraction vs. the laser diffraction fraction. The grainsize for the sedigraph is held constant at $<2\ \mu\text{m}$. In the top graph, the grainsize for the laser is set to $<8\ \mu\text{m}$, in the middle graph the laser grainsize corresponds to $<5.5\ \mu\text{m}$ and in the bottom graph the laser grainsize is set to $<5\ \mu\text{m}$.

In the above figure it is clear that for laser $<8\ \mu\text{m}$ vs. sedigraph, the laser overestimates the clay fraction. A better fit is obtained for smaller fractions. The according silt fractions can be found in the appendix B.

Further test were conducted to test the influence of this improved grain size for the laser. Therefore the resulting permeabilities and porosities were compared to the permeabilities and porosities with the standard correlation, i.e. $8\ \mu\text{m}$ for the laser and $2\ \mu\text{m}$ for the sedigraph and the improved correlation. The graphs on the next page, were selected randomly and present a good average for all of the boreholes taken in the Rupel clay Member.

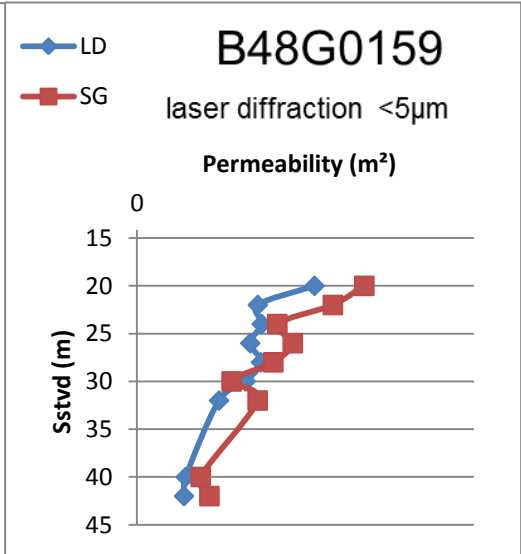
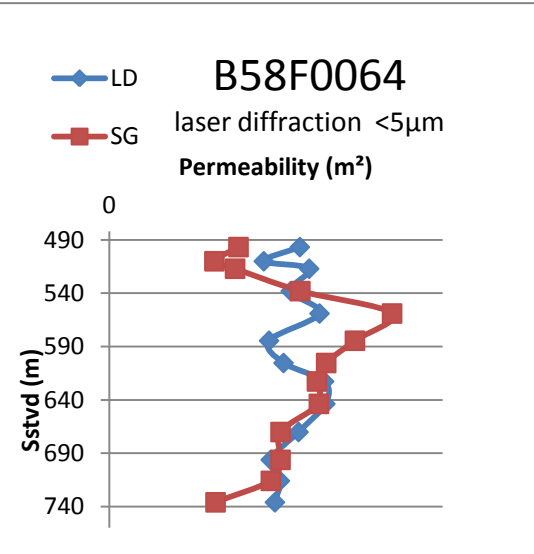
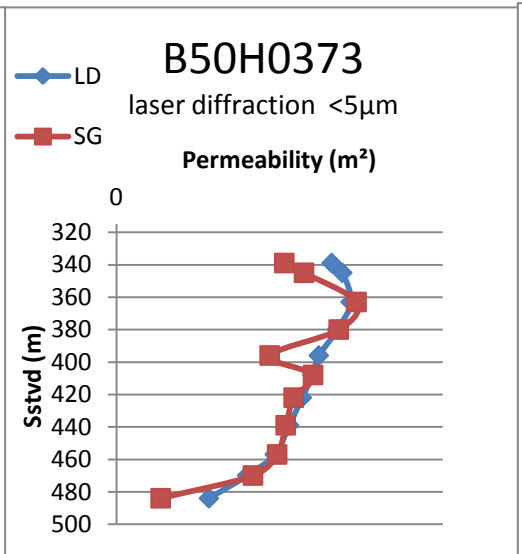
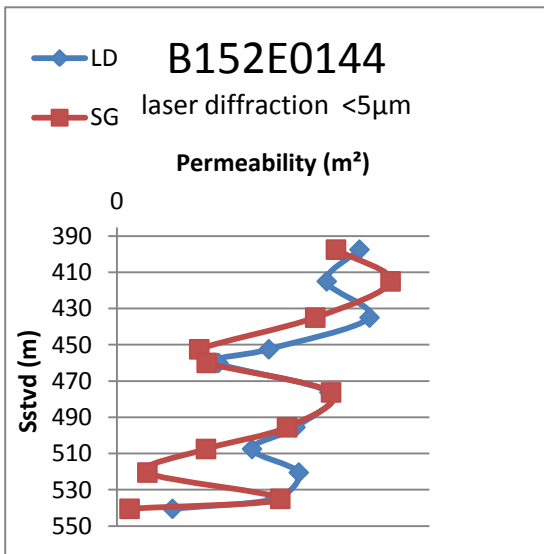
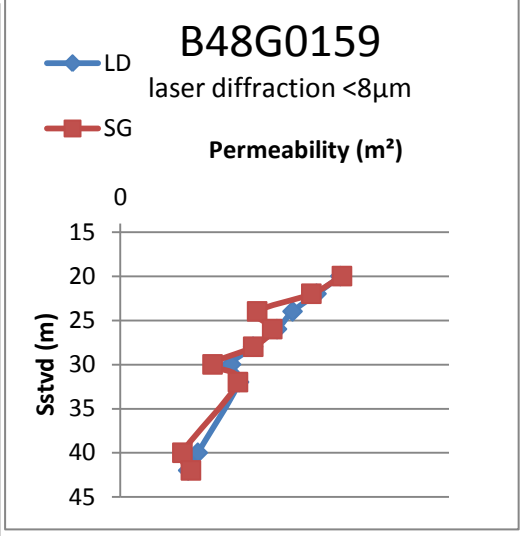
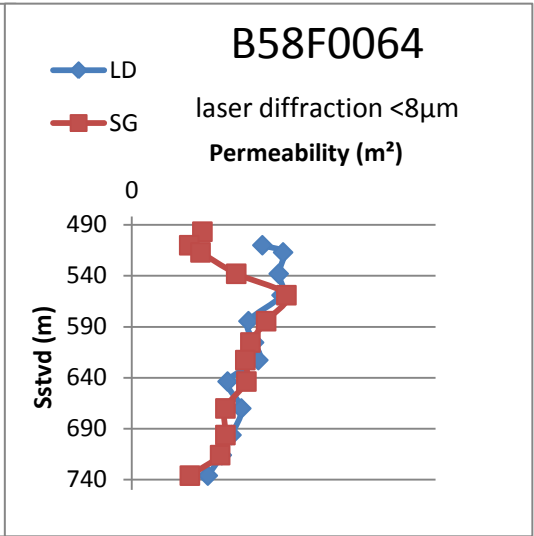
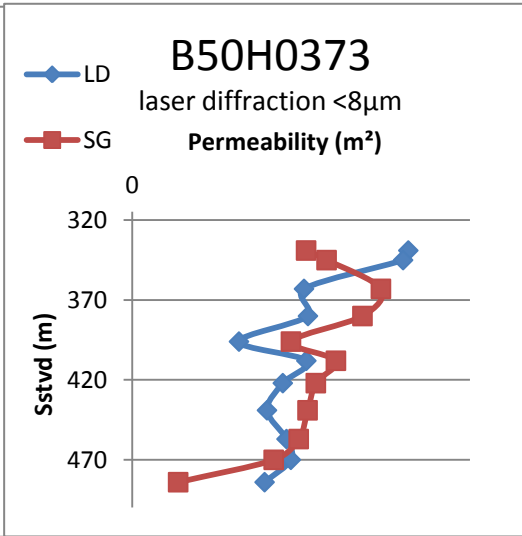
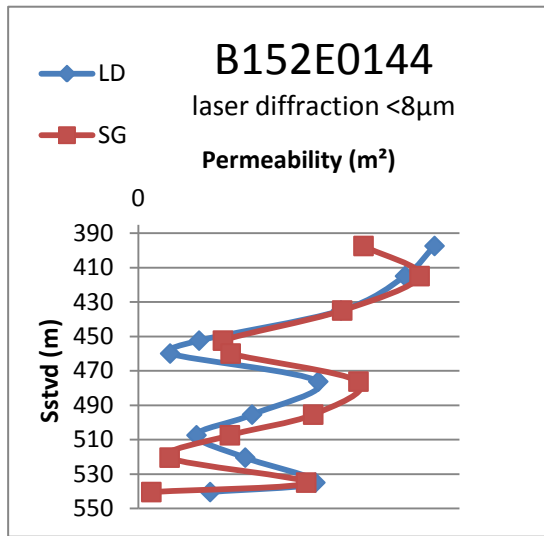


Figure 12. Permeability vs. depth for four random cores. The top graphs are representative for the 8 μm grain size boundary for the sedigraph and the lower graphs are representative for the 5 μm grain size boundary.

In general the permeability decreases with increasing depths, what is to be expected. Also, when comparing the curves, it is observed that only in about 50% of the cases a better fit for permeability is obtained when the grainsize of the laser diffraction is adapted. As mentioned before, these boreholes are chosen to represent the best average. Therefore, some of the boreholes are derived from, when considering figure 11., the parts that show close resemblance, e.g. sample number 85-95, and parts that show deviation, e.g. sample numbers 1-22.

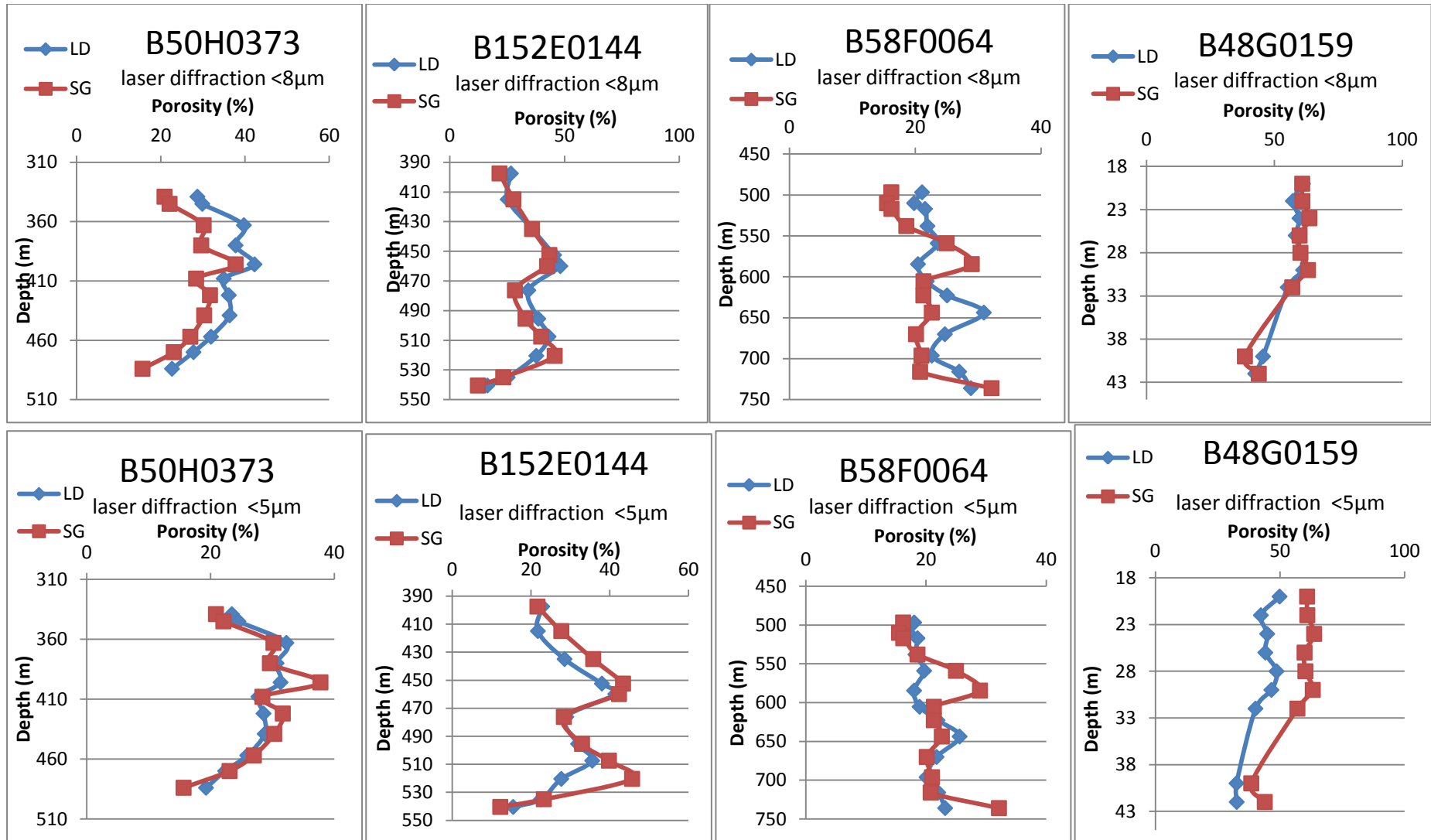


Figure 13. Porosities vs. depth. In the top graphs, the laser diffraction grain size was set at 8 μm , in the bottom graphs on 5 μm .

In the majority of the graphs a decrease in porosity is observed with increasing depth. When comparing the porosities for the different clay fractions, also here it is observed that only in about 50% of the cases a better fit is obtained with the improved grain size correlation.

A further step is to investigate the resulting porosities and permeabilities of all the different clay contents of the laser diffractor with the sedigraph. The table underneath presents an overview of the results.

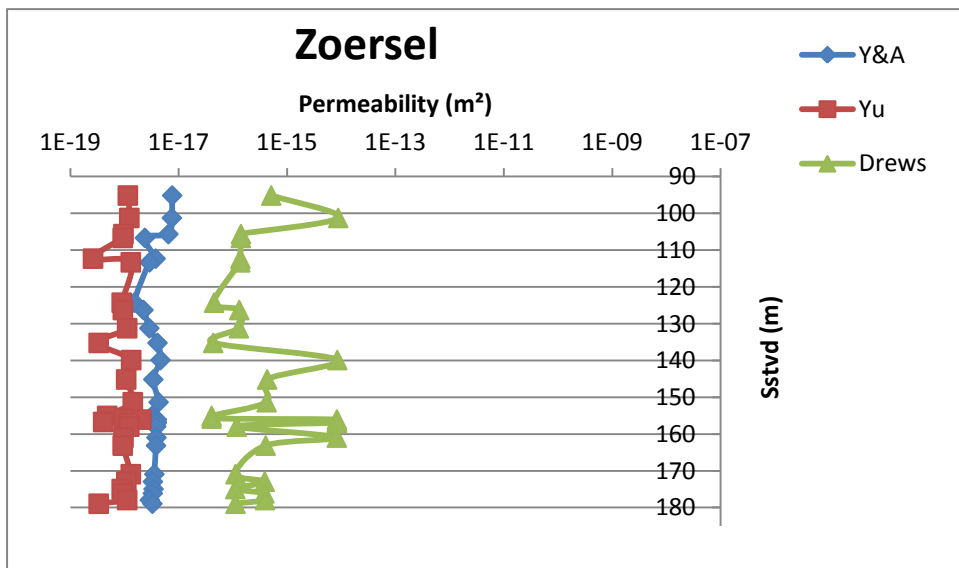
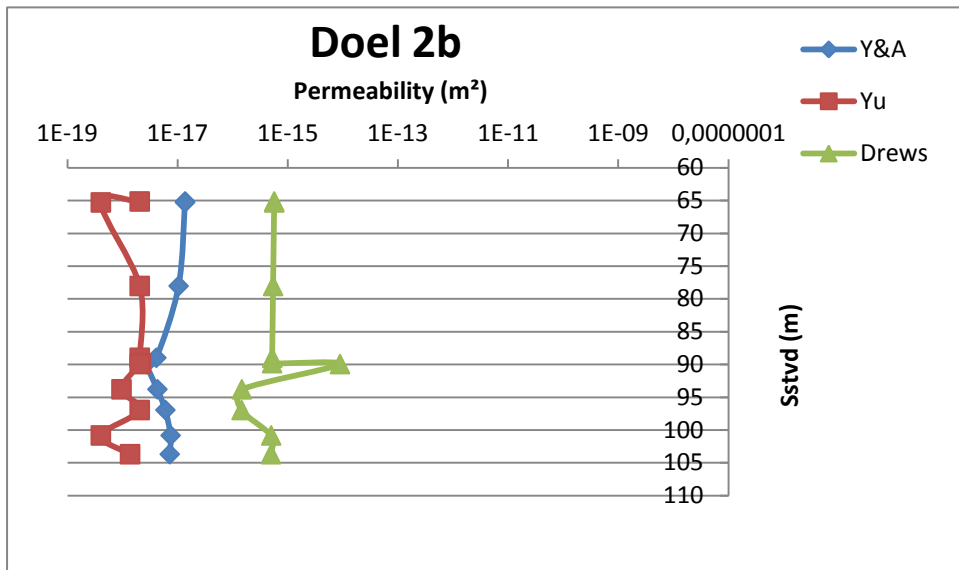
clay content laser diffractor	Difference in porosity	Difference in permeability
2 μm	0,14	2,69E-18
5 μm	0,06	8,02E-19
5,5 μm	0,03	1,89E-19
6,5 μm	0,01	1,11E-19
8 μm	0,007	1,77E-19

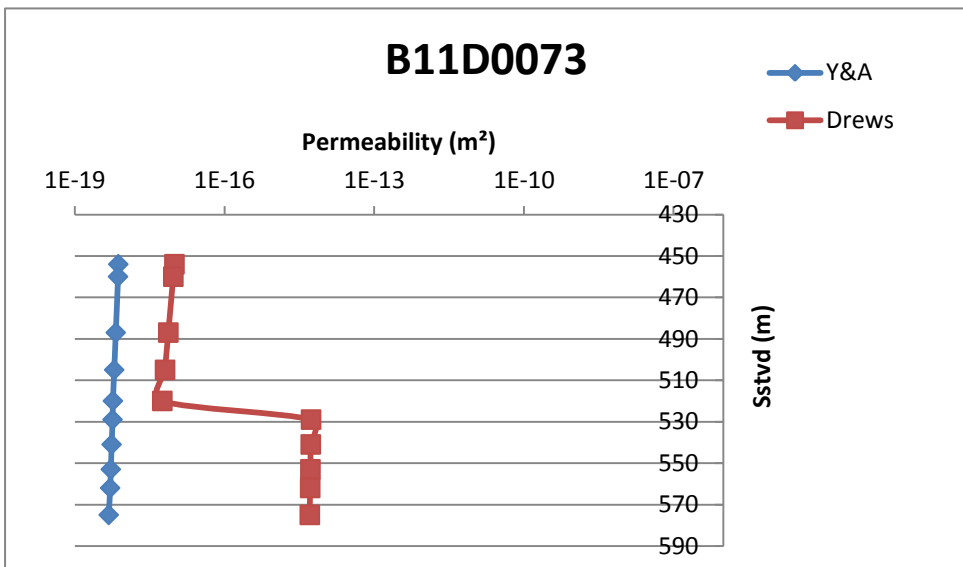
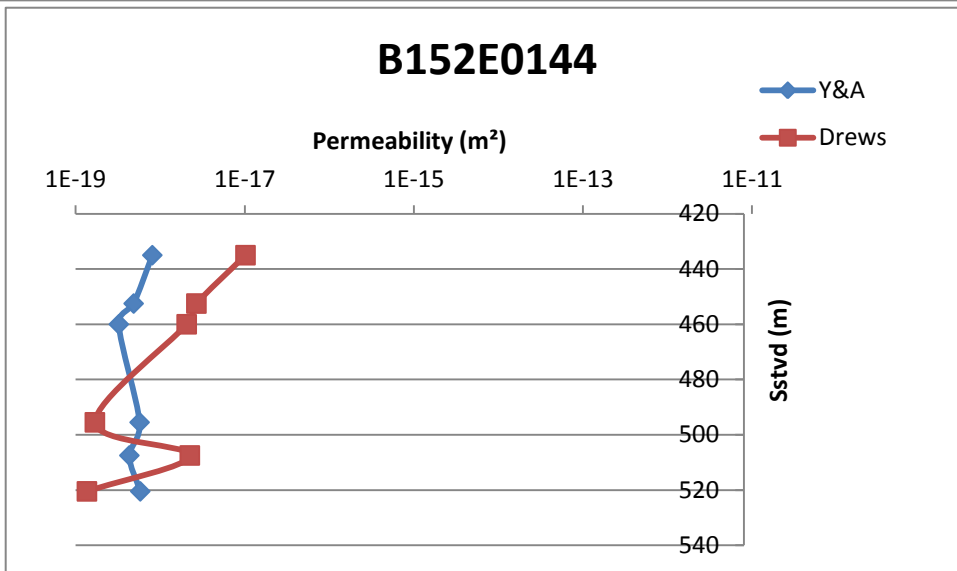
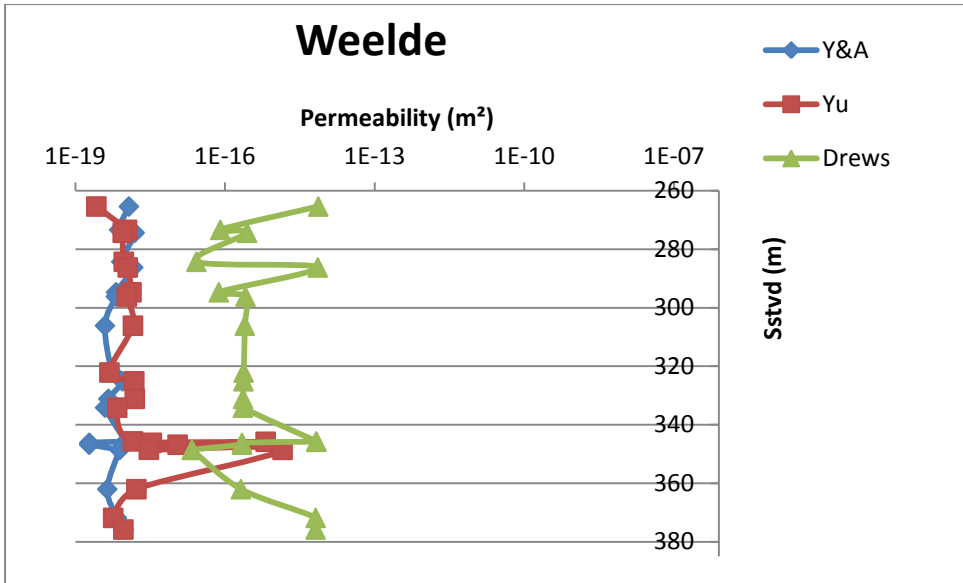
Table 3. Porosity and permeability values of the difference between the according clay fraction of the laser diffractor and the sedigraph.

Results Method 2 for homogeneous mudrocks (Yang & Aplin) + method 3 for heterogeneous mudrocks (Drews).

Porosity- effective stress and porosity-permeability calculations

In order to evaluate both methods, permeability values from the Boom Clay in Belgium and the Rupel Clay formation are used to compare the permeability values according to both methods. Hydraulic conductivity investigations have been carried out for over 30 years and Yu *et al.*, 2011, have integrated the results in a synthesis of this research. Several boreholes were presented with the measured hydraulic conductivities at certain depths. To integrate the results in this research, the hydraulic conductivities were converted to permeability. For the conversion method, and the resulting permeabilities, see appendix C.





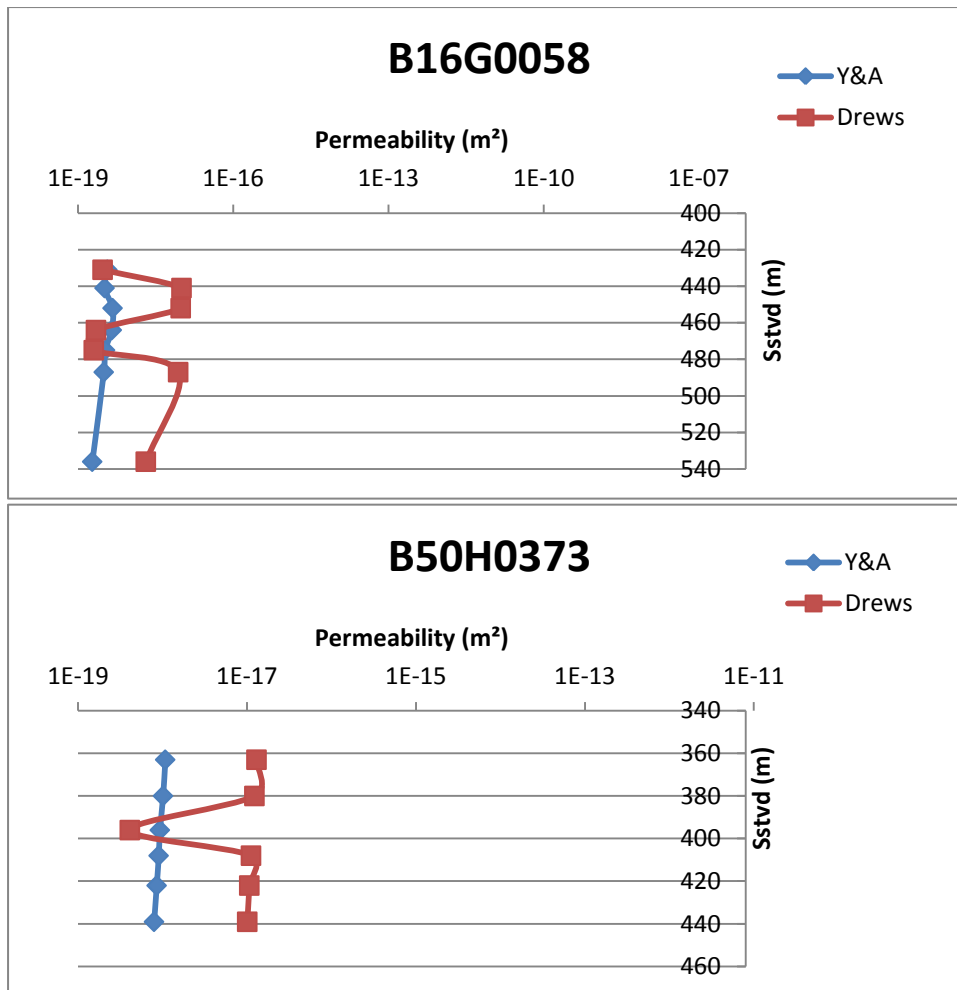


Figure 14. Permeability data from four boreholes in the Belgian Boom Clay and four boreholes from the Rupel Clay Member. In each plot the permeability values vs. depth for the three or two different methods are presented. Y&A stands for the integration of Yang and Aplin's formulas (method 2.).

First of all it should be mentioned that the results from Yu *et al.*, 2011 are measured values and are used in this research as calibration values. Therefore these values should be considered as the most correct values. From the above graphs of the Boom Clay (Zoersel, Weelde and Doel), the permeability values for Y&A and Yu *et al.*, 2011 are more consistent than the values for Y&A and Drews, 2012 or Yu *et al.*, 2011 and Drews, 2011 respectively. Yu *et al.*, 2011 obtains the smallest permeability values, while Drews, 2011 obtains the highest. The widest range in permeability values is observed in the data by Drews, 2012, followed by Yu *et al.*, 2011. Y&A, displays a very narrow range in permeability values.

For the graphs from the Rupel Clay formation (B152E0144; B50H0373; B11D0073 and B16G0058), the permeability values of both methods differ in extreme cases 5 orders in magnitude. The permeabilities by Y&A show a distinct trend of decreasing permeabilities with increasing depth, as expected. While the permeability values by Drews, 2012, change more abruptly with increasing depth.

Results Method 4. Sampling, new grain size analysis, new calculations and calibration

54 samples, of the shallow gas fields offshore northern Netherlands, were collected and analyzed with the laser diffractor. In Appendix D an overview is given of the samples that were incorporated and excluded from this research. Appendix F Provides an overview of the results of the grain size analysis. Most calculations were carried out with samples that contained a sand fraction of less than 10%. When applying this criteria, the total number of samples is 25. Samples with a sand fraction ranging between 10-25% were preferentially not incorporated, although exceptions were made for:

	Depth (mTVDss)	Sand fraction	Comments
A12-03	452m	12.3%	
	650m	11.2%	
B16-01	417m	47.7%	clay fraction: 50.6%
	463m	14.2%	

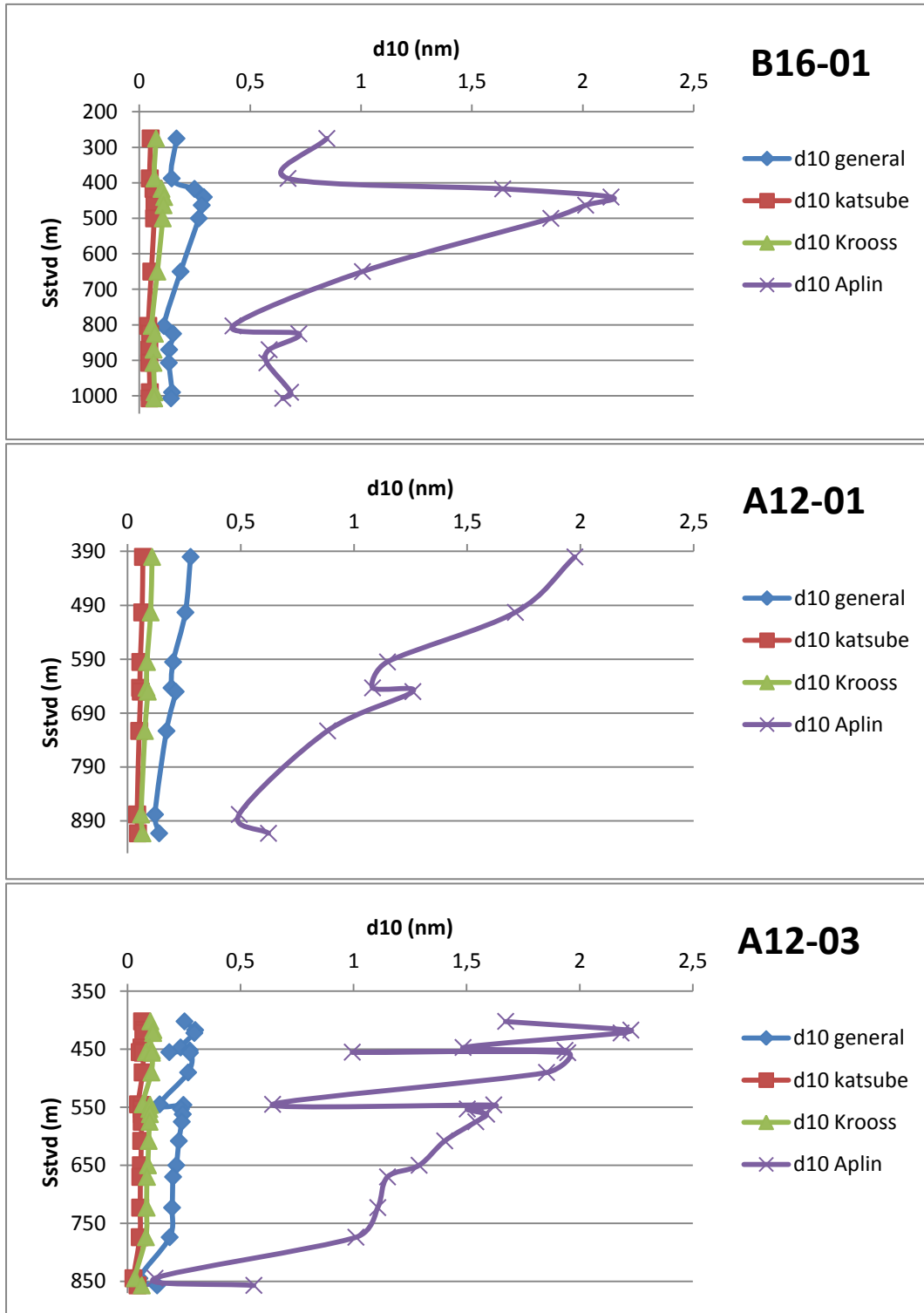
Table 4. Exceptions included in the calibration data.

All samples are situated above (stacked) gas accumulations or NPHI-RHOB cross-overs. Information about the NPHI-RHOB cross-overs was used to calibrate the resulting seal capacities (m). Also depth contour maps of top reservoir and GWC were used to calibrate the computed seal capacities.

Results Method 5. Calculation of pore throat and capillary seal capacity

1. d10 method

Samples from the 3rd data set, the gas fields offshore northern Netherlands, are implemented in the workflow and the d10 values of the different methods are plotted and compared.



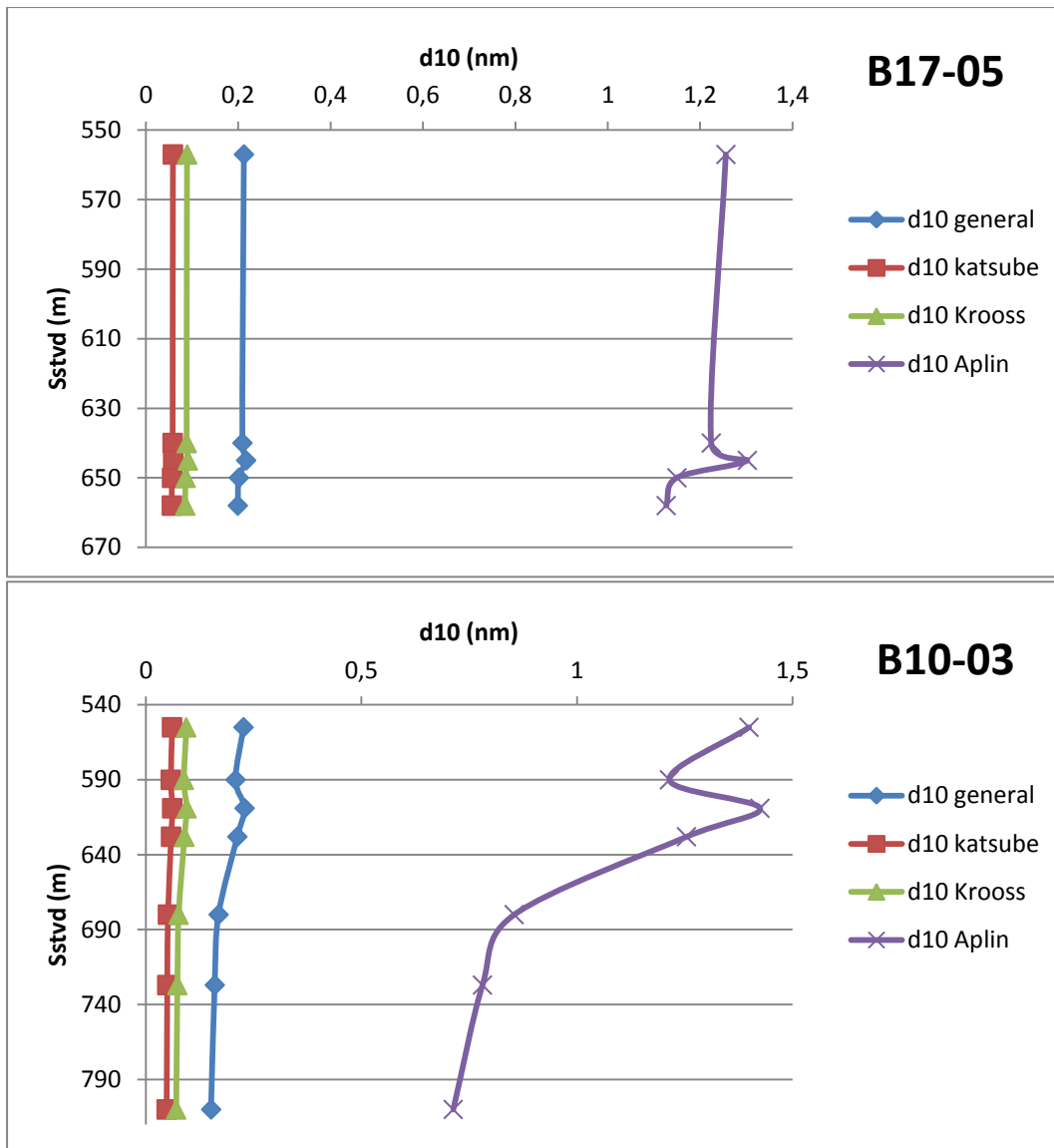
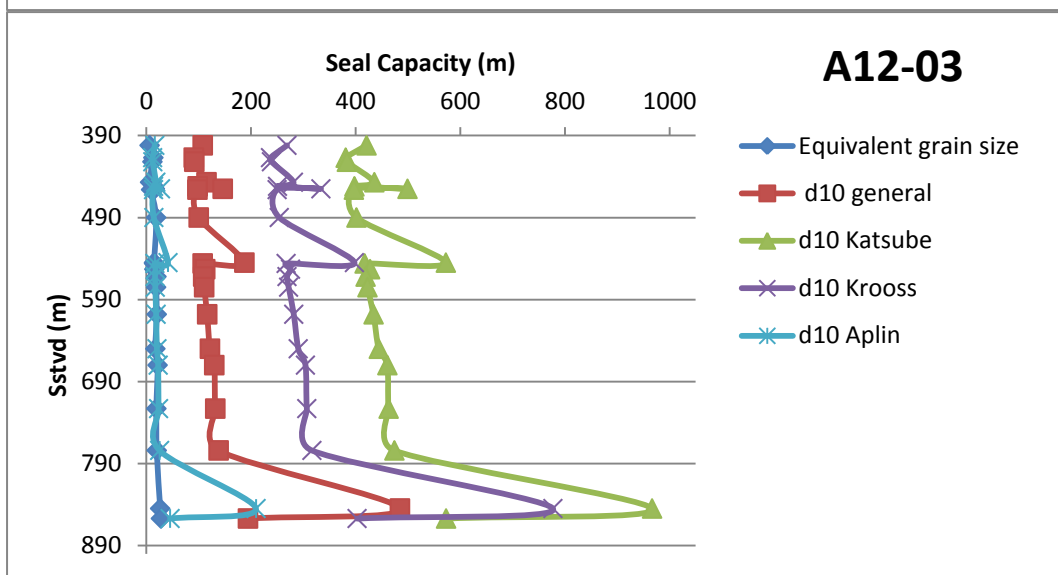
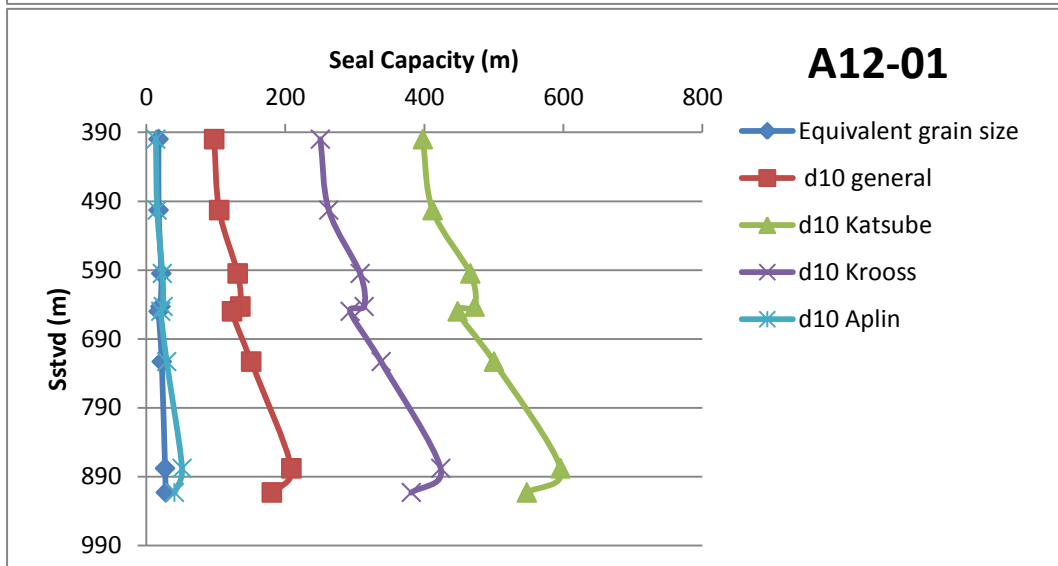
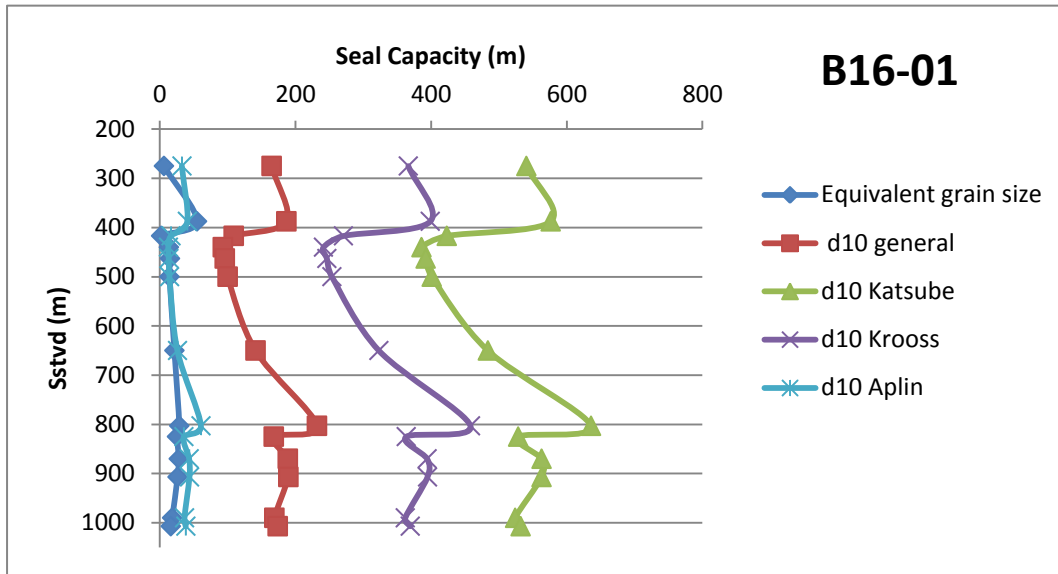


Figure 15. Depth vs. critical grain size for all d_{10} methods.

It is clear that the data from Katsube and the data from Schlömer show the best correlation and display the same trend. The data from the d_{10_All} , also displays the subtle trends observed in the two previous discussed data sets, albeit with more variability. The values are in general 1.3 times larger when compared to the values of the two previous data sets. The data from Aplin shows the widest variability, however the subtle trends observed in the other data set are also observed in this data set. The values of this data set are in general 1.5-3 times larger than the other data set values. In general, the critical grain size diameter becomes smaller with increasing depth.

2. Seal Capacity, d10 methods and equivalent grain size method



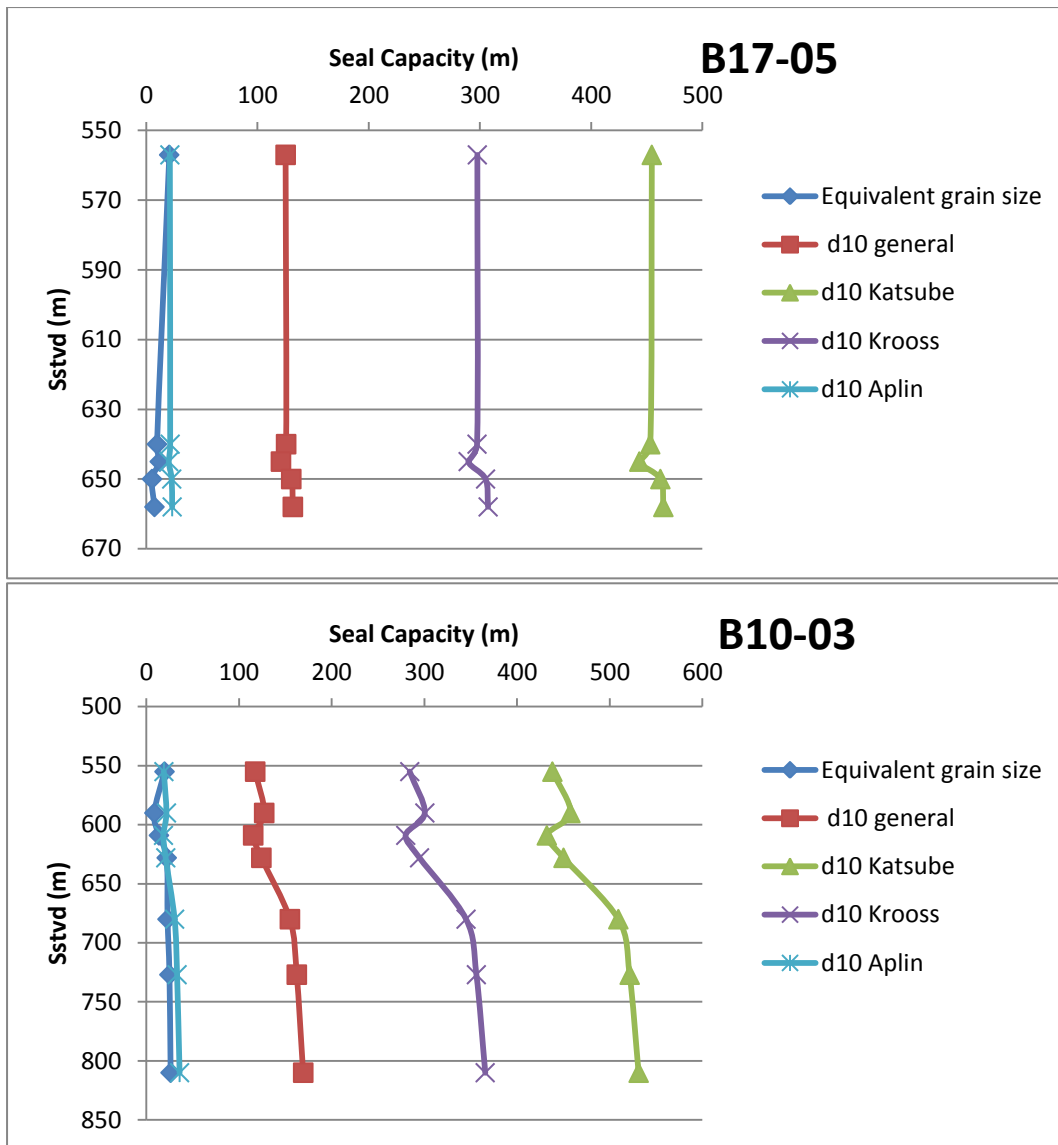


Figure 16. All seal capacities vs. depth for all the different methods.

Two major features are visible on the above graphs. The first is that the data from Katsube, Schlömer and the d10_All seal capacity, show the same trend and they are approximately at the same spacing from each other. The data from Katsube displays the widest variability. The second feature is that the equivalent grain size seal capacity and the data from Aplin, are consistent. The data from Aplin does follow the same trend as the other 3 methods.

Overall it is visible that the seal capacity increases with increasing depth, as is to be expected.

Appendix G gives an overview of the computed porosity, permeability, pore throat diameter and the seal capacities for d10_Aplin and EGM1_D.

Discussion

An overall remark regarding the grain size boundary is that the use of 2 μm as representative grain size for clay minerals is somewhat arbitrary. Many clay minerals are actually larger than 2 μm , and other non-clay minerals are smaller than 2 μm (Casey *et al.*, 2013).

Method 1. Laser diffraction vs. sedigraph

For this specific data set the preferred grain size for the laser diffraction was set to 5 μm . It is not a perfect fit but it is definitely an improvement when compared to the curve of the clay fraction of 8 μm for the laser diffraction. This fit differs somewhat of the fit found by Ramaswamy and Rao, 2006. An explanation could be found in the sampling area. Their sample set was obtained in the Northern Andaman Sea, which differs from the tectonic and geologic setting of the samples obtained in this research. It is likely that the best fit will be depended on the data set itself.

For the clay fraction 5 μm represents the best fit. For the silt fraction, the best fit is obtained for 8-62.5 μm . When the whole sample is taken into account, the best fit is when the clay fraction is <5.5 μm .

The graphs of the cores represented in the results part were carefully selected to represent an objective average of the general trend observed in the graphs. With the further test carried out concerning the permeabilities and porosities, it seems that in a small majority of the cases a better fit is obtained with the 5 μm grain size boundary.

To evaluate the method by Drews, a closer look was taken at the porosities computed in the synthesis research and the porosities obtained by Drews.

Boreholes	Average porosity by Yu et al., 2011(%)	Average porosity by Drews, 2012 (%)
Zoersel	40.5	42.4
Weelde	40.5	39.7
Doel	42.3	42.5

Table 5. Overview of the porosities of the boreholes derived from the Belgian Boom clay.

The results in table 5. are, for both methods, an average for the entire borehole. The values by Yu *et al.*, 2011, are measured values and are considered most correct. Therefore it seems that the porosities by Drews, 2012, are fairly comparable to the porosity values computed by Yu *et al.*,2011.

Method 2. And 3.

A first general remark is that for all the calculations of the effective stress a constant value is used for all depths. In reality this is not the case therefore are the values of the effective stresses more an approximation than an accurate value.

Approximately half of the permeability results obtained with Y&A seem to correspond reasonably to the permeability values combined by Yu *et al.*, 2011. In half of the cases, an underestimation of 1-2 orders is made. In Yu *et al.*, 2011 hydraulic conductivity values are presented and correlated to certain depths. The values of the hydraulic conductivity are a result of a synthesis of different researches with different methods, e.g. in situ and laboratory experiments, borehole measurements and indirect derivation from secondary data. So, seen that the permeability values in this report from Yu *et al.*, 2011 are actually a synthesis of different measurement techniques, it is possible that with the combination of all these results the specific errors were not taken into account. Also, with the conversion of hydraulic conductivity to permeability, the possible error margins were not taken into account. These reasons could explain why this discrepancy between the two results is observed.

When comparing the permeability results for all three methods, it is clear that the variability in permeability values for both Y&A and Yu *et al.*, 2011 is more smooth when compared to the range in permeability values obtained by Drews, 2012. This difference could be explained by the fact that for Drews, 2012, for every depth a distinct mud content is measured and the calculation of the permeabilities is carried out based on this distinct mud content. This, in order to include the heterogeneity in the mud interval. From the research carried out in Belgium, it is clear that the Boom clay displays banded layers, with different mud contents. The other two methods do not take heterogeneity into account and therefore the same relationships and equations are used for the whole mud interval. It is therefore possible that slight changes in mud content will go unnoticed.

Another feature is that the method of Drews, 2012 results in the highest permeability values. This could be a result of the cohesive fraction on which all the equations are based. In this methodology, grain sizes <10 µm are incorporated. This exceeds the clay fraction and includes also fine silt. While in the other calculations, for Yu *et al.*, 2011 a 2 µm grain size is taken into account, and for Y&A, 2012 a 5.5 µm grain size is considered. Incorporation larger grain sizes could lead to higher permeabilities. One more interesting feature of this method is, when reviewing figure 14., all the same clay fraction give a specific range of permeabilities. For 50% clay, all permeability values are situated in between $1-8 \cdot 10^{-15}$; for 60% clay, permeability values range between $2-5 \cdot 10^{-16}$; for 70% clay, permeabilities range between $1 \cdot 10^{-16}$ and $8 \cdot 10^{-17}$; and finally for 80% clay, the range is $2-4 \cdot 10^{-17}$. With increasing depth the permeability values become smaller as expected. So for a given grain size only a certain range of permeability values is to be expected, with the lowest permeability values for the lowest clay contents.

Moreover, the method of Drews is based on several equations all for a specific mud content. When a closer look is taken at these relationships, only small differences are noticeable.

$$\begin{array}{l} 7.86e+000\phi^2 + 8.11e+000\phi - 2.09e+001 \\ \hline 6.80e+000\phi^2 + 7.67e+000\phi - 2.12e+001 \\ \hline 6.85e+000\phi^2 + 7.33e+000\phi - 2.13e+001 \\ \hline 4.91e+000\phi^2 + 7.09e+000\phi - 2.14e+001 \\ \hline 4.20e+000\phi^2 + 6.83e+000\phi - 2.14e+001 \\ \hline 3.82e+000\phi^2 + 6.58e+000\phi - 2.14e+001 \end{array}$$

Figure 17. Snapshot of some of the equations, Drews, 2012. The equations are for ascending mud contents, from 50% to 100%.

All these equations are of the same order and sometimes only differ in the first number behind the comma, while the mud content doubles going from the top equation to the bottom equation, figure 17.

Lastly it is important to keep in mind that the relationships developed by Drews, 2012 are for cm-scale samples. This implies that the smaller scale porosity and permeability distributions, as in this research, could be improved.

Method 5. Alternative pore throat calculations

2. The d10 method

2.1. The Schlömer and Krooss, 1997 data set

In the paper by Schlömer and Krooss, Jurassic shales, mudrocks and red Carboniferous and Permian claystones were used in a study to investigate the hydrocarbon sealing efficiency of clastic sediments. Mercury porosimetry injection was applied in order to obtain permeabilities, porosities, HG displacement pressures, etc. This data set is based on principles precedently laid out by Schowalter (1979), who used the value of capillary pressure at mercury saturation of 10% as an estimate for the displacement pressure. Nordgård Bolås *et al.*, 2005, used this specific displacement pressure to calculate the critical pore throats and defined it as follows “*The displacement pressure is defined as the pressure required to form a continuous filament on nonwetting fluid through the largest interconnected pore throats of the rock. The pore throats corresponding to the displacement pressure are therefore equal to the critical pore throat diameter.*”, Nordgård Bolås *et al.*, 2005, p. 587.

The equation obtained by Nordgård Bolås *et al.*, 2005, was based on all the 27 samples presented by Schlömer and Krooss. When this data was investigated, it seemed that for some of the results not all the necessary information could be computed. This was also noted as n.m. in the tables or as an estimate, e.g. < 0.1. Nordgård Bolås *et al.*, 2005 did not state that this data was (not) included into the calculations of the dc.

More importantly, when recalculations were made of the calculations, the same equations were not obtained.

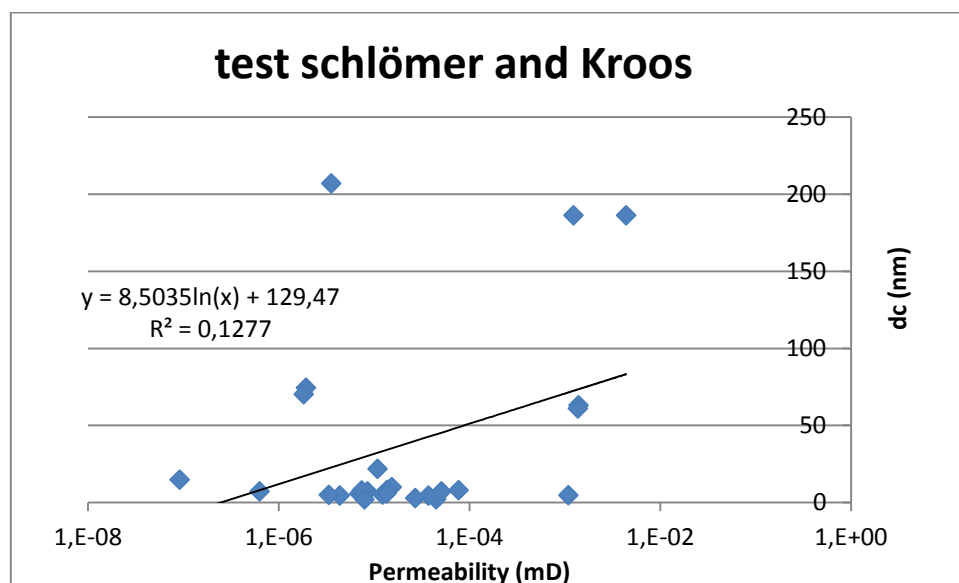


Figure 18. Re-calculations based on data from Nordgård Bolås *et al.*, 2005.

The obtained regression line and according coefficient of correlation are

$$d_c = 8,5035\ln(K) + 129,47 \quad R^2 = 0,1277,$$

which remarkably differs from the equation by Nordgård Bolås *et al.*, 2005, even when the conversion was made from log base 10 to natural logarithm.

$$\text{Log } d_c S = 0.3085 * \text{Log } K + 3.0103 \quad R^2 = 0.4798.$$

Several regression lines were created, some including the results with estimates and not measurable results, others without. In not one of those cases a regression line was obtained that was similar or slightly similar with respect to the regression line obtained by Nordgård Bolås *et al.*, 2005.

Another remark is that the coefficient of correlation is rather low, $R^2 = 0.4798$, which implicates that this method is probably not too accurate.

2.2. The Yang and Aplin data set.

This data set was submitted by Yang and Aplin, but no references towards this data set were noted in Nordgård Bolås *et al.*, 2005. This makes it hard to verify the data or to replicate them. Also, the assumptions made by Yang and Aplin are not stated. Nordgård Bolås *et al.*, 2005, p 588, did state the following “the d_{10} data should be directly comparable with the pore throat diameters that were calculated from the displacement pressures provided by Schlömer and Krooss, as the d_{10} data should provide close approximations of the critical diameters of the samples.” The obtained equation has a rather acceptable correlation coefficient,

$$\text{Log } d_c Y = 0.7187 * \log K + 5.5655 \quad R^2 = 0.8970.$$

In spite of not being able to verify this data set, the obtained correlation coefficient is much better when compared to all the other data sets and the combined data set.

2.3. The Katsube *et al.*, data set

In this paper 22 samples of shales are presented. The critical pore size is not presented in this paper, instead a mean pore size is given. These pore sizes cannot directly be compared to the critical pore throat sizes presented by Schlömer and Krooss and Yang and Aplin. Therefore Nordgård Bolås *et al.*, 2005, made a conversion of the data set. For this, data from Yang and Aplin, submitted, was used, who presented the critical grain size and the mean pore size. Nordgård Bolås *et al.*, 2005, plotted these different pore sizes against each other and calculated the regression line, see figure 19. Based on this regression line a conversion was made for the mean pore throat sizes to critical pore throat sizes. Based on these new values another regression line and correlation coefficient were computed.

$$\log d_c K = 0.2454 * \log K + 2.6099 \quad R^2 = 0.2934.$$

General remarks are that for the conversion, no error estimates are given; the data set of Yang and Aplin, submitted, cannot be found; the correlation coefficient is quite poor. Therefore this equation to calculate critical pore throats, should better not be used.

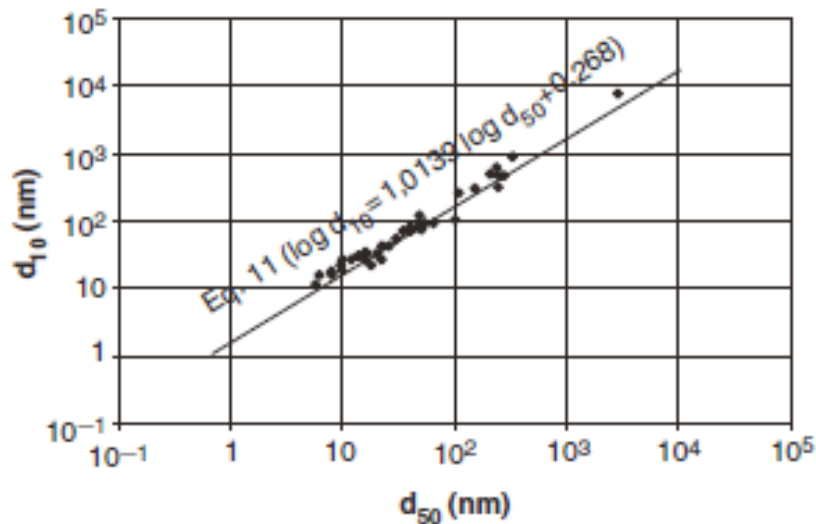


Figure 19. d10 and d50 data from Yang and Aplin, submitted, Nordgård Bolås *et al.*, 2005.

2.4. All data sets combined

Nordgård Bolås *et al.*, 2005, combined all data sets and plotted the permeabilities against critical pore throats, again a regression line and correlation coefficient were computed.

$$\text{Log } d_{cAll} = 0.4295 * \log K + 3.8013 \quad R^2 = 0.4359.$$

When reviewing all the remarks on the individual data sets, this correlation is based on many assumptions, approximations and conversions of data sets. The correlation coefficient is again rather low. Therefore, equation should better not be used to calculate critical pore throat-diameters.

2.5. Comparison d10 graphs

When Figure 15. is investigated, the wide variability observed in the Yang and Aplin d10 values and the more subtle variation in the other curves, can easily be explained by reviewing the equations.

$$\log d_{cY} = 0.7187 * \log K + 5.5655$$

$$d_{cAll} = 0.4295 * \log K + 3.8013$$

$$\text{Log } d_{cS} = 0.3085 * \log K + 3.0103$$

$$\text{Log } d_{cK} = 0.2454 * \log K + 2.6099$$

The coefficients of the Yang and Aplin equation are the largest, therefore are the obtained d10 values also the largest. When reviewing the graphs, the curves are in successive order,

with the Katsube curve displaying the smallest d_{10} values and the Yang and Aplin curve displaying the largest d_{10} values.

When a closer look is taken at the actual critical pore throat diameters, the average size values differ quite a bit.

method	Average pore throat diameter (nm)
d10_Katsube	0.06
d10_Krooss	0.08
d10_All	0.2
d10_Aplin	1.2

Table 6 . Overview of the average d10_pore throat values.

The obtained results with methods d10_Katsube and –Kroos, are quite small. Reported pore throat values for mudstones or shales, by Cranganu *et al.*, 2009, range between 0.042-0.88 μ m (diameter), and by Milliken *et al.*, 2012 range between 5.2-8.6 nm (diameter). Cranganu, used a mercury saturation of 35% to calculate the pore throats. Schlömer and Krooss, used a mercury saturation of 10%. That makes this results not directly comparable but it gives an indication that the calculation of the pore throats with this d10 method renders too small pore throat diameters. The critical pore throats calculated by d10_Aplin, results in more credible diameters.

2.6. Comparison seal capacity graphs

When reviewing Figure 16, it is clear that certain methods overestimate the seal capacity. In this part of the North Sea, especially for the shallow gas fields, where gas is trapped in subtle structures, gas columns usually range between 10-45m, EBN 2013. Therefore methods d10_Katsube, d10_Kroos and d10_general should be discarded. Methods that do give promising results are d10_Aplin and EGM1. These two curves are approximately similar and differences in results differ less than one order, except for one measurement.

2.7. Evaluation of the different methods

A12-03

Well A12-03 is part of shallow gas field A12-FA, together with well A12-01. These wells cut through several stacked bright spots. The structure is not fault bounded and the bright spots are classified as 4 way dip closure bright spots. Seal capacities were derived for the following depths (in mTVDs) 402m; 452m; 546m; 562m; 608m and 650m. The according calculated gas columns range from a couple mm to over 460m. On the next page an overview will be given of the different methods and according gas columns. The NPHI-RHOB cross over is determined from the well log, the GWC-top well or GWC-top trap is determined from depth contour maps, when available, from nlog.nl. See Appendix E for the contour maps in more details.

Well A12-03 does not cut through the top of the reservoir, therefore are the observed NPHI-RHOB cross-overs not corresponding to the maximal seal capacity of the mudstone. It is estimated that the maximal seal capacity according to the cross-section, see figure 20., would be 3/2 if the total gas column.

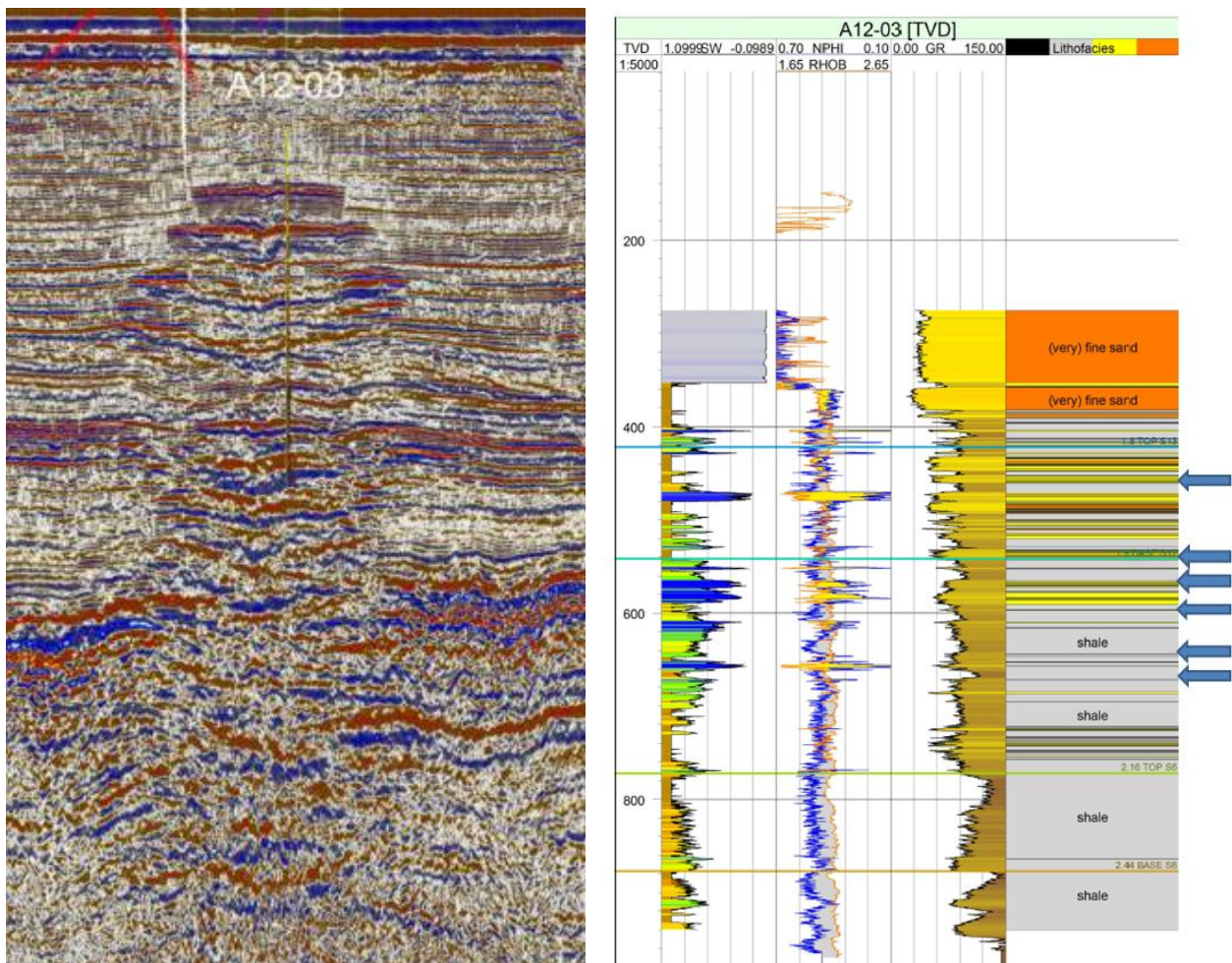


Figure 20. Left: seismic section showing the location of well A12-03 cutting through stacked bright spots. Right: Interpreted log, with lithology, NPHI-RHOB cross over and gas accumulations. Arrows indicate the location of the mudstone samples.

A12-03		Seal capacity (m)														
Seal depth (mTVDss)	Sample depth (mTVDss)	EGM1	EGM2	d10_All	d_10Katsube	d_10 Schlömer	d_10 Aplin	EGM1_D	EGM2_D	d10_D_All	d10_D_Katsube	d10_D_Schlömer	d10_D_Aplin	NPHI_RHOB cross over (m)	GWC-Top well (m)	GWC-top trap (m)
456	452	14,5	10.3	98.2	397.8	250.8	14	/	/	/	/	/	/	4	/	/
553	546	14.9	10.5	107.8	417.3	267.2	16.5	/	/	/	/	/	/	8	25	29
566	562	19.4	13.4	108.8	419.1	268.9	16.7	/	/	/	/	/	/	18	21	25
612	608	20.0	13.7	116.4	434.4	281.7	18.8	/	/	/	/	/	/	13	20	29
655	650	17.4	12.0	121.7	444.4	290.3	20.4	/	/	/	/	/	/	15	/	/
671	670	21.6	14.8	129.9	460.8	304.1	22.8	17.4	11.8	2.6	49.4	18.4	0.03	6	/	/

Table 7. Overview of the seal capacity results of all 12 methods, with according depths of the mudstone samples for well A12-03. The last six seal capacity methods all are indicated with a “_D_”, this refers to the incorporation of heterogeneity in the calculations. The porosities and permeabilities were calculated according to the methods described by Drews. NPHI-RHOB cross-over are estimated from the interpreted logs, GWC-top well or GWC-top trap are derived from the contour maps, from nlog.nl.

A12-01

This well is part of the A12-FA shallow gas field, as mentioned before. The trap geometry resembles the geometry of well A12-03, see figure 20. In some of the accumulations, A12-01 does cut through the crest of the reservoir and therefore corresponds the computed gas column the maximum seal capacity. Seal capacities were derived for the following depths (in mTVDss) 400m; 503m; 595m; 643m and 723m. The according calculated gas columns range from a couple mm to over 500m.

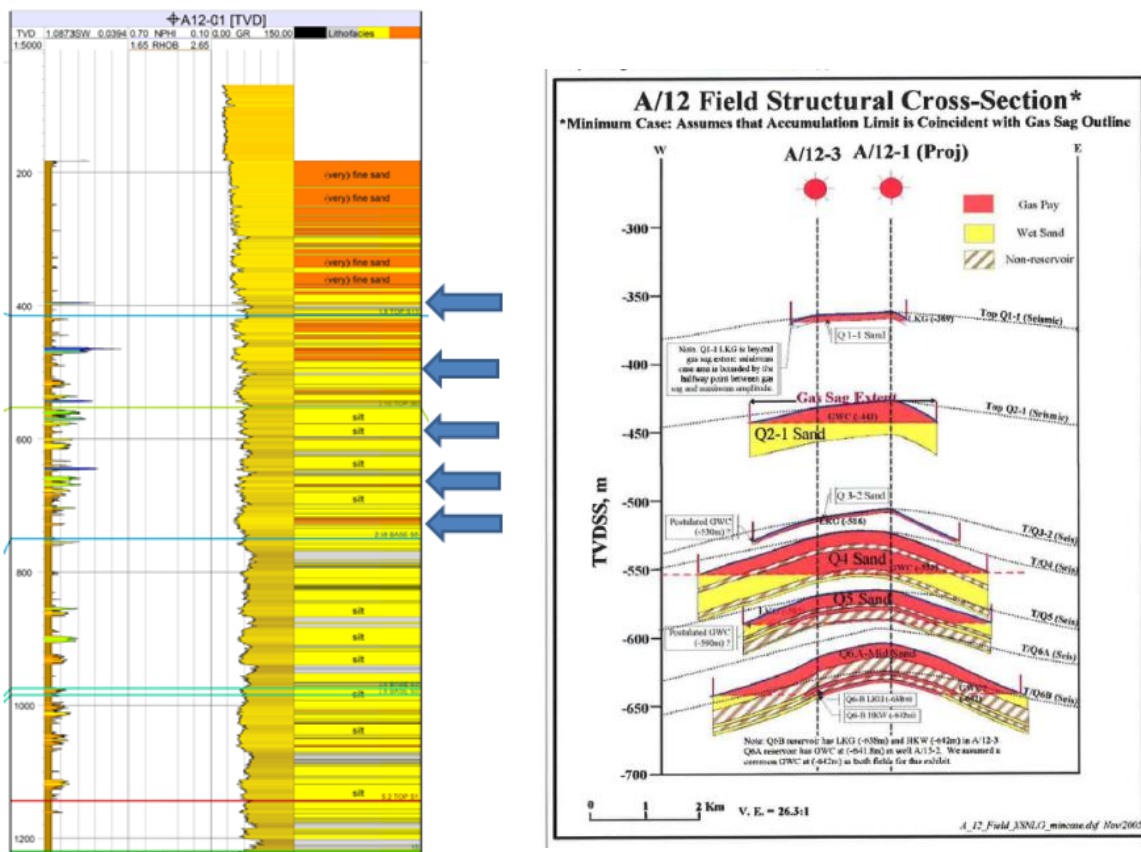


Figure 21. Left: Interpreted log, with lithology and arrows indication the location of the mudstone samples. Right: Overview of the stacked gas accumulations with GWC and trap geometry for well A12-01 and A12-03, from nlog.nl.

A12-01		Seal capacity (m)														
Seal depth (mTVDss)	Sample depth (mTVDss)	EGM1	EGM2	d10_All	d10_Katsube	d10_Schlörner	d10_Aplin	EGM1_D	EGM2_D	d10_D_All	d10_D_Katsube	d10_D_Schlörner	d10_D_Aplin	NPHI-RHOB cross over (m)	GWC-Top well (m)	GWC-top trap (m)
403	400	17.6	11.7	97.7	397.8	250.4	13.8	18.8	12.6	11.4	116.9	53.7	0.4	/	16	16
508	503	17.7	11.9	104.9	411.9	262.4	15.6	15.0	10.1	2.3	46.5	16.9	0.02	/	26	29
595	595	21.6	14.5	131.5	466.1	307.6	23.1	21.5	14.4	15.8	138.9	67.2	0.7	/	21q6	24
653	643	20.4	13.8	135.3	472.3	313.4	29.4	20.0	13.5	2.6	48.9	18.1	0.03	/	/	/
724	723	22.2	15.1	150.9	500.2	337.8	29.4	15	10	1.9	40.5	14.3	0.02	/	/	/

Table 8. Overview of the seal capacity results of all 12 methods, with according depths of the mudstone samples for well A12-01. The last six seal capacity methods all are indicated with a “_D_”, this refers to the incorporation of heterogeneity in the calculations. The porosities and permeabilities were calculated according to the methods described by Drews. NPHI-RHOB cross-over are estimated from the interpreted logs, GWC-top well or GWC-top trap are derived from the contour maps, from nlog.nl.

B16-01

Well B16-01 is part of the shallow gas field B16-FA. The structure is fault bounded and seems to be filled-to-spill. The well is not cutting through the crest of the reservoir therefore are the computed gas columns, therefore is the NPHI-RHOB cross-over not corresponding to the maximal seal capacity. Seal capacities were derived for the following depths (in mTVDss) 417m; 463m and 650m. The according calculated gas columns range from a couple mm to over 483m.

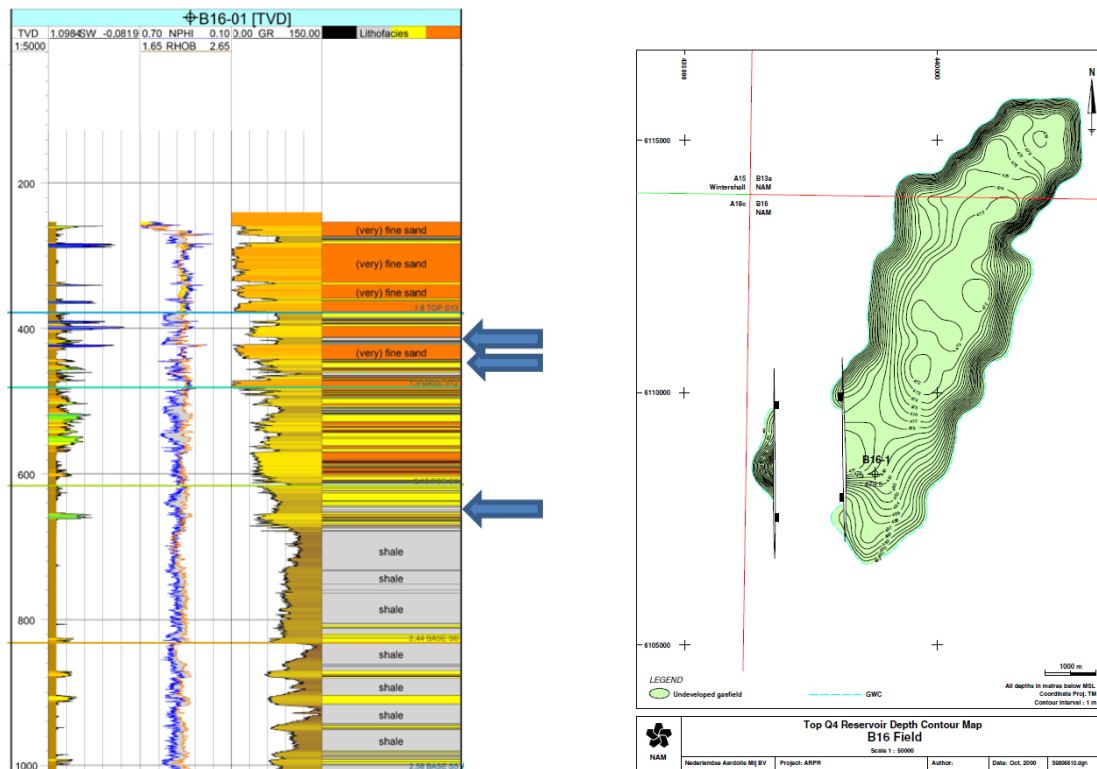


Figure 22. Left: interpreted well log, with NPHI-RHOB cross-over, lithology and arrows indication the location of the mudstone samples. Right: Contour map of the gas field, with GWC and location of the well, from nlog.nl.

B16-01		Seal capacity (m)														
Seal depth (mTVDss)	Sample depth (mTVDss)	EGM1	EGM2	d10_All	d10_Katsube	d10_Schlömer	d10_Aplin	EGM1_D	EGM2_D	d10_D_All	d10_D_Katsube	d10_D_Schlömer	d10_D_Aplin	NPHI_RHOB cross over (m)	GWC-Top well (m)	GWC-top trap (m)
420	417	1.9	1.3	108.9	423.1	270.6	16.6	/	/	/	/	/	/	2	13	20
466	463	14.9	10.2	95.7	391.9	246.2	13.4	/	/	/	/	/	/	8	/	/
659	650	21.5	14.5	141.1	483.6	323.0	26.1	22.5	15.2	2.6	49.1	18.2	0.03	2	/	/

Table 9. Overview of the seal capacity results of all 12 methods, with according depths of the mudstone samples for well B16-01. The last six seal capacity methods all are indicated with a “_D_”, this refers to the incorporation of heterogeneity in the calculations. The porosities and permeabilities were calculated according to the methods described by Drews. NPHI-RHOB cross-over are estimated from the interpreted logs, GWC-top well or GWC-top trap are derived from the contour maps, from nlog.nl. Keep in mind that the first sample (417m) contains a very large sand fraction and is therefore not too reliable.

B17-05

Well B17-05 is part of the gas field B17-FB. This field is characterized by many north-south trending faults. The well does not cut through the crest of the reservoir and the reservoir is fault bounded. The reservoir is not filled-to-spill and one of the faults surrounding the reservoir is leaking. Seal capacity was derived for the following depth (in mTVDss): 557m and the according calculated gas columns range from a couple mm to over 454m.

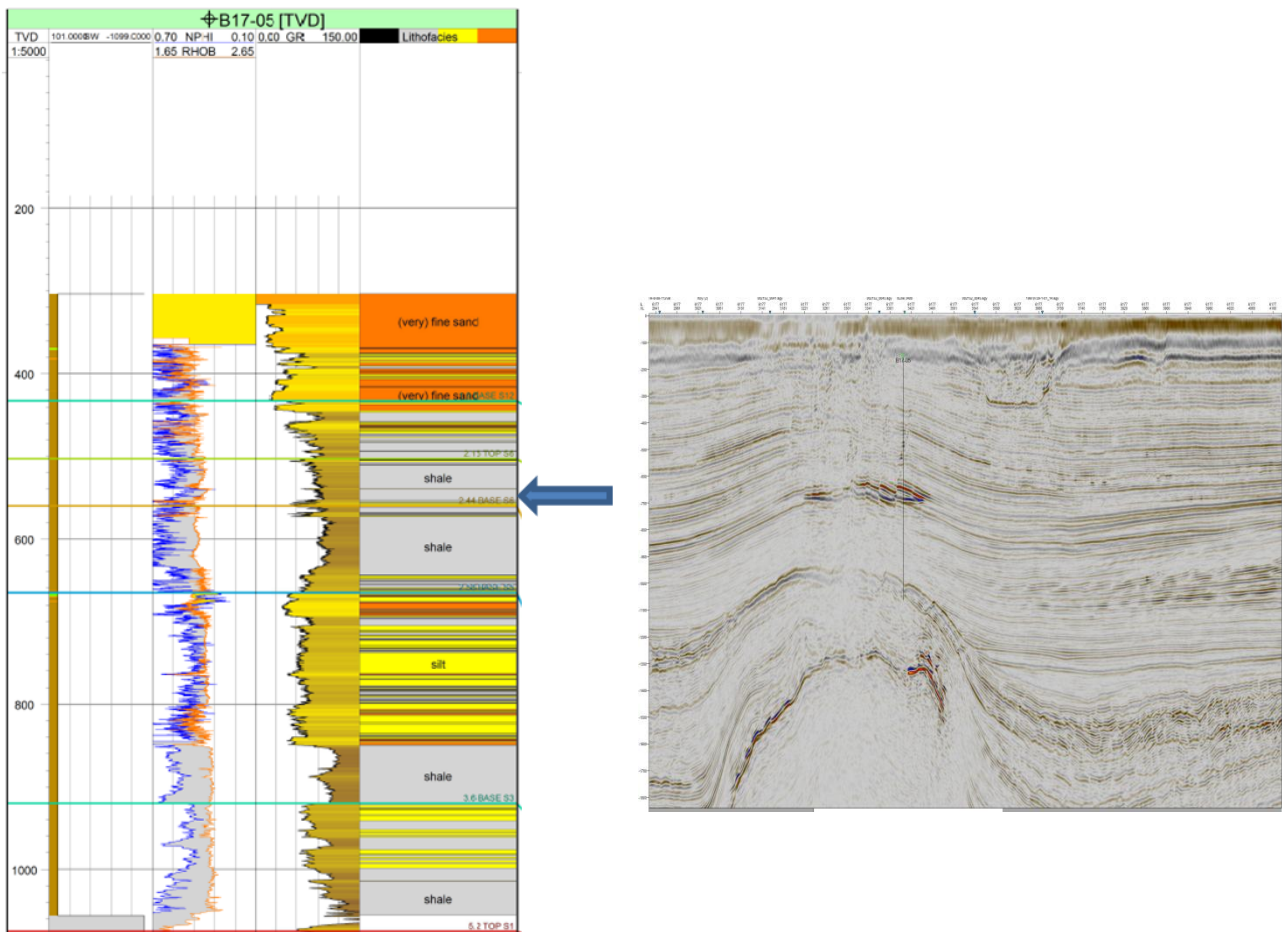


Figure 23. Left: the interpreted well log, with lithology, NPHI-RHOB cross-over and the arrow indication the location of the mudstone sample. Right: seismic section indicating the location of the well. Several faults are clearly visible.

B17-05		Seal capacity (m)														
Seal depth (mTVDss)	Sample depth (mTVDss)	EGM1	EGM2	d10_All	d10_Katsube	d10_Schlömer	d10_Aplin	EGM1_D	EGM2_D	d10_D_All	d10_D_Katsube	d10_D_Schlömer	d10_D_Aplin	NPHI_RHOB cross over (m)	GWC-Top well (m)	GWC-top trap (m)
640	557	20.6	13.8	125.3	454.5	297.6	21.2	31.3	21.3	2.4	47.4	17.4	0.03	15	24	40

Table 10. Overview of the seal capacity results of all 12 methods, with according depths of the mudstone samples for well B17-05. The last six seal capacity methods all are indicated with a “_D_”, this refers to the incorporation of heterogeneity in the calculations. The porosities and permeabilities were calculated according to the methods described by Drews. NPHI-RHOB cross-over are estimated from the interpreted logs, GWC-top well or GWC-top trap are derived from the contour maps, from nlog.nl.

B10-03

Well B10-03 is part of the shallow gas field B10-FA. The well cuts through bright spots classified as stacked 4 way dip closures and the structure is not fault bounded. The well is not cutting through the crest reservoir, the top is actually located at approximately 1.7 km from the well. Seal capacities were derived for the following depths (in mTVDs) 555m; 628m; 680m; 727m and 810m. The according calculated gas columns range from a couple mm to over 531m.

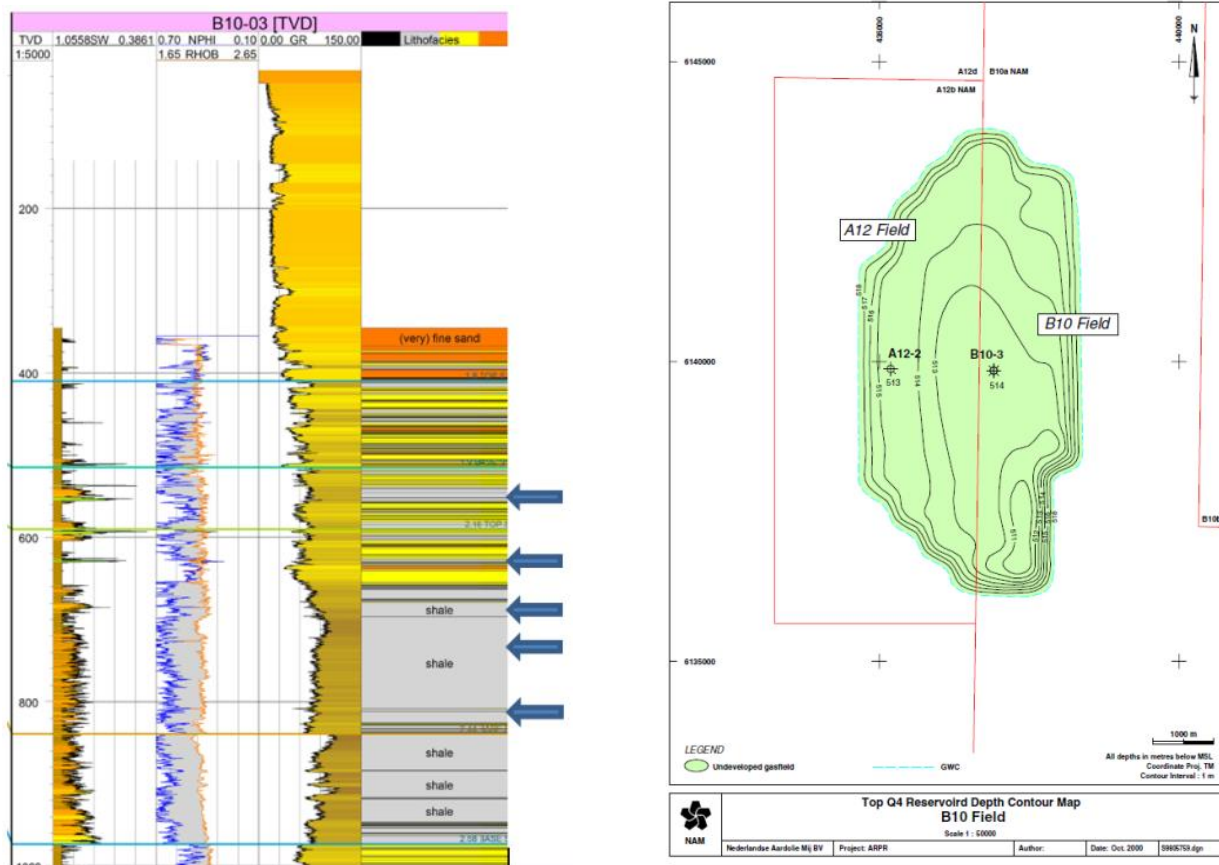


Figure 24. Left: interpreted well log with lithology, NPHI-RHOB cross-over and arrows indicating the location of the mudstone samples. Right: contour map, with the crest of the gas field, the well location and the GWC, from nlog.nl.

B10-03		Seal capacity (m)														
Seal depth (mTVDss)	Sample depth (mTVDss)	EGM1	EGM2	d10_All	d10_Katsube	d10_Schlömer	d10_Aplin	EGM1_D	EGM2_D	d10_D_All	d10_D_Katsube	d10_D_Schlömer	d10_D_Aplin	NPHI_RHOB cross over (m)	GWC-Top well (m)	GWC-top trap (m)
558	555	19.7	13.3	117.5	438.1	284.2	19.0	18.6	12.5	2.4	47.4	17.3	0.03	/	/	/
630	628	22.0	15.0	124.1	450.1	294.8	21.0	18.2	12.3	2.5	48.7	18.0	0.03	4	/	/
690	680	22.9	15.4	154.9	509.2	335.0	30.6	26.2	17.7	2.6	49.6	18.4	0.03	/	/	/
732	727	25.0	16.8	162.4	521.5	356.1	33.3	26.5	17.9	19.2	154.2	76.9	0.9	/	/	/
812	810	26.2	17.8	169.3	531.2	365.6	36.0	25.6	17.4	21.6	163.7	83.3	1.1	/	/	/

Table 11. Overview of the seal capacity results of all 12 methods, with according depths of the mudstone samples for well B10-03. The last six seal capacity methods all are indicated with a “_D_”, this refers to the incorporation of heterogeneity in the calculations. The porosities and permeabilities were calculated according to the methods described by Drews. NPHI-RHOB cross-over are estimated from the interpreted logs, GWC-top well or GWC-top trap are derived from the contour maps, from nlog.nl.

2.8. Overview methods

As mentioned in the introduction this part of the Dutch offshore is characterized by shallow gas fields, which occasionally display multiple reservoir-seal pairs. The height of the traps is maximum 40 meters and in most cases the hydrocarbon column height varies between 10-20m. From seismics it is hard to exactly establish the height of the columns due to the very subtle structure of these traps and due to the pull down effect of deeper reflectors. Therefore the height of the lower gas accumulation only can be estimated from seismics. In order to have more calibration points, depth contour maps, production plans and NPHI-RHOB cross-overs, were taken into account. Keeping this in mind, an evaluation of the different methods is made.

The first thing that strikes the eye is that the d10_All; d10_Katsube; d10_Schlömer and d10_D_Katsube methods result in an overestimation of the gas column in all wells. The d10_D_aplin and d10_D_All methods result in an underestimation. That leaves methods EGM1, EGM2, d10_Aplin, EGM1_D, EGM2_D and d10_Schlömer. In well A12-03, keeping in mind that the well does not cut through the crest of the reservoir, methods EMG1, d10_Aplin, and EMG1_D, give the best results. In well A12-01, the methods that give the best representation of the seal capacity are EMG1 and EMG1_D. Well B16-01 is also not cutting through the crest of the reservoir and the seal capacity is best represented by methods EMG2 and EMG2_D. In well B17-05, seen the possibility that some of the faults are leaking the gas column could be much larger than computed, the methods giving the best representation of the seal capacity are d10_Aplin, EGM1_D and EMG2_D. In well B10-03, the seal capacity is best represented by methods EMG1, d10_Aplin and EMG1_D.

When the results from section 2.5 and 2.6 are incorporated, several methods can be discarded. The three methods that are based on the calculations by Nordgård Bolås *et al.*, 2005, with the poor correlation coefficients, result in unrealistic pore throat diameters and seal capacities, with and without incorporation of heterogeneity. The d10_Aplin with incorporation of heterogeneity displays unrealistic hydrocarbon columns, in most cases the hydrocarbon column is only a couple cm high. The EGM2 which is based on actual mudstone data, renders in an underestimation of the seal capacity, both with and without incorporation of heterogeneity.

When all this information is combined, the methods resulting in the best outcomes are first EGM1_D, and on a shared second place d10_Aplin and EGM1. Figure 25. presents the three best methods. EGM1_D is in the majority of the cases situated in between EGM1 and d10_Aplin. The most pronounced differences the curve displays when compared to the curve of EGM1, is the variability. The influence of the specific clay fraction is more pronounced. The EGM1_D and d10_Aplin curve display approximately the same trend, which is remarkable seen that the formulae used to obtain these results are not analogue.

It is however hard to conclude from the computed seal capacities which of the methods are over- and underestimating the hydrocarbon column. With the seismic resolution being rather poor and the very subtle structure of the traps it is hard to state whether traps are filled to spill or under filled. Only when a closer look is taken at gas fields A12-01 and A12-03 and compare them to the calibrated gas columns derived from the depth contour maps, the methods EGM1, EGM2, d10_Aplin result in an underestimation of the seal capacity.

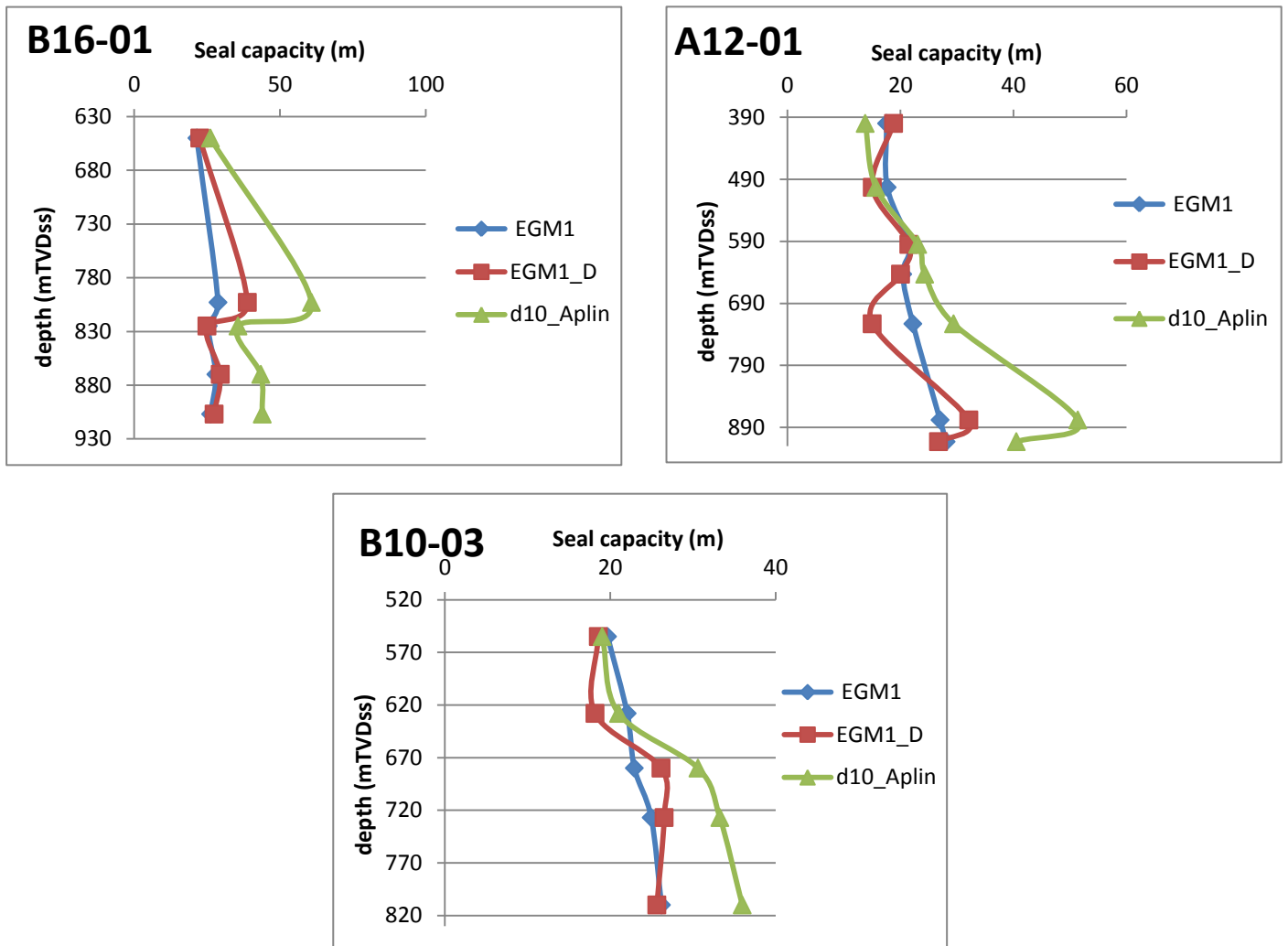


Figure 25. Seal capacities computed by the methods EGM1, EGM1_D and d10_Aplin.

Conclusions and outlook

Method 1. Laser diffraction vs. sedigraph

It has been shown that the postulated correlation for sedigraph and laser diffraction results, should be improved. For the samples of the Rupel Clay Formation onshore Netherlands, the 8 μm grain size is an overestimation and in this research a correlation of 5 μm has been found to give the best correlations. It is possible that the best correlation is dependent on the specific data set.

Method 2. Porosity- effective stress and porosity-permeability calculations with Belgian Boom Clay measurements

The carried out calibration of the porosity and permeability results obtained with the Yang and Aplin's formulae and the obtained data from the Belgian Boom Clay leads to the following conclusion: the proposed porosity-effective stress and porosity-permeability by Yang and Aplin, 2004, 2010, results in reliable calculations of the porosity and permeability, respectively. Although when compared to the calibrated values, the Yang and Aplin method results in an overestimation, in most cases, of the permeability by 1-2 orders.

Method 3. Application of heterogeneity: Drews methodology

This method can only be applied to mudstones with a clay content of at least 50%. The application of heterogeneity results in curves that display more variability. This is due to the fact that each sample has its own specific clay fraction and this is represented in the obtained results. A sample with a specific clay fraction will always result in a narrow range of permeabilities, the only factor influencing the results is the depth, i.e. effective stress. This method could be considered as an improvement for mudstone calculations, seen that most other methods are assuming homogeneous clays or mudstones. However the relationships developed are generally developed for larger scale samples. Another feature is its applicability, for many different bed forms and structures according relationships were developed, each specific for each situation.

It would be useful that the workflow developed by Drews, 2012 is extended to the whole spectrum of clay fractions and not only 50-100%.

Method 5. Alternative pore throat calculations

1. The equivalent grain size method (1)

The first equivalent grain size method results in the most reliable results, when compared to EGM2. This method can also be combined with heterogeneity calculations, only if the clay fraction exceeds 50%.

2. The d10 method

By analyzing each method separately, checking the original data set, the obtained critical pore throats and finally the seal capacities, it can be concluded that methods d10_Katsube, d10_Schlömer and d10_all, should better not be used. d10_Aplin does present reliable results. When this method is combined with the heterogeneity calculations, the results unreliable. The values are approximately 1-2 orders too small, this is a consequence of the applied formula.

3. Seal capacity

The methods leading to the most accurate seal capacity are EGM1_D, d10_Aplin and EGM1. All of these seal capacities fall in the same range of results, but mostly result in an underestimation of a couple meter in hydrocarbon column. With certainty, methods d10_Katsube; d10_Schlömer; d10_All and d10_D_Aplin render unrealistic hydrocarbon columns.

Acknowledgments

First of all I would like to thank Dr. Hanneke Verweij, who supervised my thesis and was always there for questions and discussions. I also would like to thank Prof. Dr. Jan de Jager, my university supervisor who mentioned this opportunity to combine my thesis with an internship, and for his guidance.

References

- Aertsens M., Wemaere I., and Wouters L., 2004. Spatial variability of transport parameters in the Boom Clay, *Applied Clay Science*, Vol. 26, pp. 37-45.
- Amyx, J.W., Bass, D.M. and Whiting, R.L., 1960. Petroleum Reservoir engineering, Physical properties, McGraw-Hill, New York, 160pg.
- Aplin, A.C., Yang, Y.L. and Hansen, S., 1995. Assessment of β , the compression coefficient of mudstones and its relationship to detailed lithology, *Marine and Petroleum Geology*, Vol. 12, pp. 955-963.
- Aplin, A.C. and Macquaker, J.H.S., 2010. Mudstone diversity: origin and implications for source, seal and reservoir properties in petroleum systems, *AAPG Bulletin*, Vol. 95, pp. 2031-2059.
- Arriaga, F.J., Lowery, B., Mays, M.D., 2006. A fast method for determining soil particle size distribution using a laser instrument, *Soil Science*, Vol. 171, pp. 663-674.
- Barboza, S.A., Always, R., Akpulat, T., Esch, W.L., Hicks Jr., P.J. and Gerdes, M.L., 2009. Stochastic evaluation of fluvial to marginal marine sealing facies, *Marine and Petroleum Geology*, Vol. 26, pp. 445-456
- Burland, J.B., 1990. On the compressibility and shear strength of natural clays, *Geotechnique*, Vol. 40, pp. 329-378.
- Buurman, P., Pape, Th., Reijneveld, J.A., Jong, F. de, Gelder, E. van, 2001. Laser diffraction and pipette-method grain sizing of Dutch sediments: correlations for fine fractions of marine, fluvial and loess samples, *Geologie en Mijnbouw/Netherlands Journal of Geosciences*, Vol. 80, pp. 49-57.
- Carman, P.C., 1956. The flow of gases through porous media, Academic press, New York.
- Casey, B., Germaine, J.T., Flemings, P.B., Reece J.S., Gao, B. and Betts, W., 2013. Liquid limit as predictor of mudrock permeability, *Marine and petroleum Geology*, Vol. 44, pp. 256-263.
- Chiles, J. P. and Delfiner, P. 1999. Geostatistics: modeling spatial uncertainty. Wiley, New York, pp. 695.
- Clayton, C. and Hay, S., 1994. Gas migration mechanisms from accumulation to surface, *Bulletin of the geological Society of Denmark*, Vol.44, pp. 12-23.
- Cranganu, C., Villa, M.A., Saramet, M., and Zakharova N., 2009. Petrophysical characteristics of source and reservoir rocks in the Histria Basin, western Black Sea, *Journal of Petroleum Geology*, Vol. 32, pp. 357-372.
- Daza Cajigal, V.A.D., 2012, Sampling and particle size analysis by laser diffraction technique, internship report. TNO and Department of Environment, Land and Infrastructure_DIATA, Politecnico di Torino, Italy,
- Daza Cajigal, V.A.D., 2012, The evaluation of sealing properties of mudstone layers for shallow gas accumulations in the Dutch northern offshore. Master of science thesis. TNO and Department of Environment, Land and Infrastructure_DIATA, Politecnico di Torino, Italy,
- De Haan, H., Godderij, R., Van Hulst, F., Scheffer, B., 2010. Unconventional gas in the Netherlands. PGK lecture, 21. April 2010.
- Deutsch, C. V. 2002. Geostatistical Reservoir Modeling. Oxford University Press, USA, pp. 384.
- Dewhurst, D. N., Yang, Y. and Aplin, A.C., 1999. Permeability and fluid flow in natural mudstones, Geological Society, London, Special Publications, Vol. 158, pp 23-43.
- Downey, M.W., 1984. Evaluating seals for hydrocarbon accumulations, *The American Association of Petroleum Geologist*, Vol. 68, pp. 1752-1763.
- Drews, C.M., 2012. Modelling stress-dependent effective porosity-permeability relationships of metre-scale heterogeneous mudstones, Doctor of Philosophy thesis, Newcastle University.

- Dullien, F. A. L., 1992. Porous media, fluid transport and pore structure, Academic Press, San Diego.
- EBN, 2013. Shallow gas, 75th EAGE conference and Exhibition incorporation SPE EUROPEC 2013, London, UK, 10-13 June 2013.
- Fawad, M., Mondol, N.H., Jahren, J. and Bjørlykke, 2010. Microfabric and rock properties of experimentally compressed silt-clay mixtures, *Marine and Petroleum Geology*, Vol. 27, pp. 1698-1712.
- Ferro, V. and Mirabile, S., 2009. Comparing particle size distribution analysis by sedimentation and laser diffraction method, *Journal of Agricultural Engineering*, Vol. 2, pp. 35-43.
- Giesche H., 2006. Mercury Porosimetry: a general (practical) overview, *Particle and Particle Systems Characterization*, vol. 23, pp. 1-11.
- Herngreen, G.F.W., van Konijnenburg-van Cittert, J.H.A. and Oosterink, H.W., 2005. New geological data (Middle Triassic, Rhaetian-Liassic and Oligocene) of the Winterswijk Quarry, the eastern Netherlands, *Netherlands Journal of Geosciences*, Vol. 84, pp. 409-413.
- Hildenbrand, A., Schlömer, S. and Krooss, B.M., 2002. Gas breakthrough experiments on fine grained sedimentary rocks, *Geofluids*, Vol. 2., pp. 3-22.
- Ingram, G.M., Urai, J.L. and Naylor, M.A., 1997, Sealing processes and top seal assessment, Norwegian Petroleum Society Special Publications, Vol. 7, pp. 165-174.
- Katsube, T.J., Issler, D.R. and Cox, W.C., 1998. Shale permeability and its relation to pore-size distribution, *Current Research*, Vol. 1998-D, pp. 51-57.
- Klimkowski, L., and Smulski, R., 2012. Laboratory method to measure sealing capacity of caprocks, *Archives of Mining Sciences*, Vol. 57, pp. 471-481.
- Konert, M., and Vandenberghe, J., 1997. Comparison of laser grain size analysis with pipette and sieve analysis: a solution for the underestimation of the clay fraction, *Sedimentology*, Vol. 44, pp. 523-535.
- Kowalenko, C.G. and Babuin, D., 2013. Inherent factors limiting the use of laser diffraction for determining particle size distributions of soil and related samples, *Geoderma*, Vol. 193-194., pp. 22-28.
- Li, S., dong, M., Li, Z., Huang, S., Aing, H. and Nickel, E., 2005. Gas breakthrough pressure for hydrocarbon reservoir seal rocks: implication for the security of long term CO2 storage in the Weyburn field, *Geofluids*, Vol. 5, pp. 326-334.
- Macquaker, J. H. S. and Gawthorpe, R. L. 1993. Mudstone lithofacies in the Kimmeridge Clay Formation, Wessex Basin, southern England: Implications for the origin and controls of the distribution of mudstones, *Journal of Sedimentary Petrology*, Vol. 63, pp. 1129-1143.
- Milliken, K.L., Esch, W.L., Reed, R.M., and Whang, T., 2012. Grain assemblages and strong diagenetic overprinting in siliceous mudrocks, Barnett Shale (Mississippian), fort Worth Basin, Texas, *AAGP Bulletin*, Vol. 96, pp. 1553-1578.
- Mondol, N. H., Bjørlykke, K., Jahren, J., and Høeg, K., 2007. Experimental mechanical compaction of clay mineral aggregates – changes in physical properties of mudstones during burial, *Marine Petroleum Geology*, Vol. 24, pp. 289-311.
- Muntendam-Bos, A.G., Wassing, B.B.T., Heege, J.H., van Bergen, F., Schavemaker, Y.A., van Gessel, S.F., de Jong, M.L., Nelskamp, S., van Thienen-Visser, K., Guasti, E., van den Belt, F.J.G. and Marges, V.C., 2009. Inventory non-conventional gas, TNO report, 158 pg's.
- Nakayama K. and Sato D., 2002. Prediction of sealing capacity by the equivalent grain size method, Norwegian Petroleum Society Special Publications, Vol. 11, pp. 51-60.
- Nordgård Bolås, H.M., Hermanrud, C. and Teige, G.M.G, 2005. Seal capacity estimation from subsurface pore pressures, *Basin Research*, Vol. 17, pp. 583-599.

- Norhdal, K. and Ringrose, P. S., 2008. Identifying the representative elementary volume for permeability in heterolithic deposits using numerical rock models, *Mathematical geosciences*, Vol. 40, pp. 753-771.
- Overeem, I., Weltje, G.J., Bishop-Kay, C., Kroonenberg, S.B., 2010. The Late Cenozoic Eridanos delta system in the Southern North Sea Basin: a climate signal in sediment supply?, *Basin Research*, Vol. 13, pp. 293-312.
- Pieri, L., Bittelli, M., Pisa, P.R., 2006. Laser diffraction, transmission electron microscopy and image analysis to evaluate a bimodal Gaussian model for particle size distribution in soils, *Geoderma*, Vol. 135, pp. 118–132.
- Ramaswamy, V., and Rao, P.S., 2006. Grain size analysis of sediments from the Northern Andaman Sea: Comparison of laser diffraction and sieve pipette Techniques, *Journal of Coastal Research*, Vol. 224, pp. 1000-1009.
- Sawamura, F., and Nakayama, K., 2005. Estimating the amount of oil and gas accumulation from top seal and trap geometry, *AAGP Memoir*, Vol. 85, pp. 33-42.
- Schieber, J. 1999. Distribution and Deposition of Mudstone Facies in the Upper Devonian Sonyea Group of New York, *Journal of Sedimentary Research*, Vol. 69, pp. 909–925.
- Schlömer, S., and Krooss, B.M., 1997. Experimental characterization of the hydrocarbon sealing efficiency of cap rocks, *Marine and Petroleum Geology*, Vol. 14, pp. 565-580.
- Schneider, J., Flemings, P.B., Day-Stirrat, R. J., and Germaine, J. T., 2011. Insights into pore scale control on mudstone permeability through re-sedimentation experiments, *Geology*, Vol. 39, pp. 1011-1014.
- Schowalter, T.T., 1979. Mechanics of secondary hydrocarbon migration trapping, *American Association of Petroleum Geologist Bulletin*, Vol. 63, pp. 723-760.
- Skempton, A.W. 1970. The consolidation of clays by gravitational compaction, *Quarterly Journal of the Geological Society of London*, Vol. 125, pp. 373–411.
- Skempton, A.W., 1944. Notes on the compressibility of clay, *Quaternary Journal of the Geological society of London*, Vol. 100, pp. 119-135.
- Tavenas, F. Jean, P., Leblond, P. and Leroueil, S., 1983. The permeability of natural soft clays, Part 2: Permeability characteristics, *Canadian Geotechnical Journal*, Vol. 20, pp. 629-644.
- Veen, J.H. ten, Verweij, H., donders, T.H., Geel, G.R. Bruin, G. de, Munsterman, D.K., Verreussel, R.M.C.H., Daza Cajigal, V.A., Harding, R., Cremer, H., 2013. Anatomy of the Cenozoic Eridanos Delta hydrocarbon system, TNO 2013 R10060, pp. 216.
- Tokunaga, T., Hosoya, S., Kojima, K. and Tosaka, H., 1994. Change of hydraulic properties of muddy deposits during compaction: assessment of mechanical and chemical effect, Proceedings of the international association of engineering geologist conference, Vol. 7, pp. 635-643.
- Yang, Y.L., and Aplin, A.C., 1998. Influence of lithology and effective stress on the pore size distribution and modelled permeability of some mudstones from the Norwegian margin, *Marine Petroleum Geology*, Vol. 15, pp. 163-175.
- Yang, Y. and Aplin, A.C., 2004. Definition and practical application of mudstone porosity – effective stress relationships, *Petroleum Geoscience*, Vol. 10, pp. 153-162.
- Yang, Y. and Aplin, A. C. 2010. A permeability-porosity relationship for mudstones, *Marine and Petroleum Geology*, Vol. 27, pp. 1692-1697.

Yu, L., Gedeon, M., Wemaere, I., Marivoet, J. and De Crean, M., 2011. Boom Clay Hydraulic Conductivity a synthesis of 30 years of research, SCK-CEN-ER, 101 pg's.

Websites:

<http://www.engineeringtoolbox.com/>

<http://www.nlog.nl>

Appendix A: shallow gas field data.

Field	n° monster	Depth (tvd, m)	MD (m)
B16-01	1	275m (±5m)	312,4
	2	387,5m (±2,5m)	424,9
	3	417m (±3m)	454,4
	4	440m (±5m)	477,4
	5	463m (±2m)	500,4
	6	500m (±2m)	537,4
	7	650m (±5m)	687,4
	8	803m (±2m)	840,4
	9	825m (±2m)	862,4
	10	870m (±3m)	907,4
	11	907m (±2m)	944,4
	12	990m (±2m)	1027,4
	13	1007m (±3m)	1044,4
A12-01	14	400m (±2m)	434
	15	503m (±1m)	546
	16	595m (±2m)	629
	17	650m (±2m)	684
	18	643m (±2m)	677
	19	723m (±1m)	757
	20	878m (±1m)	912
	21	913m (±2m)	947
A12-03	22	402m (±3m)	439,2
	23	417m (±2m)	454,2
	24	422m (±2m)	459,2
	25	447m (±2m)	484,2
	26	456m (±3m)	493,2
	27	490m (±2m)	527,2
	28	546m (±2m)	583,2
	29	553m (±2m)	590,2
	30	562m (±3m)	599,2
	31	575m (±2m)	612,2
	32	608m (±2m)	645,2

	33	650m (±3m)	687,2
	34	670m (±2m)	707,2
	35	723m (±1m)	760,2
	36	774m (±2m)	811,2
	37	857m (±2m)	894,2
B17-05			
	39	557m (±2m)	592,66
	40	640m	675,66
	41	645m	680,66
	42	650m	685,66
	43	658m (±2m)	693,66
B10-03	44	590m (±2m)	628,3
	45	628m (±2m)	666,3
	46	555m (±2m)	593,3
	47	609m (±1m)	647,3
	48	680m (±4m)	718,3
	49	727m (±2m)	765,3
	50	810m (±2m)	848,3

Table 1. overview of all the cuttings. Cutting n°38 is intentionally left blank.

Field	n° monster	Depth (tvd, m)	MD (m)
A12-03	26b	455 m	493m
	28b	545-546 m	583-584m
	29b	452 m	590m
B10-03	45b	590 m	629m

Table 2. overview of the cores samples.

All the sample depths were chosen from interpreted boreholes. The depths targeted were located just above possible gas accumulations in the sealing mud layer. The center of this layer was taken as reference depth, the ranges are represented by the values in between brackets.

Appendix B: results sedigraph vs. laser diffraction

Samples from the 16 boreholes of the onshore Rupel Clay formation, Netherlands.

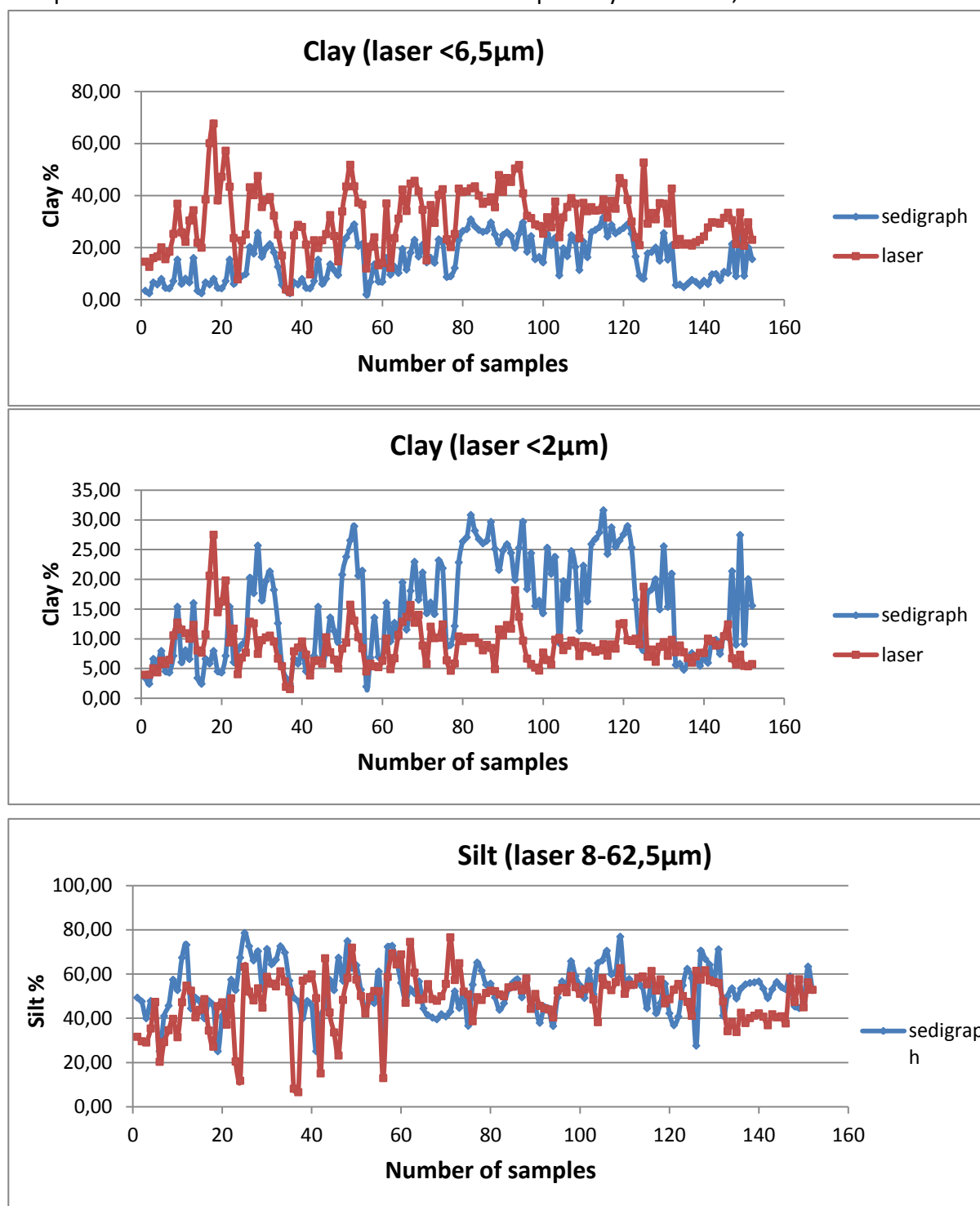


Figure 1. The above graphs represent the sedigraph clay fraction vs. the laser diffraction fraction. The grainsize for the sedigraph is held constant at $<2\ \mu\text{m}$. In the top graph, the grainsize for the laser is set to $<6.5\ \mu\text{m}$, the bottom graph is set to $<2\ \mu\text{m}$.

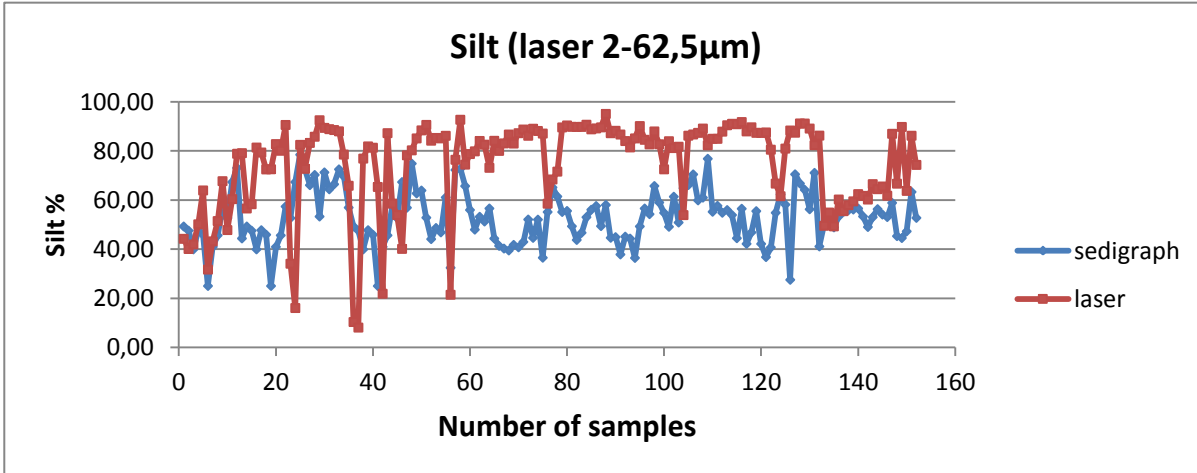
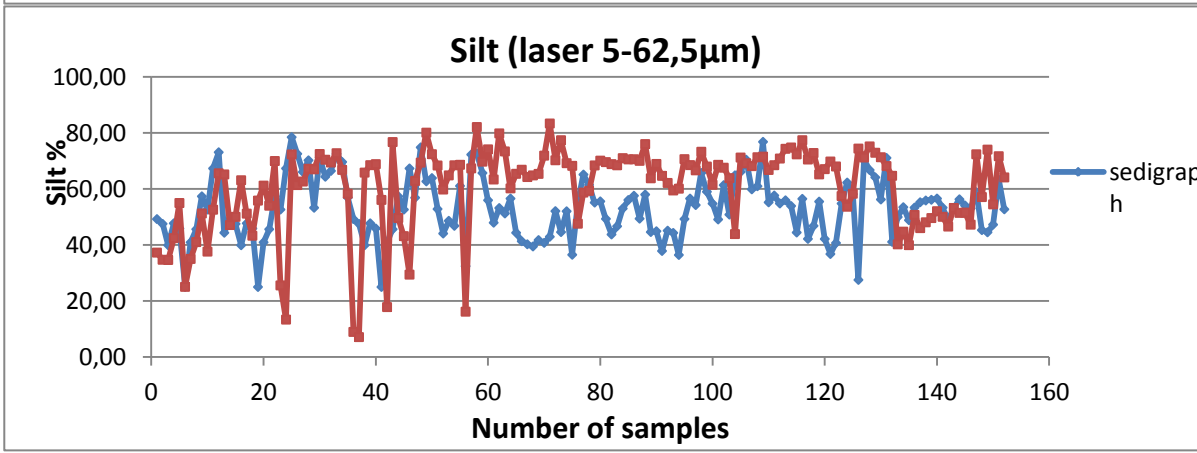
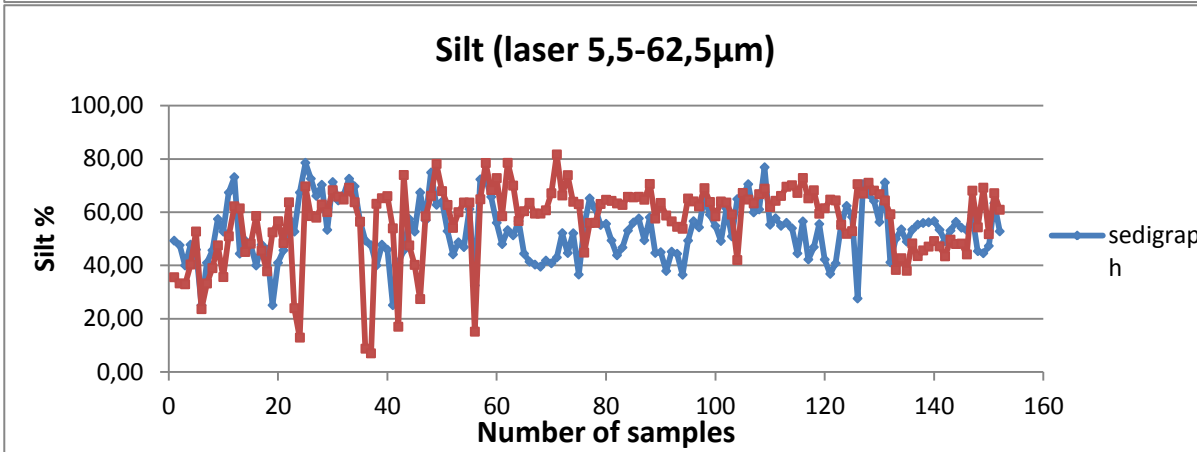
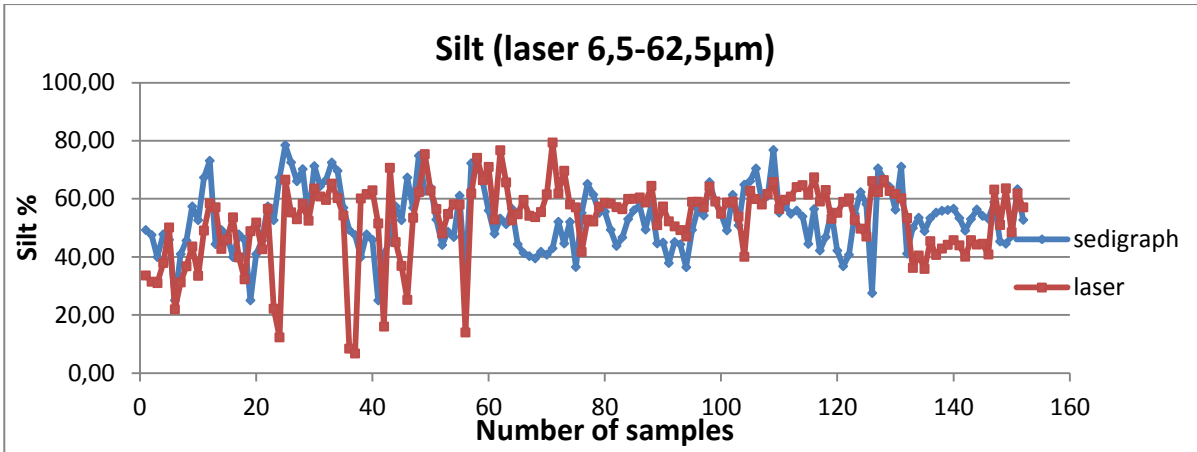


Figure 2 . The silt fractions are represented for the sedigraph (blue) and laser diffraction (red). The silt fraction for the sedigraph are held constant at 2-62.5 μm . In the top graph A), the silt fraction for the laser is set to 8-62.5 μm , in B) the silt fraction is 6.5-62.5 μm , in C) 5.5-62.5 μm , in D) 5-62.5 μm and in the bottom one E) 2-62.5 μm .

sample nr.	sedigraph clay %	sedigraph silt %	Laser < 2 μm	Laser < 5 μm	Laser < 5,5 μm	Laser < 6,5 μm	Laser < 8 μm	Laser 2-62,5 μm	Laser 5-62,5 μm	Laser 5,5-62,5 μm	Laser 6,5-62,5 μm	Laser 8-62,5 μm
I-1	3,42	49,26	3,96	10,90	12,67	14,59	16,63	44,24	37,30	35,53	33,61	31,57
I-2	2,43	47,56	3,97	9,32	10,86	12,60	14,51	40,10	34,75	33,21	31,47	29,56
I-3	6,62	39,93	5,04	12,32	14,10	15,99	17,97	41,95	34,67	32,89	31,00	29,02
I-4	5,83	47,76	4,36	12,05	14,20	16,59	19,18	50,15	42,46	40,31	37,92	35,33
I-5	7,96	45,91	6,31	15,24	17,55	20,10	22,89	63,93	55,00	52,69	50,14	47,36
I-6	4,53	25,03	5,78	12,43	13,95	15,55	17,21	31,72	25,07	23,55	21,95	20,29
I-7	4,33	40,96	6,47	14,63	16,48	18,43	20,47	43,19	35,03	33,18	31,23	29,19
I-8	7,14	45,64	10,58	21,00	23,11	25,28	27,51	51,48	41,05	38,94	36,77	34,54
I-9	15,40	57,39	12,75	29,18	32,96	36,86	40,77	67,71	51,27	47,49	43,59	39,68
I-10	6,06	52,66	11,56	21,71	23,77	25,86	27,97	47,81	37,66	35,60	33,50	31,39
I-11	8,08	67,35	10,94	18,74	20,45	22,26	24,14	60,41	52,62	50,91	49,09	47,21
I-12	6,61	73,12	10,02	23,28	26,72	30,40	34,21	78,88	65,62	62,18	58,50	54,69
I-13	16,01	44,39	12,34	26,26	30,08	34,36	39,05	79,12	65,20	61,38	57,10	52,41
II-1	3,42	49,26	8,04	17,49	19,62	21,87	24,22	56,60	47,15	45,02	42,77	40,42
II-2	2,43	47,56	7,67	15,93	17,88	19,99	22,24	58,33	50,07	48,12	46,01	43,76
II-3	6,62	39,93	10,75	29,01	33,62	38,51	43,54	81,39	63,13	58,52	53,63	48,60
II-4	5,83	47,76	20,63	48,79	54,50	60,15	65,59	79,37	51,21	45,50	39,85	34,41
II-5	7,96	45,91	27,51	56,66	62,25	67,70	72,87	72,49	43,34	37,75	32,30	27,13
II-6	4,53	25,03	14,48	31,18	34,66	38,18	41,67	72,56	55,87	52,39	48,87	45,38
II-7	4,33	40,96	16,26	37,85	42,50	47,22	51,89	82,80	61,21	56,56	51,84	47,17
II-8	7,14	45,64	19,81	45,86	51,53	57,25	62,83	80,09	54,04	48,37	42,65	37,07
II-9	15,40	57,39	9,41	30,01	36,33	43,41	51,03	90,59	69,99	63,67	56,59	48,97
II-10	6,06	52,66	11,71	20,23	21,92	23,65	25,41	34,11	25,59	23,89	22,16	20,41
II-11	8,08	67,35	4,05	6,72	7,26	7,82	8,40	16,06	13,39	12,85	12,29	11,71
III-1	9,00	78,50	6,85	16,99	19,69	22,73	26,13	82,49	72,34	69,64	66,60	63,21
III-2	9,83	72,56	7,69	19,01	21,92	25,07	28,41	72,74	61,42	58,51	55,35	52,01
III-3	20,28	66,08	12,89	33,51	38,28	43,20	48,14	83,29	62,67	57,90	52,98	48,04
III-4	17,68	70,24	12,61	31,19	35,58	40,18	44,92	85,80	67,22	62,83	58,23	53,49
III-5	25,69	53,31	7,48	32,98	40,01	47,52	55,21	92,52	67,02	59,99	52,48	44,79
III-6	16,44	71,28	9,77	26,68	30,97	35,60	40,50	89,41	72,50	68,21	63,58	58,68
III-7	19,71	64,38	10,24	28,68	33,33	38,31	43,52	88,89	70,45	65,80	60,82	55,61
III-8	21,34	66,45	10,53	29,60	34,36	39,42	44,66	88,53	69,46	64,70	59,64	54,40
III-9	18,24	72,52	9,55	24,76	28,42	32,30	36,37	88,00	72,78	69,13	65,25	61,18
III-10	12,62	69,65	6,68	18,40	21,53	24,96	28,65	78,55	66,82	63,69	60,27	56,58
III-11	5,70	56,96	5,40	12,94	14,86	16,96	19,27	65,84	58,30	56,38	54,27	51,96
IV-1	3,42	49,26	1,93	3,31	3,60	3,89	4,19	10,37	8,99	8,70	8,41	8,11
IV-2	2,43	47,56	1,55	2,51	2,71	2,91	3,11	8,10	7,14	6,94	6,74	6,54
IV-3	6,62	39,93	7,90	18,95	21,70	24,67	27,85	76,91	65,86	63,11	60,14	56,96

IV-4	5,83	47,76	8,53	21,87	25,18	28,73	32,46	81,86	68,52	65,21	61,66	57,93
IV-5	7,96	45,91	9,55	22,01	24,90	27,94	31,10	81,33	68,88	65,99	62,95	59,78
IV-6	4,53	25,03	7,35	16,60	18,81	21,17	23,67	65,36	56,11	53,90	51,54	49,04
IV-7	4,33	40,96	3,83	7,86	8,77	9,71	10,68	21,88	17,85	16,94	16,00	15,03
IV-8	7,14	45,64	6,27	16,77	19,61	22,83	26,47	87,26	76,76	73,92	70,70	67,06
IV-9	15,40	57,39	6,37	15,30	17,49	19,86	22,39	58,58	49,65	47,46	45,09	42,56
IV-10	6,06	52,66	5,82	16,57	19,58	22,83	26,21	53,92	43,18	40,17	36,91	33,53
IV-11	8,08	67,35	10,26	20,96	23,07	25,19	27,28	40,14	29,44	27,33	25,21	23,12
V-1	13,60	56,90	7,74	23,09	27,56	32,48	37,71	78,23	62,88	58,41	53,49	48,27
V-2	11,32	74,86	6,51	17,35	20,68	24,46	28,60	80,26	69,42	66,09	62,31	58,17
V-3	9,45	62,72	5,02	10,03	12,04	14,74	18,27	85,12	80,11	78,10	75,40	71,88
V-4	20,79	63,90	8,36	24,32	28,88	33,91	39,29	88,39	72,43	67,87	62,84	57,46
V-5	23,80	52,85	9,38	31,61	37,34	43,51	49,96	90,62	68,39	62,66	56,49	50,04
V-6	26,56	44,11	15,74	40,12	45,88	51,83	57,81	84,20	59,82	54,06	48,11	42,13
V-7	28,93	48,65	13,06	33,50	38,41	43,56	48,83	85,30	64,86	59,95	54,80	49,54
V-8	20,61	46,85	10,29	26,95	31,83	37,27	43,14	85,13	68,47	63,59	58,15	52,28
V-9	21,46	61,10	8,40	25,95	31,01	36,55	42,40	86,19	68,64	63,58	58,04	52,19
V-10	1,96	32,46	4,51	9,75	10,88	11,99	13,05	21,46	16,22	15,09	13,98	12,92
V-11	6,83	72,29	5,83	14,88	17,44	20,34	23,58	76,42	67,37	64,81	61,91	58,67
V-12	13,56	72,70	5,38	15,96	19,65	23,96	28,81	92,71	82,13	78,44	74,13	69,28
VI-1	6,96	65,71	5,24	9,93	11,41	13,22	15,40	74,45	69,76	68,28	66,47	64,29
VI-2	6,87	55,98	6,31	10,91	12,31	14,06	16,25	78,76	74,16	72,76	71,01	68,82
VI-3	16,04	47,97	10,03	26,48	31,45	36,99	42,92	79,85	63,40	58,43	52,89	46,97
VI-4	9,57	53,22	4,90	9,13	10,49	12,24	14,49	84,08	79,85	78,49	76,74	74,49
VI-5	12,69	51,27	6,74	15,90	19,36	23,64	28,74	82,57	73,41	69,95	65,67	60,57
VI-6	10,26	56,60	10,64	23,57	27,15	31,15	35,48	73,16	60,23	56,64	52,64	48,31
VI-7	19,49	44,38	12,88	31,60	36,71	42,32	48,29	84,15	65,43	60,32	54,71	48,73
VI-8	11,54	41,36	13,69	26,85	30,25	34,09	38,36	80,04	66,88	63,48	59,64	55,37
VI-9	18,08	40,27	15,70	34,51	39,36	44,62	50,17	83,09	64,28	59,43	54,17	48,62
VI-10	22,96	39,49	12,71	34,54	39,97	45,68	51,51	86,69	64,86	59,43	53,72	47,89
VI-11	16,56	41,78	14,03	31,66	36,41	41,62	47,17	83,04	65,41	60,66	55,45	49,89
VI-12	21,16	40,77	8,87	24,21	29,04	34,55	40,62	87,25	71,91	67,08	61,57	55,50
VII-1	14,30	42,96	5,77	11,12	12,87	15,11	17,98	88,74	83,38	81,64	79,40	76,53
VII-2	16,11	52,11	12,04	27,97	32,00	36,36	40,97	86,20	70,27	66,24	61,88	57,27
VII-3	14,17	44,62	10,12	21,76	25,32	29,51	34,34	89,06	77,42	73,86	69,67	64,84
VII-4	23,20	52,05	10,20	29,13	34,47	40,27	46,35	88,15	69,22	63,88	58,08	52,00
VII-5	21,88	36,53	12,42	31,25	36,56	42,45	48,76	87,10	68,27	62,96	57,07	50,76
VII-6	8,70	55,15	6,40	17,33	20,18	23,21	26,34	58,56	47,62	44,77	41,74	38,61
VII-7	8,97	65,16	4,64	14,32	17,10	20,20	23,56	68,40	58,72	55,94	52,84	49,49
VII-8	12,16	61,46	5,85	18,11	21,51	25,24	29,21	71,60	59,34	55,94	52,21	48,23
VIII-1	22,87	55,16	10,40	31,58	36,96	42,68	48,60	89,60	68,42	63,04	57,32	51,40
VIII-2	26,38	55,59	9,61	29,88	35,39	41,36	47,63	90,39	70,12	64,61	58,64	52,37
VIII-3	27,09	49,35	10,18	30,39	35,79	41,64	47,79	89,82	69,61	64,21	58,36	52,21
VIII-4	30,84	43,78	10,15	31,06	36,70	42,80	49,20	89,80	68,89	63,25	57,15	50,75
VIII-5	28,20	46,70	10,20	31,53	37,31	43,55	50,08	89,80	68,47	62,69	56,45	49,92

VIII-6	26,78	53,04	9,31	28,98	34,28	40,02	46,08	90,69	71,02	65,72	59,98	53,92
VIII-7	26,05	56,08	8,07	26,30	31,35	36,85	42,67	88,81	70,58	65,53	60,03	54,21
VIII-8	26,52	57,60	8,96	27,52	32,42	37,69	43,24	89,19	70,64	65,74	60,47	54,92
VIII-9	29,67	49,41	8,48	28,04	33,46	39,34	45,53	89,62	70,06	64,64	58,76	52,57
VIII-10	25,14	58,02	4,91	23,96	29,45	35,52	42,03	95,09	76,04	70,55	64,48	57,97
IX-1	21,59	44,65	11,59	35,00	41,25	47,88	54,63	87,24	63,83	57,58	50,95	44,20
IX-2	24,84	44,93	10,60	25,03	35,40	41,46	47,88	88,22	68,94	63,42	57,36	50,94
IX-3	25,92	37,88	12,32	28,96	40,31	46,76	53,46	86,70	64,70	58,71	52,26	45,56
IX-4	24,45	45,13	11,72	28,41	39,27	45,25	51,32	84,05	62,17	56,50	50,52	44,45
IX-5	19,92	44,33	18,18	35,43	45,18	50,39	55,69	81,46	59,49	54,46	49,25	43,95
IX-6	25,31	36,45	13,70	32,82	45,09	51,78	58,49	85,13	60,13	53,74	47,05	40,34
IX-7	29,69	49,29	9,69	24,28	34,75	40,87	47,37	90,15	70,66	65,09	58,97	52,47
IX-8	18,38	56,58	6,68	18,73	27,23	32,23	37,57	84,56	68,54	64,01	59,01	53,67
IX-9	24,42	54,27	5,77	17,77	26,35	31,37	36,74	82,69	66,67	62,11	57,09	51,72
IX-10	15,52	65,75	5,16	16,07	24,12	28,92	34,07	87,95	73,30	68,99	64,19	59,04
IX-11	16,43	59,02	4,67	15,69	23,62	28,32	33,37	82,74	68,01	63,78	59,09	54,04
IX-12	14,31	54,80	7,69	16,03	21,82	25,34	29,23	72,53	61,51	58,40	54,88	50,99
X-1	25,32	49,13	6,43	21,78	26,43	31,67	37,38	83,98	68,63	63,98	58,74	53,03
X-2	20,94	61,39	5,71	19,30	23,32	27,81	32,68	81,18	67,60	63,58	59,09	54,22
X-3	23,75	50,87	9,85	27,70	32,51	37,70	43,12	81,73	63,88	59,07	53,88	48,46
X-4	9,31	64,88	10,16	20,14	22,08	24,00	25,86	53,89	43,92	41,98	40,06	38,20
X-5	19,70	66,11	8,10	23,10	27,16	31,59	36,27	86,23	71,24	67,17	62,75	58,07
XI-1	16,69	70,47	8,85	26,38	30,86	35,62	40,54	86,72	69,19	64,71	59,95	55,03
XI-2	24,76	59,88	9,69	28,90	33,80	39,01	44,39	87,38	68,17	63,27	58,06	52,68
XI-3	22,09	61,00	9,43	27,21	31,84	36,88	42,24	89,13	71,35	66,72	61,68	56,32
XII1	11,37	76,84	7,11	17,88	20,65	23,66	26,87	82,33	71,57	68,80	65,79	62,57
XII2	22,31	55,24	8,79	26,96	31,90	37,21	42,74	84,98	66,81	61,87	56,56	51,03
XII3	16,30	57,68	8,74	25,19	29,45	34,00	38,70	84,95	68,50	64,24	59,69	54,99
XII4	25,93	54,84	8,46	25,46	30,27	35,55	41,18	87,88	70,88	66,07	60,79	55,16
XII5	26,81	55,96	7,83	23,95	28,79	34,25	40,23	90,48	74,35	69,52	64,06	58,08
XII6	27,89	53,94	8,06	24,31	29,06	34,41	40,29	91,07	74,82	70,07	64,72	58,84
XII7	31,63	44,47	9,10	27,63	32,81	38,54	44,71	90,90	72,37	67,19	61,46	55,29
XII8	24,27	56,49	7,17	21,52	26,16	31,54	37,62	91,78	77,43	72,79	67,41	61,33
XIII1	28,75	42,20	9,06	26,50	31,87	37,94	44,53	87,98	70,54	65,17	59,10	52,51
XIII2	25,48	46,84	8,35	25,14	29,80	34,94	40,47	89,64	72,85	68,19	63,05	57,52
XIII3	26,53	55,51	12,48	34,65	40,49	46,73	53,17	87,39	65,22	59,38	53,14	46,70
XIII4	27,56	42,17	12,64	32,90	38,56	44,79	51,42	87,36	67,10	61,44	55,21	48,58
XIII5	28,97	36,80	9,77	27,50	32,64	38,33	44,43	87,54	69,81	64,67	58,98	52,88
XIII6	25,34	40,73	9,65	22,13	25,80	30,01	34,71	80,53	68,05	64,38	60,17	55,47
XIII7	16,57	54,84	10,02	19,27	21,53	24,03	26,76	66,74	57,49	55,23	52,73	50,00
XIII8	9,20	62,31	9,07	16,98	18,83	20,92	23,28	61,59	53,68	51,83	49,74	47,38
XIII9	8,04	58,17	18,77	41,42	46,91	52,71	58,67	80,97	58,32	52,83	47,03	41,07
XIII10	17,79	27,55	7,00	20,91	24,85	29,22	33,94	88,34	74,43	70,49	66,12	61,40
XIV1	18,32	70,50	8,20	24,39	28,68	33,32	38,21	87,44	71,25	66,96	62,32	57,43
XIV2	20,02	66,76	6,14	22,14	26,35	30,89	35,68	91,21	75,21	71,00	66,46	61,67

XIV3	14,96	64,16	8,66	26,89	31,78	37,12	42,81	91,17	72,94	68,05	62,71	57,02
XIV4	25,57	56,27	9,43	27,21	31,84	36,88	42,24	89,13	71,35	66,72	61,68	56,32
XV1	15,37	71,10	7,14	21,32	25,15	29,29	33,65	82,36	68,19	64,36	60,22	55,86
XV2	20,94	41,13	9,83	31,38	36,90	42,69	48,56	86,26	64,71	59,19	53,40	47,52
x	5,60	49,98	7,76	17,05	19,03	21,08	23,19	49,55	40,26	38,28	36,23	34,12
x	5,81	53,51	8,88	19,04	21,15	23,33	25,56	54,93	44,78	42,67	40,49	38,26
x	4,79	48,88	7,74	17,08	19,09	21,18	23,31	49,31	39,97	37,96	35,87	33,74
x	6,16	53,37	6,77	16,25	18,79	21,58	24,57	60,24	50,76	48,22	45,43	42,44
x	7,60	55,27	5,99	15,44	18,01	20,79	23,69	55,50	46,04	43,47	40,69	37,79
x	6,80	55,90	7,05	16,87	19,39	22,11	24,97	57,95	48,12	45,60	42,88	40,02
x	5,46	56,16	7,65	17,49	20,09	22,94	25,99	59,48	49,64	47,04	44,19	41,14
x	7,24	56,60	7,62	17,97	20,95	24,28	27,89	62,44	52,09	49,10	45,77	42,16
x	5,97	53,35	10,03	21,66	24,60	27,76	31,07	61,72	50,09	47,14	43,98	40,67
x	9,70	49,05	9,61	23,23	26,45	29,75	33,04	60,23	46,61	43,39	40,09	36,80
x	9,84	53,04	8,87	22,14	25,73	29,60	33,63	66,50	53,24	49,64	45,77	41,74
x	7,45	56,33	9,03	21,99	25,46	29,21	33,11	64,45	51,49	48,01	44,26	40,36
x	10,71	54,12	10,44	24,39	27,82	31,44	35,14	65,54	51,59	48,16	44,54	40,84
x	10,24	53,09	12,43	26,94	30,12	33,37	36,60	61,80	47,29	44,11	40,86	37,63
Covra	21,37	58,86	6,72	21,32	25,68	30,53	35,77	87,00	72,39	68,04	63,19	57,95
Covra	9,00	45,33	5,69	15,26	18,12	21,39	25,01	66,70	57,13	54,27	51,00	47,37
Covra	27,47	44,55	7,32	23,05	27,94	33,48	39,54	89,79	74,06	69,17	63,63	57,57
Covra	9,15	47,28	5,45	14,69	17,50	20,71	24,29	63,76	54,52	51,71	48,49	44,91
Covra	20,04	63,32	5,39	19,89	24,51	29,73	35,41	86,20	71,71	67,09	61,86	56,18
Covra	15,57	52,76	5,76	15,96	19,22	23,01	27,27	74,33	64,13	60,87	57,08	52,82

Table 1. Overview of the input values of the different clay and silt fractions for the sedigraph and laser diffraction.

Appendix C permeability values

The data is derived from the 5 boreholes in the Belgian Boom clay. In the next table an overview will be given of the computed permeability values by Yu et al, 2011; Drews, 2012 and Y&A.

Yu *et al.*, 2011 made a synthesis of hydraulic conductivity values which were converted to permeability values. The conversion was carried out as follows

$$K = \frac{k\eta}{\gamma_w}$$

Where K is the permeability in m²; k the hydraulic conductivity in ms⁻¹; η the dynamic fluid viscosity in 10⁻³kgm⁻¹s⁻¹; and γw the unit weight of water in kNm⁻³.

The temperature was computed as in formula (22); η and γw are dependent on T, the values were established by implementing values from (http://www.engineeringtoolbox.com/water-dynamic-kinematic-viscosity-d_596.html), the values change according to T.

	SSTVD	Y&A	Yu	Drews
Doel 2b	65,15	1,37E-17	2,05E-18	5,68E-16
	65,3	1,36E-17	4,04E-19	5,67E-16
	78,04	1,04E-17	2,05E-18	5,42E-16
	88,99	4,11E-18	2,05E-18	5,22E-16
	89,81	2,66E-18	2,15E-18	5,2E-16
	89,95	2,65E-18	2,05E-18	8,88E-15
	93,8	4,3E-18	9,6E-19	1,47E-16
	96,96	6E-18	2,05E-18	1,45E-16
	100,84	7,48E-18	4,04E-19	5E-16
	103,7	7,2E-18	1,37E-18	4,95E-16
Zoersel	95,12	7,58E-18	1,15E-18	5,1E-16
	101,22	7,49E-18	1,23E-18	8,78E-15
	105,61	6,46E-18	9,58E-19	1,41E-16
	106,65	2,38E-18	9,26E-19	1,4E-16
	112,28	3,76E-18	2,63E-19	1,38E-16
	113,28	2,91E-18	1,31E-18	1,37E-16
	124,26	1,52E-18	8,88E-19	4,5E-17
	126,26	2,24E-18	9,32E-19	1,31E-16
	131,2	2,87E-18	1,12E-18	1,29E-16

	135,2	4,07E-18	3,34E-19	4,34E-17
	139,86	4,63E-18	1,33E-18	8,45E-15
	145,14	3,4E-18	1,07E-18	4,28E-16
	151,32	4,26E-18	1,42E-18	4,19E-16
	155,04	3,24E-18	4,8E-19	4,06E-17
	155,77	3,22E-18	9,73E-19	4,05E-17
	156,04	3,96E-18	2,05E-18	8,31E-15
	156,69	3,93E-18	4,04E-19	8,31E-15
	156,95	3,93E-18	1,15E-18	8,31E-15
	157,95	3,85E-18	1,23E-18	1,18E-16
	160,94	3,89E-18	9,58E-19	8,27E-15
	163,12	3,81E-18	9,26E-19	4,03E-16
	170,89	3,55E-18	1,31E-18	3,92E-16
	172,92	3,34E-18	1,08E-18	1,12E-16
	174,92	3,44E-18	8,88E-19	3,87E-16
	176,1	3,32E-18	9,32E-19	1,11E-16
	177,92	2,93E-18	1,12E-18	3,83E-16
	178,92	3,27E-18	3,34E-19	1,1E-16
Weelde-1	265,39	1,18E-18	2,63E-19	7,4E-15
	273,36	7,52E-19	1,08E-18	8,02E-17
	274,36	1,54E-18	8,88E-19	2,76E-16
	284,28	8,28E-19	9,32E-19	2,65E-17
	286,22	1,44E-18	1,12E-18	7,23E-15
	294,7	6,51E-19	1,33E-18	7,49E-17
	296,17	6,45E-19	1,07E-18	2,57E-16
	306,13	3,9E-19	1,42E-18	2,49E-16
	322,13	5,48E-19	4,8E-19	2,36E-16
	325,13	8,76E-19	1,51E-18	2,34E-16
	331,13	4,58E-19	1,55E-18	2,29E-16
	334,13	3,93E-19	6,86E-19	2,27E-16
	345,68	1,01E-18	1,42E-18	6,76E-15
	345,82	1,01E-18	6,51E-16	6,76E-15
	346,16	1,89E-19	3,4E-18	2,18E-16
	346,82	1,89E-19	1,12E-17	2,18E-16
	348,52	7,68E-19	2,97E-18	2,16E-17
	348,57	7,68E-19	1,42E-15	2,16E-17
	362,03	4,35E-19	1,67E-18	2,07E-16
	371,82	6,79E-19	5,72E-19	6,56E-15
	375,81	9,31E-19	9,15E-19	6,53E-15

Table 1. Permeability values for the different methods. Grey squares in the sstvd column indicate different boreholes, according to order: Doel, Zoersel, Essen, Mol and Weelde.

Appendix D: selection shallow gas field samples

Overview of the collected and analyzed samples, with the criteria to be useful for clay fraction based calculations. Samples with a sand fraction of less than 10% were incorporated in the calculations, samples with sand fractions ranging between 10-25% were preferentially not incorporated in the calculations and samples with sand fractions over 25%, were excluded from the calculations. Each category was assigned with an appropriate color. For convenience the clay fraction is also presented.

Field	Depth (tvd, m)	% clay	% sand
B16-01	275	1,11	97,38
	387,5	2,47	37,91
	417	50,67	47,74
	440	34,24	23,69
	463	32,99	14,2
	500	26,64	20,5
	650	45,05	6,57
	803	59,78	0,02
	825	43,7	9,86
	870	47,8	1,45
	907	46,12	3,54
	990	23,97	23,44
	1007	21,7	26,85
A12-01	400	45,94	6,6
	503	37,29	8,59
	595	45,07	3,04
	650	33,26	11,04
	643	42,82	6,55
	723	43,79	3,18

	878	52,33	1,45
	913	42,94	1,81
A12-03	402	11,82	56,94
	417	21,42	20,16
	422	21,13	33,84
	447	12,08	53,12
	456	20,19	32,89
	455	7,15	22,95
	490	33,83	5,99
	546	23,49	21,45
	545	5,49	49,34
	553	19,77	19,19
	452	19,38	12,32
	562	29,14	7,68
	575	26,59	7,4
	608	31,94	6,19
	650	30,5	11,23
	670	36,78	4,6
	723	24,59	14,13
	774	27,63	16,65
	857	49,96	3,92
	844,8	79,73	0
B17-05	557	45,36	6,4
	640	19,51	39,65
	645	24,58	33,32
	650	17,91	59,26
	658	17,8	48,75
B10-03	590	15,57	47,34
	628	37,26	5,07
	555	40,94	5,91
	609	28,42	25,03
	680	48,33	4,62
	727	47,86	4,51
	810	45,11	2,68

Table 1. Results of the laser diffraction analysis.

Appendix E: contour maps shallow gas fields

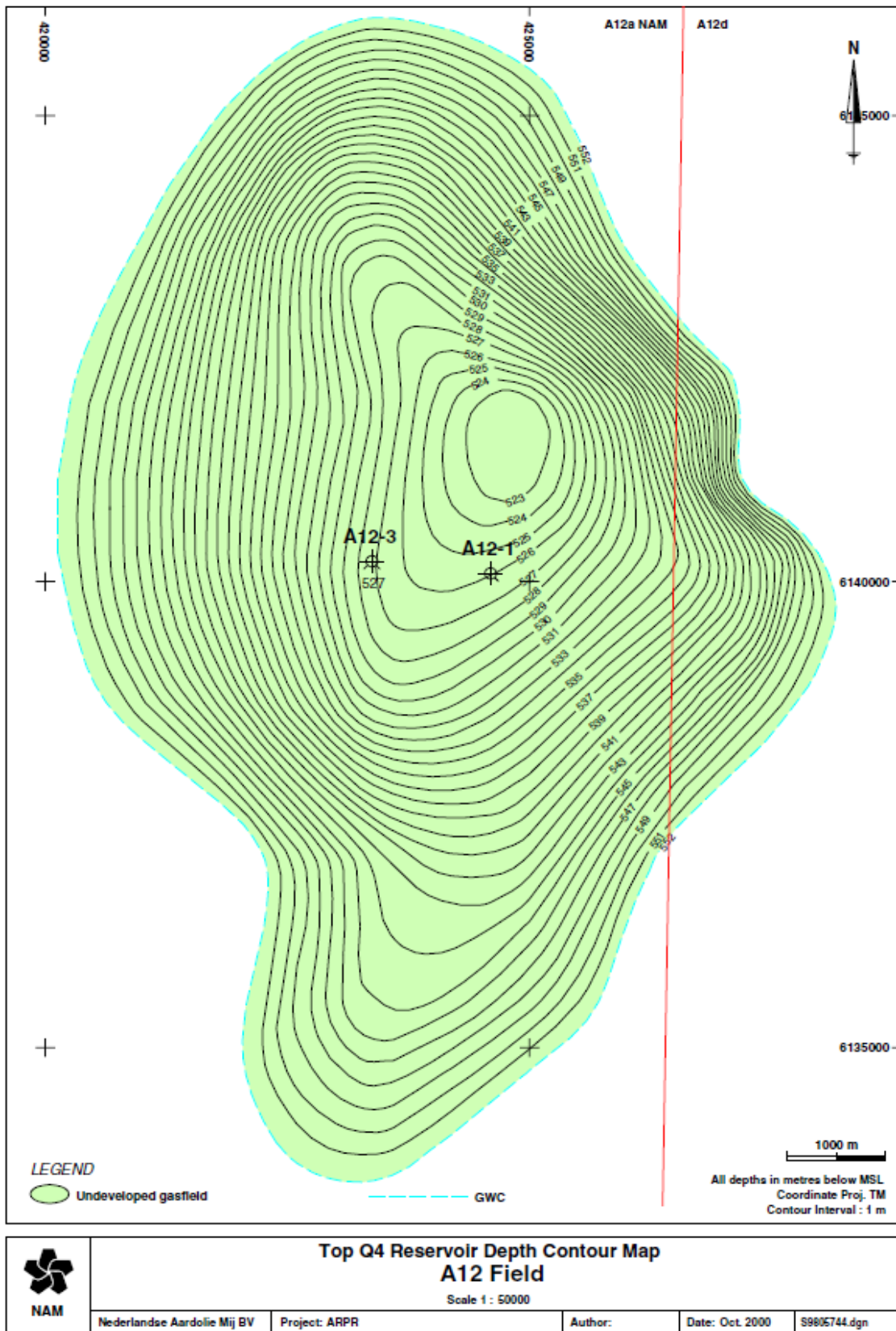


Figure 1. Gas field A12-FA, with both A12-03 and A12-01, from nlog.nl

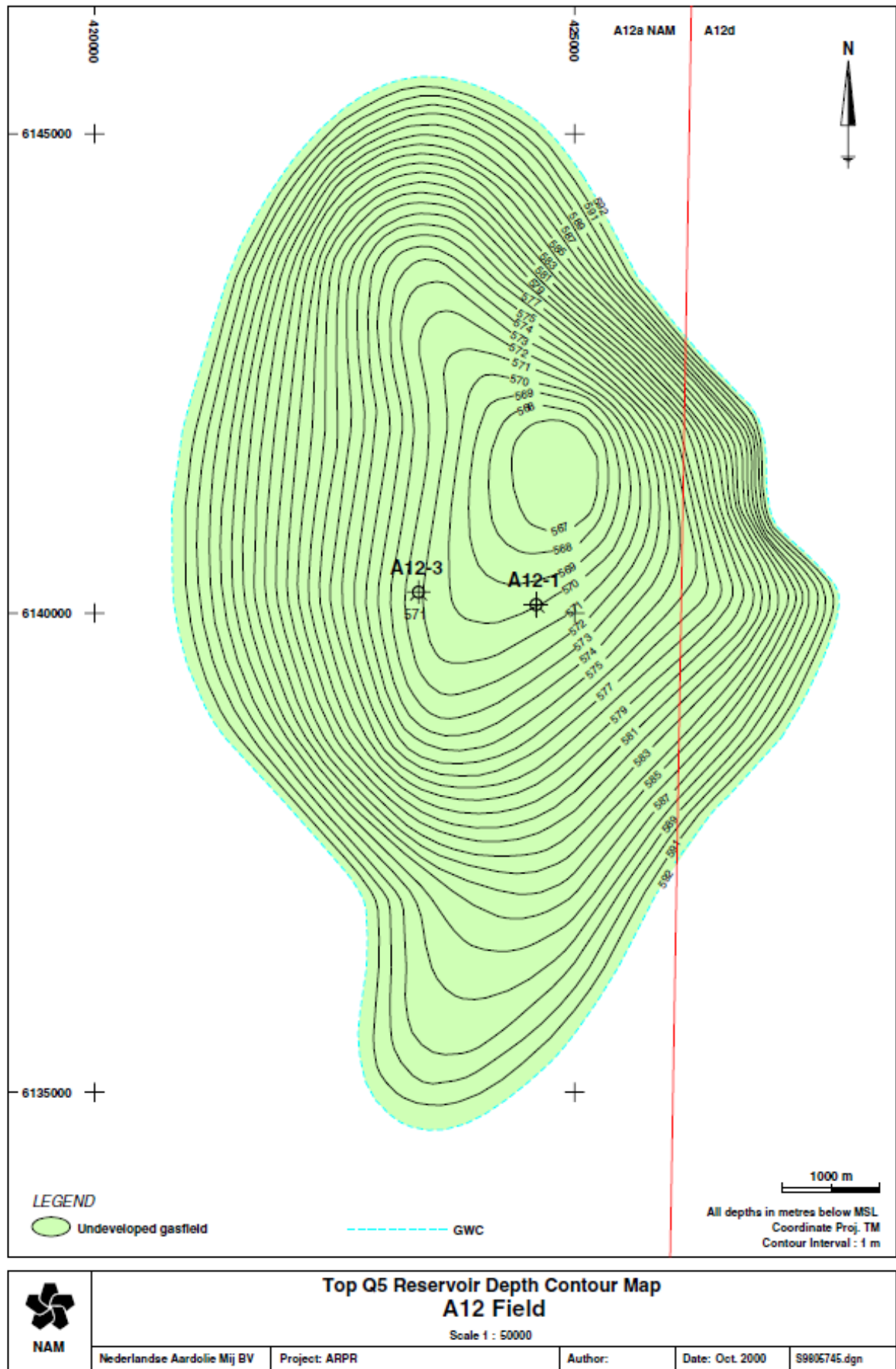
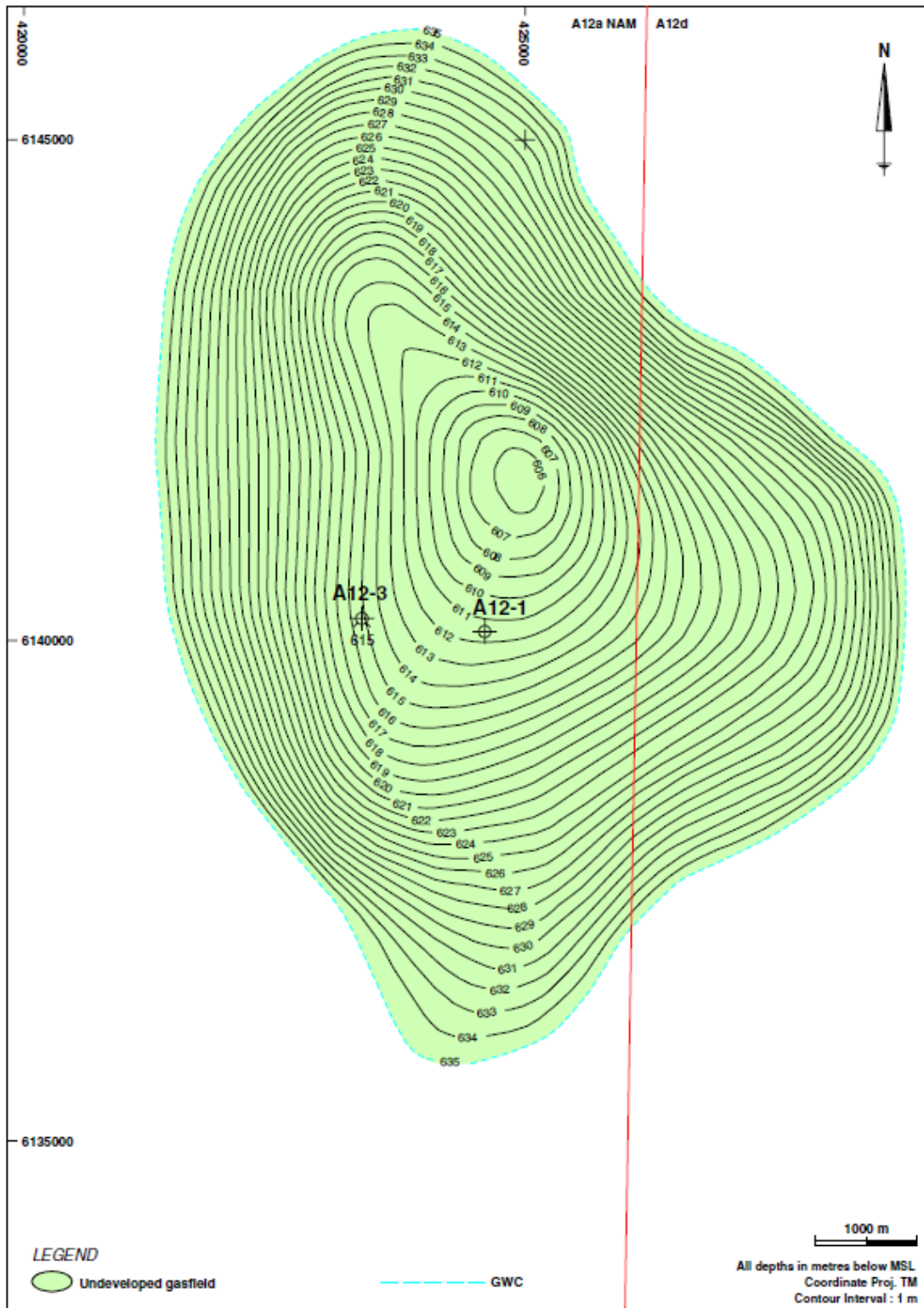


Figure 2. Gasfield A12-FA, with both A12-03 and A12-01, from nlog.nl.




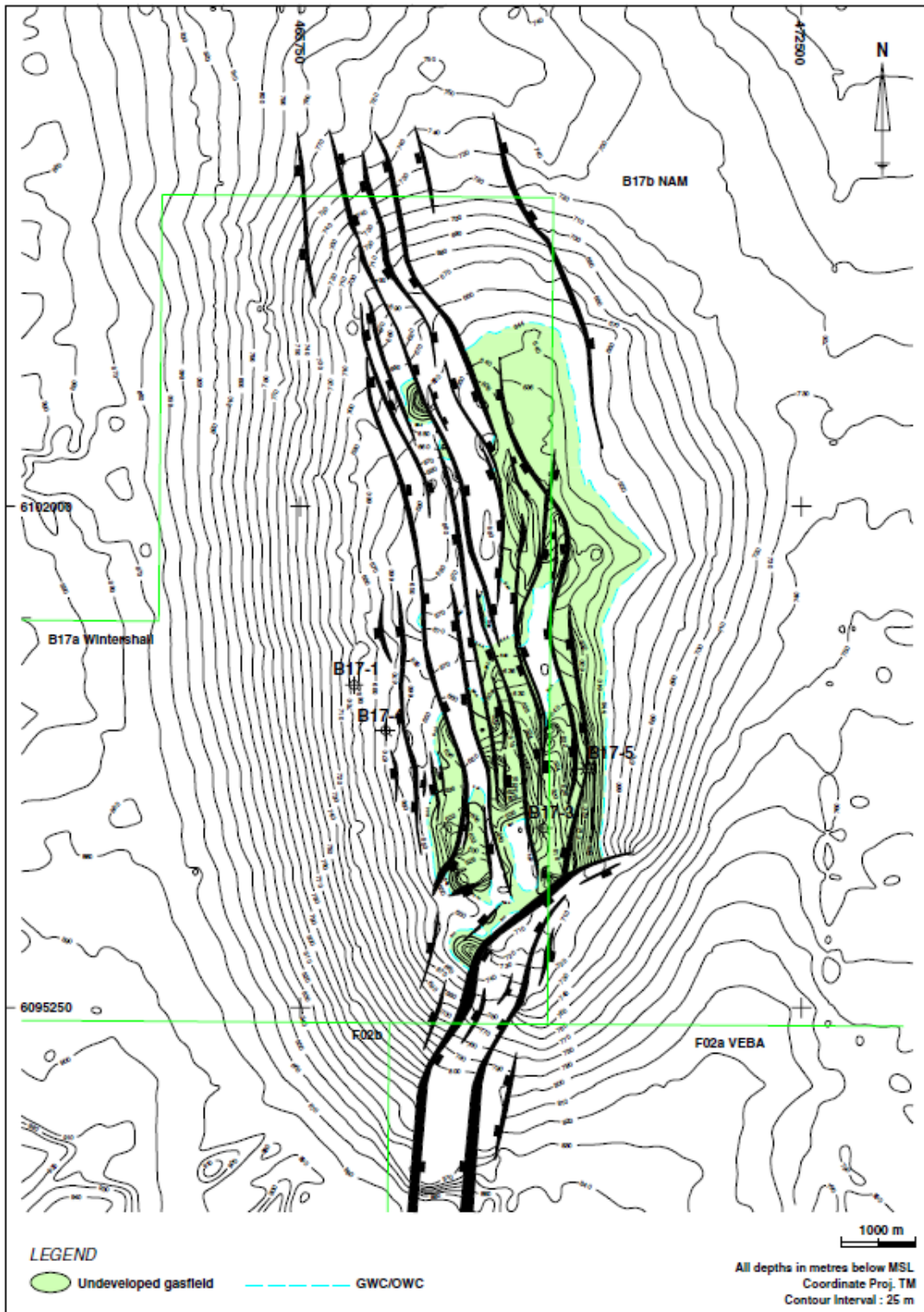
 NAM	Top Q6 Reservoir Depth Contour Map A12 Field Scale 1 : 50000			
	Nederlandse Aardolie Mij BV	Project: ARPR	Author:	Date: Oct. 2000

Figure 3. Gas field A12-FA, with both A12-03 and A12-01, from nlog.nl.




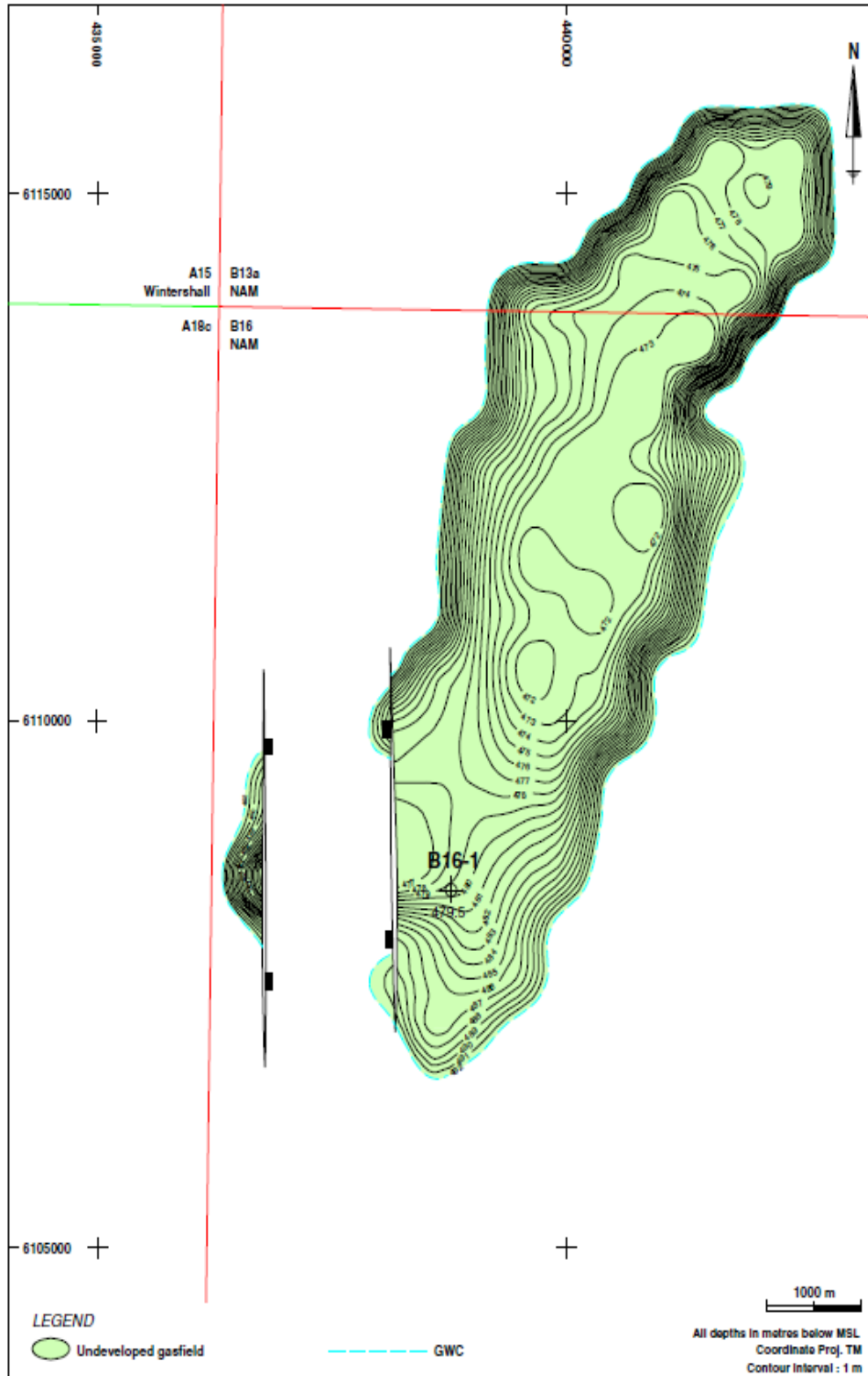
 NAM	Top T1 Reservoir Depth Contour Map B17 Field Scale 1 : 67500				
	Nederlandse Aardolie Mij BV	Project: ARPR	Author:	Date: Oct. 2000	S000023.dgn

Figure 4. Gas field B17-Fa, from nlog.nl.



 NAM	Top Q4 Reservoir Depth Contour Map B16 Field Scale 1 : 50000			
	Nederlandse Aardolie Mij BV	Project: ARPR	Author:	Date: Oct. 2000

Figure 5. Gas field B16A, from nlog.nl

Appendix F: Grain size analysis results: shallow gas fields

Well	Sample depth		Clay(<5µm)	Silt (5-63µm)	Sand (63-2000µm)	Median grain size	Sample
Name	MD (m)	mTVDss	%	%	%	µm	type
B16-1	312	275	1.06	1.55	97.41	158.35	Cutting
B16-1	424	387	26.87	35.16	37.98	18.3	Cutting
B16-1	454	417	18.88	33.29	47.83	51.84	Cutting
B16-1	477	440	31	45.22	23.81	12.74	Cutting
B16-1	500	463	29.82	55.86	14.29	12.21	Cutting
B16-1	537	500	23.77	55.55	20.66	17.25	Cutting
B16-1	687	650	41.26	52.08	6.65	6.92	Cutting
B16-1	840	803	54.27	45.69	0.02	4.06	Cutting
B16-1	862	825	39.02	51.04	9.97	7.08	Cutting
B16-1	907	870	42.95	55.56	1.44	5.92	Cutting
B16-1	944	907	39.49	56.95	3.56	6.83	Cutting
B16-1	1027	990	21.45	54.89	23.65	23.36	Cutting
B16-1	1044	1007	19.32	53.45	27.15	29.67	Cutting
A12-01	434	400	41.38	51.96	6.65	6.43	Cutting
A12-01	546	503	33.53	57.77	8.69	9.3	Cutting
A12-01	629	595	40.25	56.69	3.06	6.55	Cutting
A12-01	684	650	29.98	58.85	11.2	12.23	Cutting
A12-01	677	643	39.13	54.23	6.65	7.73	Cutting
A12-01	757	723	37.33	59.43	3.24	7.41	Cutting
A12-01	912	878	45.23	53.33	1.46	5.47	Cutting
A12-01	947	913	38.1	60.05	1.84	7.02	Cutting
A12-03	439	402	10.44	32.37	57.18	76.36	Cutting
A12-03	454	417	18.75	60.86	20.35	21.03	Cutting
A12-03	459	422	18.67	47.31	34	24.69	Cutting
A12-03	484	447	10.64	35.97	53.37	68.7	Cutting
A12-03	493	456	18.23	48.64	33.15	34.24	Cutting
A12-03	493	455	6.44	70.18	23.37	44.43	Core

A12-03	527	490	30.71	63.24	6.09	9.69	Cutting
A12-03	583	546	20.67	57.65	21.68	19.86	Cutting
A12-03	583	545	4.97	45.11	49.89	62.4	Core
A12-03	590	553	17.35	63.26	19.42	23.22	Cutting
A12-03	590	452	17.31	70.21	12.47	22.56	Core
A12-03	599	562	25.38	66.83	7.77	12.13	Cutting
A12-03	612	575	23.19	69.29	7.52	14.17	Cutting
A12-03	645	608	28.01	65.72	6.28	11.06	Cutting
A12-03	687	650	27.28	61.31	11.4	13.99	Cutting
A12-03	707	670	32.6	62.72	4.65	9.08	Cutting
A12-03	760	723	21.54	64.15	14.31	17.29	Cutting
A12-03	811	774	24.32	58.88	16.8	15.3	Cutting
A12-03	894	857	44.97	51.06	3.95	5.53	Cutting
A12-03	882	844	63.39	36.63	0	3.1	Core
B17-5	592	557	40.72	52.81	6.45	6.56	Cutting
B17-5	675	640	17.45	42.67	39.87	41.21	Cutting
B17-5	680	645	21.85	44.63	33.5	25.61	Cutting
B17-5	685	650	12.16	28.4	59.46	84.59	Cutting
B17-5	693	658	15.99	35.03	48.97	60.06	Cutting
B10-03	628	590	13.59	38.93	47.49	53.81	Cutting
B10-03	666	628	35.18	59.7	5.14	8.43	Cutting
B10-03	593	555	36.66	57.36	5.97	7.82	Cutting
B10-03	647	609	25.71	49.05	25.21	18.6	Cutting
B10-03	718	680	43.4	51.93	4.68	6.08	Cutting
B10-03	765	727	43.98	51.46	4.55	5.89	Cutting
B10-03	848	810	39.99	57.32	2.7	6.5	Cutting

Table 1. Overview of the grain size analysis for the shallow gas field samples.

Appendix G: Shallow gas fields: Calculated properties

Well			Results grain size analysis		Calculated properties						
	Sample depth		Clay (<5µm)	Median grain size	porosity	permeability	Pore throat rad.	Gas column height	Gas column height	Gas column height	Sample
Name	MD (m)	mTVDss	%	µm	%	(m ²)	µm	EGM1_D (m)	d10_Aplin (m)	EGM1 (m)	type
B16-1	312	275	1.06	158.35	14.72	2,1E-19	2,26		32,69	6,09	Cutting
B16-1	424	387	26.87	18.3	14.40	1,53E-19	0,24		40,61	54,87	Cutting
B16-1	454	417	18.88	51.84	27.04	8,62E-19	3,02		11,64	1,96	Cutting
B16-1	477	440	31	12.74	31.14	7,6E-19	1,01		12,71	13,37	Cutting
B16-1	500	463	29.82	12.21	30.10	7,04E-19	0,90		13,39	14,98	Cutting
B16-1	537	500	23.77	17.25	26.27	6,29E-19	0,94		14,45	14,21	Cutting
B16-1	687	650	41.26	6.92	32.71	2,68E-19	0,61	22,47	26,10	21,48	Cutting
B16-1	840	803	54.27	4.06	36.24	8,02E-20	0,44	38,76	60,74	28,70	Cutting
B16-1	862	825	39.02	7.08	29.62	1,68E-19	0,50	24,91	35,55	25,37	Cutting
B16-1	907	870	42.95	5.92	30.65	1,26E-19	0,45	29,48	43,39	27,97	Cutting
B16-1	944	907	39.49	6.83	29.52	1,23E-19	0,48	27,37	43,88	26,17	Cutting
B16-1	1027	990	21.45	23.36	19.92	1,56E-19	0,68		36,51	18,19	Cutting
B16-1	1044	1007	19.32	29.67	18.88	1,45E-19	0,76		38,39	16,16	Cutting
A12-01	434	400	41.38	6.43	37.79	6,86E-19	0,77	18,78	13,76	17,55	Cutting
A12-01	546	503	33.53	9.3	31.55	5,62E-19	0,75	15,02	15,65	17,65	Cutting
A12-01	629	595	40.25	6.55	33.62	3,22E-19	0,61	21,50	23,05	21,57	Cutting
A12-01	684	650	29.98	12.23	27.42	3,67E-19	0,73		20,84	17,86	Cutting
A12-01	677	643	39.13	7.73	31.84	2,97E-19	0,64	20,02	24,29	20,41	Cutting
A12-01	757	723	37.33	7.41	31.06	2,24E-19	0,58	15,00	29,40	22,20	Cutting
A12-01	912	878	45.23	5.47	32.28	9,95E-20	0,46	32,11	51,40	27,02	Cutting
A12-01	947	913	38.1	7.02	28.21	1,38E-19	0,44	26,74	40,52	28,09	Cutting
A12-03	439	402	10.44	76.36	19.58	5,44E-19	2,15		16,25	6,31	Cutting
A12-03	454	417	18.75	21.03	24.73	8,09E-19	1,00		12,19	13,48	Cutting
A12-03	459	422	18.67	24.69	24.50	7,88E-19	1,15		12,42	11,72	Cutting
A12-03	484	447	10.64	68.7	19.21	4,61E-19	1,85		18,20	7,29	Cutting
A12-03	493	456	18.23	34.24	23.51	6,72E-19	1,46		13,86	9,23	Cutting
A12-03	493	455	6.44	44.43	16.41	2,64E-19	0,82		27,15	16,30	Core
A12-03	527	490	30.71	9.69	30.06	6,27E-19	0,71		14,49	18,85	Cutting
A12-03	583	546	20.67	19.86	24.05	5,2E-19	0,89		16,45	14,93	Cutting
A12-03	583	545	4.97	62.4	14.78	1,43E-19	0,90		41,55	14,76	Core
A12-03	590	553	17.35	23.22	22.08	4,69E-19	0,86		17,72	15,46	Cutting

A12-03	590	452	17.31	22.56	23.13	6,66E-19	0,92		13,95	14,54	Core
A12-03	599	562	25.38	12.13	26.65	5,06E-19	0,68		16,74	19,42	Cutting
A12-03	612	575	23.19	14.17	25.22	4,85E-19	0,70		17,23	18,74	Cutting
A12-03	645	608	28.01	11.06	27.37	4,26E-19	0,66		18,83	19,95	Cutting
A12-03	687	650	27.28	13.99	26.14	3,79E-19	0,75		20,36	17,35	Cutting
A12-03	707	670	32.6	9.08	28.75	3,23E-19	0,60	17,38	22,77	21,62	Cutting
A12-03	760	723	21.54	17.29	22.57	3,06E-19	0,67		23,47	19,27	Cutting
A12-03	811	774	24.32	15.3	23.41	2,7E-19	0,64		25,52	19,90	Cutting
A12-03	894	857	44.97	5.53	31.67	1,18E-19	0,45	50,38	209,88	26,50	Cutting
A12-03	882	844	63.39	3.1	42.57	1,42E-20	0,48	31,25	45,53	27,95	Core
B17-5	592	557	40.72	6.56	34.40	3,65E-19	0,64	22,16	21,19	20,60	Cutting
B17-5	675	640	17.45	41.21	21.02	3,52E-19	1,36		21,48	9,62	Cutting
B17-5	680	645	21.85	25.61	23.41	3,84E-19	1,08		20,18	12,13	Cutting
B17-5	685	650	12.16	84.59	20.15	3,23E-19	2,54		22,84	5,15	Cutting
B17-5	693	658	15.99	60.06	20.02	3,14E-19	1,78		23,28	7,36	Cutting
B10-03	628	590	13.59	53.81	19.57	3,48E-19	1,51		21,81	8,74	Cutting
B10-03	666	628	35.18	8.43	29.56	3,64E-19	0,59	18,56	19,03	19,67	Cutting
B10-03	593	555	36.66	7.82	32.40	4,24E-19	0,67	18,15	21,01	22,04	Cutting
B10-03	647	609	25.71	18.6	25.68	4,35E-19	0,96		18,54	13,66	Cutting
B10-03	718	680	43.4	6.08	33.64	2,14E-19	0,57	26,14	30,61	22,91	Cutting
B10-03	765	727	43.98	5.89	32.71	1,88E-19	0,52	26,51	33,26	24,95	Cutting
B10-03	848	810	39.99	6.5	30.40	1,66E-19	0,48	25,63	35,97	26,19	Cutting

Table 1. Overview of the shallow gas field samples calculated properties. Some of the cells in the column of method EGM1_D are empty due to the fact that the minimum clay fraction of the sample, needs to be at least 50%, otherwise calculations could not be carried out.